University of Texas at El Paso

ScholarWorks@UTEP

2022-12-01

Laser Powder Bed Fusion Process, Structure, and Properties: Holistic Approach to Establishing Metallurgical Quality

Hunter Taylor
University of Texas at El Paso

LASER POWDER BED FUSION PROCESS, STRUCTURE, AND

PROPERTIES: HOLISTIC APPROACH TO ESTABLISHING

METALLURGICAL QUALITY

HUNTER COLE TAYLOR

Doctoral Program in Materials Science and Engineering

APPROVED:

_____

Ryan B. Wicker, P.E., Ph.D., Chair

_____

Lawrence E. Murr, Ph.D.

_____

Francisco Medina, Ph.D.

_____

Amit J. Lopes, Ph.D.

_____

Stephen L. Crites, Jr., Ph.D.

Dean of the Graduate School

LASER POWDER BED FUSION PROCESS, STRUCTURE, AND

PROPERTIES: HOLISTIC APPROACH TO ESTABLISHING

METALLURGICAL QUALITY

by

HUNTER COLE TAYLOR, B.S.

DISSERTATION

Presented to the Faculty of the Graduate School of

The University of Texas at El Paso

in Partial Fulfillment

of the Requirements

for the Degree of

DOCTOR OF PHILOSOPHY

Materials Science and Engineering

THE UNIVERSITY OF TEXAS AT EL PASO

December 2022

Acknowledgements

I would like to thank my family, friends, colleagues, mentors, and students who have all helped enable this work. In particular, I want to acknowledge my wife who has likely made the greatest sacrifice over the last 4 years, allowing me to pursue my PhD and start a business simultaneously. I appreciate her support and patience with the hours spent in the lab, traveling, teaching, and pursuing my passion for metal additive manufacturing. In addition, I would never have had the opportunity to enter the Keck Center had she not been stationed at Ft Bliss and encouraged me to pursue a PhD. I would like to thank my parents, T.W. Taylor and Libby Taylor for never setting limits on what could be achieved and always allowing me to explore and learn things the hard way. I'd like to thank my high school frisbee coaches Paverick Nicolas and Nicholas Ligatti for volunteering an extreme amount of time to create the Ultimate Frisbee club and provide an outlet for me that led to a mental and physical attitude critical to achievement. I would also like to thank Rod Rowland, my first boss after graduating from Virginia Tech, for showing me that impact and excellence cannot be faked and that to achieve either you must outwork your competition.

Throughout my PhD I have had the opportunity to leverage the Keck Center's and Dr. Wicker's network of world leaders across all domains of additive manufacturing. There are too many to list, but I would like to specifically thank Dr. Yves Hagedorn and his team at Aconity3D team and Dr. Branden Kappes. I have also had the opportunity to lead over 25 students as part of the development and execution of GTADExP and would like to acknowledge that none of this would be possible without their individual efforts.

iv

Abstract

The advent of metal additive manufacturing (AM) was posed as a disruption to casting, forging, machining, and forming with the notion "complexity is free". However, since invention in the late 1990's the marketed potential has not been realized. Metal based AM is best viewed from the process-structure-properties-performance (PSPP) paradigm taught in material science and engineering, which links the process history to the part performance. Understanding the complex and localized process control made available by AM creates a significant challenge in defining the materials structure, properties, and performance. The lack of holistic understating of inputs and corresponding results has been identified as a major roadblock limiting the promised impact of metal AM.

Metal laser powder bed fusion is the most widely adopted form of metal 3D printing and has produced parts certified for use in space, aerospace, and biomedical applications. These success stories prove the technology is capable of high-quality material creation. The focus for AM now shifts to reproducible quality and predictable properties. America Makes partnered with ANSI to create a standards road map, with 93 gaps identified in 2018. A major theme for metal AM was to develop knowledge to fill gaps in the understanding process parameters, machine variables, geometry, and properties. Through extensive literature review the Qualification Test Artifact was developed to quantitatively address knowledge gaps. The defining characteristic of the artifact is its singular body enabling a holistic evaluation of processing condition against the resulting structure/properties across relevant geometric features. The complexity of the artifact created a need for a complete data management solution leading to the development and funding of the Global Test Artifact Data Exchange Program (GTADExP). GTADExP is designed to bring

an end to qualitative assertions in the LPBF community through pedigree data driven and holistic analysis of process to properties.

Analysis of artifacts from different machines uncovered variability that could not be explained based on the known input parameters. Investigation of microsecond controls of the LPBF process, which are typically hidden from the user, revealed macroscopic impacts to include porosity, spatter, microstructure, and mechanical properties. Utilizing an AconityMIDI+ open architecture LPBF system power ramp rates from <10µs to 400µs were evaluated with plate melting tests. A method to determine optimal ramp rate was developed, and two qualification test artifacts (QTA) were built from IN718 with and without power ramping. Holistic evaluation of the artifacts revealed laser power ramping prevents one form of back spatter but only reduced total spatter by 5%. Laser power ramping also increased near surface porosity which led to reduced elongation to failure in uniaxial tensile tests. The impacts of microsecond control were apparent, and this work highlights the need for transparency in LPBF process control if broadly accepted material property data is to be developed.

Ultimately, the combination of applying the PSPP lens to LPBF, development of a holistic test artifact, and the deep-dive into the microsecond impacts provide the breadth and depth necessary to generate strong conclusions on why LPBF struggles with reproducible and reliable production. Industry has adopted a proprietary approach to process parameter development which is directly tied to material properties. This cascaded into every aspect of the process from academic research, small business adoption, and even industry standards. A review of traditional manufacturing standards reveals no similarities in the make/model/serial number

material property development. Utilizing the knowledge ascertained from this work, a path to repeatability and reliability is proposed. Finally, the only discernible path forward is build file transparency, along with shifting of LPBF OEM's and user value away from parameter development.

Table of Contents

List of Tables

List of Figures

Chapter 1: Introduction

1.1 METAL ADDITIVE MANUFACTURING

The definition of quality as it relates to manufacturing is not universally agreed upon but generally assumes that a quality product and therefore a quality process is void in deficiencies or that the final products meet the defined performance metrics. This work does not disagree with the above definitions but will define manufacturing quality in terms of Lincoln's 5 criteria (criteria also used in MIL-STD-1530D)[1]. These criteria include:

1. Stability
2. Producibility
3. Characterization of mechanical and physical properties
4. Predictability of structural performance
5. Supportability

A quality metal manufacturing process must be able to produce the same product function multiple times, in multiple locations, at a cost that allows for a sustainable business model where the function or performance to the product is defined from prior knowledge of the expected outcome. When a quality metal part is required, there are many established approaches to create it as shown below (Figure 1) based on starting from a particular feedstock. All five Lincoln criteria have been met for processes that start from metal in the liquid, billet, or powder forms as defined in Figure 1.
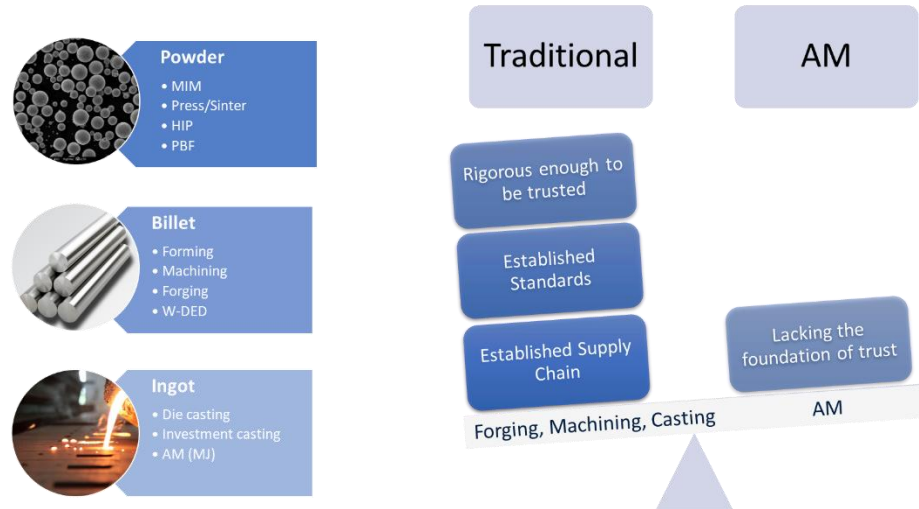
Figure 1 left) feedstock form that feed metal manufacturing right) the weight of trust that prevents LPBF from effectively competing

Metal additive manufacturing enables control over the manufacturing process at orders of magnitude smaller scales than the final part being created. This localized control enables two distinctly different and often confused advantages over other metal manufacturing techniques. First, it enables new geometric freedom of design to create shapes that would otherwise not be possible, or to create shapes that would not be possible without expensive tooling. The second is local control over the material properties by adjusting the process to alter the microstructure. Binder jetting of metal does not enable local process control whereas directed energy deposition and powder bed fusion AM do. Although distinctly different, these two aspects of metal AM cannot be turned off, meaning the control is not only available when desired but that complete control is required if predictable performance is the desired outcome.

The fundamental challenge and key differentiator of Laser Powder Bed Fusion (LPBF) AM from machining, casting, and forging is the microscale volume (voxel level) control of the process. The toolpath in Computer Numerical Control (CNC) machining does not alter the bulk material microstructure and the thermal/mechanical history in most casting and forging operations are

2

orders of magnitude slower and over a large volume. The time scale in these traditional manufacturing processes enable prediction or structure (either from simulation or experience), since the anisotropy or lack thereof can be better predicted. In LPBF, the digital file has direct control over thermal history at the microsecond and micrometer scale [2–4]. While an exciting potential for controlling and tailoring material properties, this also challenges the ability to monitor and simulate the process. Finally, in LPBF, the factors that affect thermal history extend beyond the design itself and encompass every decision from location within a build plate, number of other parts in the build, the orientation of the part in the build, the toolpath relative the chamber gas flow and[5–9]. For these complex interrelated reasons, the digital file workflow determines how much a part will cost, what its properties will be, how it will perform, and how it can be inspected. The digital workflow is not defined by the LPBF process but is instead defined by the machine make/model/serial number/firmware version/software version leading to the logical conclusion that the material properties/cost/performance are linked to a specific machine, which is precisely how the industry currently operates.

1.2 PROJECT OVERVIEW – LASER POWDER BED FUSION PROCESS SENSITIVITY

A critical barrier preventing wider adoption of metal laser powder bed fusion additive manufacturing is a lack of trust [10–12]. On a macroscopic level, there is an adequate level of understanding, i.e. high laser power at low velocity will increase the occurrence of keyhole pores, but the challenge in serial production of critical components comes with identification of rogue defects and the systematic control to reduce their occurrence that is machine manufacturer independent [13–15].

Due to the voxel level control in AM, exceedance curves must account for geometry specific effects such as overhangs and contours. Southwest Research Institute developed Design Assessment of Reliability with Inspection program (DARWIN) for traditional manufacturing and adopted a zone-based approach to probability of anomaly and probably to failure if there is an anomaly in a given zone[16]. It is logical for AM to adopt a similar methodology for reliability assessment. The successful implementation of such an approach requires detailed understanding of input variables to output results. For each geometry zone, there is a list of items that must be well understood to include:

- Type of anomalies and their frequency

- Residual stress

- Feasibility and effectiveness of inspection

- Feasibility of post processing

A pre-requisite to developing the size, type, and frequency of anomalies for a process is the understanding of what factors can affect the outcome. Specifically, LPBF still lacks fundamental understanding on what factors are relevant in terms of defect frequency and distribution. There are other factors limiting adoption including cost, access, training, and materials availability, but those issues cannot be fully addressed without first establishing a practical understanding of what factors account for 99.9% of the part quality.

Scan strategy is known to affect part quality, but there is not a universally accepted or data backed strategy for optimal quality[15,17–21]. One simple question in terms of scan strategy is as follows: Does flow optimization matter and if so to what degree? Flow optimization is described

by some machine manufacturers as a method of rastering the scan vectors so that each new vector moves closer to the cover gas inlet nozzle[22]. This is said to prevent the laser beam from scanning through spatter and smoke and therefore reduces the likelihood for rogue anomalies. EOS has shown this advantageous qualitatively but not statistically at least in the public domain [22]. In addition, negative consequences such as increases in residual stress for example have been ignored in these improvements.

As described in the example above, it is difficult to isolate the effect of one input on a singular output, and therefore, inputs must be simultaneously explored in multiple output metrics. This creates the need for a test artifact that allows for investigation of most, if not all, relevant aspects simultaneously. Such an artifact would create an opportunity to fully characterize the process-structure-property relationships in LPBF. In addition to holistic analysis, fully defined process variables are also necessary. A widely cited number of greater than 130 factors exist in LPBF that contribute to part quality [23]. Spears et al. presented a list of 50 input variables, but several are materials properties that cannot be easily quantified, while others are vague and are made up of many parameters labeled as one such as scan strategy [24]. There is no single number of parameters to control, and the number, unfortunately, depends on a few goals. To guide the quality control affecting variables, it will be helpful to separate them into buckets such as those listed here:

1. Feedstock
   o Shape
   o Size
   o Chemistry
   o Storage
2. Machine
   o Laser

- o Scanner
- o Powder Management System
- o Environmental Control Chamber
- o Gas Flow and Filtration
- o Computer Control System
3. Digital File Preparation
   - o CAD to Machine
   - o Supports
   - o Scanning Strategy
4. Post Processing
   - o Thermal Processing
   - o Surface Processing
5. Inspection
   - o Dimensional
   - o Defect
   - o Properties

Furthermore, the list above can be broken down into sub-categories shown in Table 1.

Table 1 Details of the many categories and factors of control in LPBF

Feedstock	Laser	Scanner Hardware	Powder Spreading	Chamber	Scan Strategy
Alloy	Wavelength	Working Distance	Method	Pressure	Contours
Shape	Mode	Coatings	Type	Gas Type	Infill
Size	Rayleigh Length	Beam Splitters	Return Offset	Gas Purity	Short Vectors
Chemistry	Spot Size	Tuning	Spread Velocity	Oxygen Content	Scaling
Humidity	Energy Profile	Firmware	Return Velocity	Humidity	Scan Order Plate
Apparent Density	Quality	Focal Plane Compensation	Compacting	Gas Temperature	Scan Order Part
Absorptivity	# Of Lasers		Dosing Factor		Layer Thickness
	Response Time		Layer Time		Edge/Blocked Path
Scanner Firmware	**Gas Cross Flow**	**Post Processing**	**Support**	**Build Plate**	**Component**
On Delay	Flow Velocity	Heat Treat	Type	Size	Size
Off Delay	Flow Profile	Hip	Connection Distance	Thickness	Orientation
Polygon Delay	Flow Consistency	Surface Finishing	Connection Type	Alloy	Location On Plate
Acceleration Time	Volumetric Flow		Use Req.	Pre-heat	Digital Quality
Mark Delay				Heat Uniformity	Volume
Jump Delay				Movement Accuracy	Surface Area
Skywriting					Parts On Plate

Each category in Table 1 has been shown to contribute to part quality in literature and the following section attempts to highlight some of the more useful publications on the categories and the findings.

The above paragraphs for section 1.2 were written in the summer of 2020 and have been left substantially unaltered to shed light on the nuance to the challenges in LPBF. The above plan fails to identify the source of the problem, and if completed as designed, this work would have fulfilled the requirements for this dissertation and consumed considerable resources without answering any questions definitively.

1.3 SUMMARY OF RESULTS

Throughout this work, substantial roadblocks (learning opportunities) were encountered, to include equipment breakdown, dead end side projects, proprietary restrictions to required data, and more. However, the most important findings were directly related to these roadblocks, triggering creative solutions or deeper investigation than what would have otherwise happened if everything went as planned. Likely, the most important of these roadblocks came in the form of a firmware error within the AconityONE Raylase scanner control SP-ICE3 card. Seemingly rogue porosity in a complex test geometry (produced prior to the conception of the qualification test artifact) was eventually traced back to a skywriting parameter being implemented incorrectly, causing the scanner to decelerate while the laser beam was still on, creating keyhole pores at the end of vectors Figure 2. The identification of this error required developing a basic understating of the control of the scanner galvanometer (or galvo), a fundamental aspect of the process most materials engineers and scientist do not get the opportunity to learn. This work helped lead to the development of the qualification test artifact; a major result of this dissertation is the design of complicated three-dimensional qualification test artifact for LPBF and the creation of the Global Test Artifact Data Exchange Program (GTADExP). The GTADExP was awarded a $1 million

dollar award by the National Institute for Standards and Technology (NIST). The establishment of the program has led to the conclusion that the underlying challenge preventing LPBF from achieving its potential is the lack of transparency and control of the scanning strategy, the gas flow, and the chamber conditions.

Power = 200 w
Speed = 1000 mm/s
Hatch = 0.1 mm
Stripe Width = 5 mm
Stripe Gap = 0 mm
Strip rotation 90°

On Delay = -100 µs
Off Delay = 15 µs
Mark Delay = 300 µs

On Delay = -100 µs
Off Delay = 15 µs
Mark Delay =100 µs
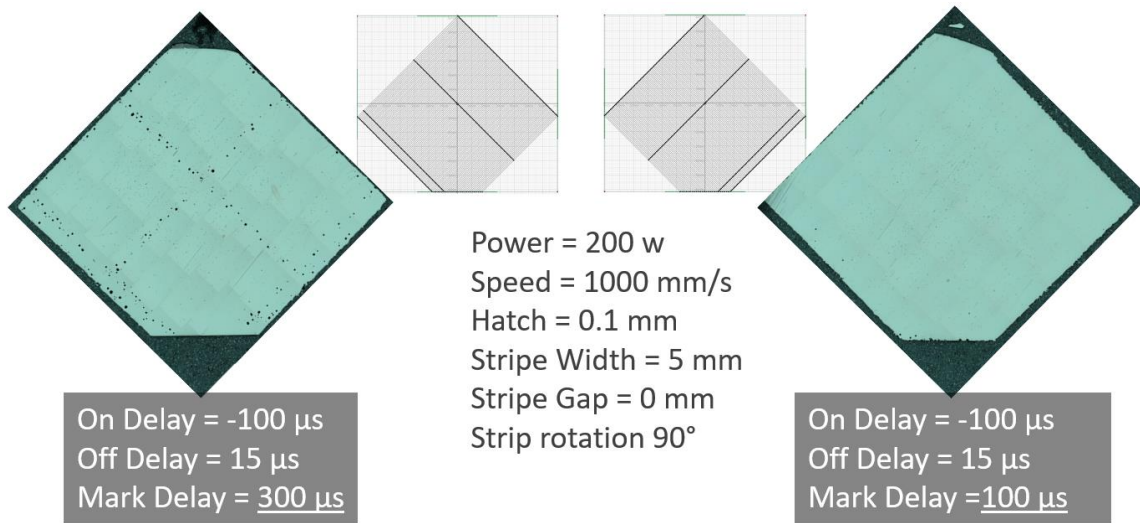
Figure 2 End of track keyhole porosity before and after identification of firmware bug

1.4 ORGANIZATION OF DISSERTATION

This work contains two publications in peer-reviewed journals as chapters with each publication containing literature review. In addition, chapter two contains a brief literature review connecting the major aspects of the LPBF process to the material structure and properties. Chapter 3 contains a self-standing publication entitled Towards a Common Laser Powder Bed Fusion Test Artifact. Chapter 3.2 goes on to describe the artifact redesign and 3.3 describes the Global Test Artifact Data Exchange program to include the data infrastructure. Chapter 4 is a self-standing publication entitled "Effects of Microsecond Control in Laser Powder Bed fusion". Chapter 5 summarizes the challenges and realities of LPBF today, reviews how qualification of highly

critical metal parts is done for other manufacturing methods, reviews the current LPBF standards and qualification landscape, and then proposes a detailed path to turning LPBF into just another manufacturing method. One significant learning outcome from this work and a conclusion of the research is that LPBF should be considered a tool in the large toolbox of manufacturing, and not a grand solution to all of the manufacturing challenges the world is facing. That is, there are many manufacturing methods capable (and more capable in many instances than LPBF) to produce metal parts, and LBPF should be used and applied appropriately. I hope my dissertation provides a foundation upon which the appropriate use of LPBF can be developed and more broadly adopted.

Chapter 2: Literature Review

Laser Powder Bed Fusion is a manufacturing process that is best viewed through the process, structure, properties, performance paradigm. The literature review presented below is not comprehensive as each chapter contains its own literature review to substantiate the claims made. This chapter attempts to provide a broad view of the LPBF literature landscape through selected examples directly relating one aspect of the LPBF process to one or multiple structure/property/performance outcomes. The importance of this review is to highlight the breadth of challenges in LPBF and that the focus of the industry has been to interrogate one variable's impact on a subset of the potential influences it has on the structure/properties/performance. It is well known that performance outcomes of parts made via metal no matter the method, are inherently linked through its entire history. Figure 3 captures the different aspects of LPBF to capture a part's history of formation. The literature review breaks down the various aspects of the LPBF process systematically by looking at its impact on structure and properties.
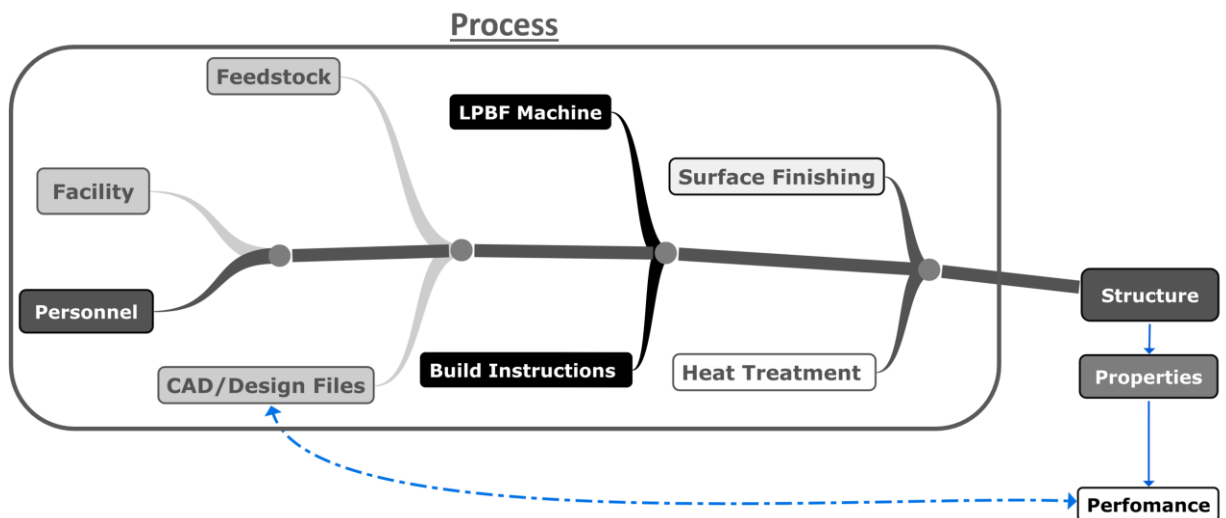
Figure 3 Aspects of the LPBF process that influence structure, properties, and performance

2.1 FACILITY AND PERSONNEL

The control of the facility and training of the personnel was not found in peer reviewed published literature outside of standards such as "ISO/ASTM 52942 Qualifying machine operators of laser metal powder bed fusion machines and equipment used in aerospace applications" [25]. Research facilities do not typically follow a quality management system and a research environment is decidedly not a production environment. Standards such as NASA-STD-6030 and NASA-STD-6030 require production facilities to have a QMS in place that conforms to ISO-9001 and AS-9100[26,27]. In addition, the NASA standards require an LPBF machine to be locked to one alloy chemistry and the facility provide evidence that powder cross contamination is unlikely to occur[26,27]. The data presented for LPBF research is often done with LPBF machines that have held multiple feedstocks of various chemistries in prior research or in facilities with two (or more) machines of different feedstock side by side. Each of these situations creates an opportunity for material contamination that could skew results. Furthermore, a significant amount of published research is performed by researchers and students not fully trained to operate the equipment in a consistent manner (e.g., according to a standard or work instruction that is part of a quality management system) creating further potential variability. An untrained user could perform a series of builds for a publication with a bad recoater, or without skywriting, or any number of small mistakes that go unnoticed and lead to inaccurate conclusions about the data.

2.2 FEEDSTOCK

The LPBF process begins with powder, known as feedstock. Low quality powder is attributed to poor build quality; however, the specific attributes of how to classify powder quality

is not straightforward. ISO/ASTM 52907 manufacturing — Feedstock Materials — Methods to characterize metallic powders lists methods to characterize feedstock size distribution, morphology, flowability, characteristic densities, contamination, and chemical composition [28]. Within each of these categories to classify powder quality there are multiple unique methods yet the relationships to build quality form one or more of these metrics does not yet exist to the authors knowledge.

Riener et al. investigated four varieties of Al10SiMg powder, three gas atomized and one plasma atomized, to evaluate the best methods for quantifying powder quality impacts on part density [29]. Under constant laser power and hatching, scan speeds were varied to produce tensile bars, surface roughness blocks, and density cubes. It was found that more spherical and narrower particle size distributions had higher bulk density, lower absorption at 1064nm, and higher spreading layer density. The more spherical powder resulted in higher density in all cases but the lowest density of any specimen was 99.8% TMD. The work also highlighted the relationship between scan speed and tensile properties, showing higher strength and lower ductility for higher scan speeds, but with density reduction at speeds greater than 2000mm/s [29].

In a review article on feedstock for powder bed fusion by Vock et al. (2019), it was concluded from dozens of articles, that there is no single metric to relate powder quality directly to final product performance [30]. The review reveals it is generally agreed that better flowing powders with high bulk density are preferred but there is difficulty in determining a quality control criterion.

To further validate the perceived importance of feedstock quality, Uniformity Labs was able to raise $38 million on their powder size distribution optimization approach to maximize powder bed packing density [31]. Their technology claims to enable 10x improvement in build time while reducing surface roughness and increasing part strength. The benefits are attributed to enhanced thermal conductivity of the powder and reduced spatter from higher pack density. Despite the clear importance of feedstock quality, the goal of defining the metric to measure and control for consistent properties has yet to be identified.

2.3 DIGITAL FILE PREPARATION

LPBF commonly utilizes the same computer aided design software as traditional manufacturing; however, the defining advantage of additive manufacturing is the freedom of design, which has led to an entirely new field of design tools such as topology optimization software. The design tools enable engineers and non-engineers to create designs that incorporate lattice structures, topology optimized features and more. Although intended to leverage AM, they inherently add complexity, not only in design but in validation, GD&T, documentation, and post processing. In addition to the digital design software, each LPBF machine requires additional software to bridge the gap between design and print. Unfortunately, the make of the machine (manufacturer) also dictates the digital workflow once the design is complete as depicted in Figure 4. To date I have not identified any resource that compares, reviews, or attempts to define how each of these different software impacts the outcome of the part. To perform this study, one entity would have to own one of each machine with each version of software to create a master list of all the similarities and differences in available options.
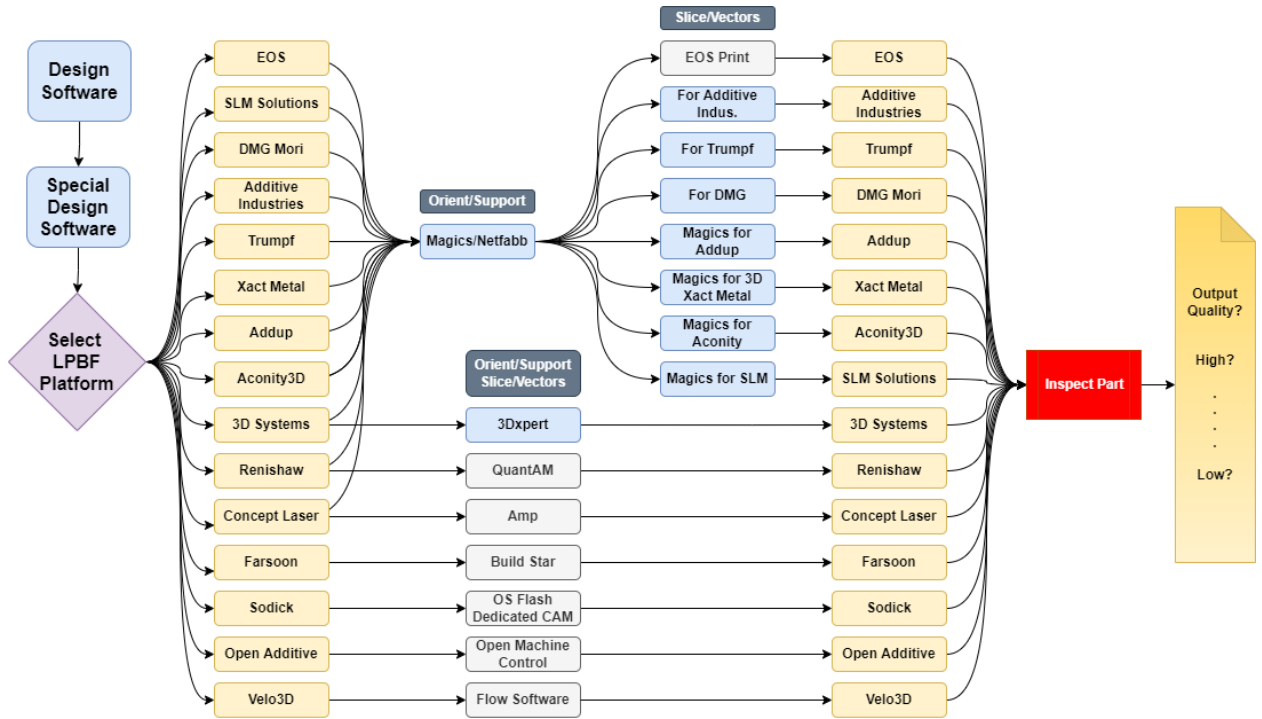
Figure 4 Digital workflow for each LPBF major OEM (illustration to demonstrate complicated workflow in LPBF…there are alternative workflows that may not be captured)

2.3.1 Parameter Selection

Although the implementation may differ between software and hardware, the general methods to identify process parameters are universal. Parameter development typically begins with a series of melts on plate to define a power/velocity map that correlates the melt pool depth to a P/V ratio, from here a series of cubes are produced to create a porosity-based process window as depicted in Figure 5. Although simulation software continues to improve, the next step in parameter development typically requires the creation of simple geometries using a design of experiments (DOE) with various power, speed, and hatch spacing.
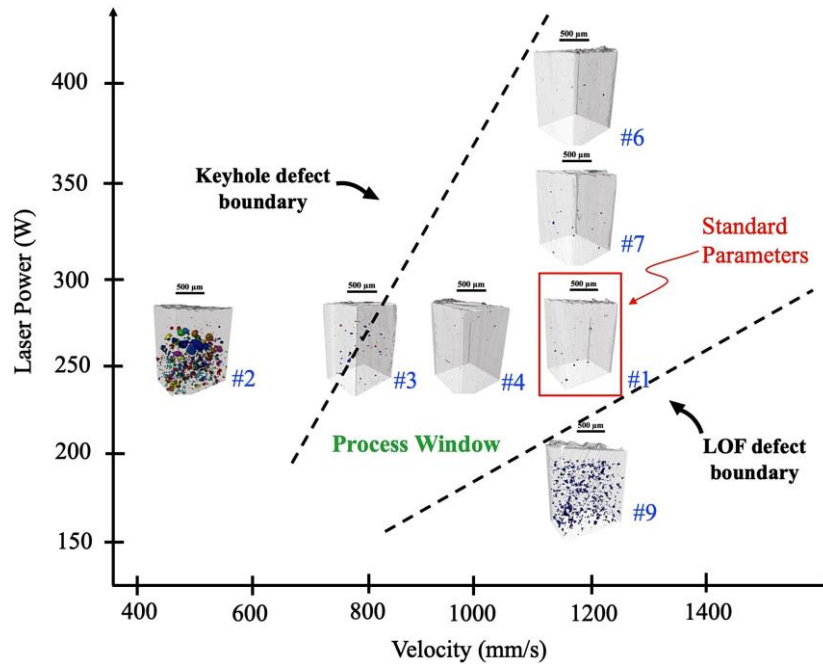
Figure 5 Power velocity process map adapted from [32] under https://creativecommons.org/licenses/by-nc-nd/4.0https://creativecommons.org/licenses/by-nc-nd/4.0/

Developing the remaining parameters for down-skin, contours, stripe width and more often utilize more DOE's of increasing complex designs. LPBF has dozens of relevant examples of parameter development or the analysis of the effect of various parameters controlled by the digital file preparation as shown in Table 2.

Table 2 List of references for a given topic related to digital file preperation

Major Topic of research article	References
Plate melt analysis	[33–43]
Cubes/blocks	[7,43,44]
Laser power/scan speed	[4,21,45]
Spot size	[35,46–48]
Hatch spacing	[49]

Hatch method (meander, stripe, chess, other)	[9,18,50,51]
Build plate temperature	[52–55]
Intervector time	[56]
Surface roughness	[6,19,57–62]
Laser on/off optimization	[2,15]
Build orientation/Geometry	[63–66]
Incident angle	[67,68]
Down-skin/overhangs	[69,70]

2.4 LPBF MACHINES

2.4.1 Six universal subsystems

All laser powder bed fusion systems are composed of six main sub systems as shown in Figure 6. Each subsystem play an important role in the overall part quality. This section reviews relevant literate related to each subsystem and its impact on the structure and properties of LPBF produced materials.

1) Laser source
2) Beam steering system
3) Powder and platform management system
4) Gas flow and filtering system
5) Environmental control chamber
6) Computer control system
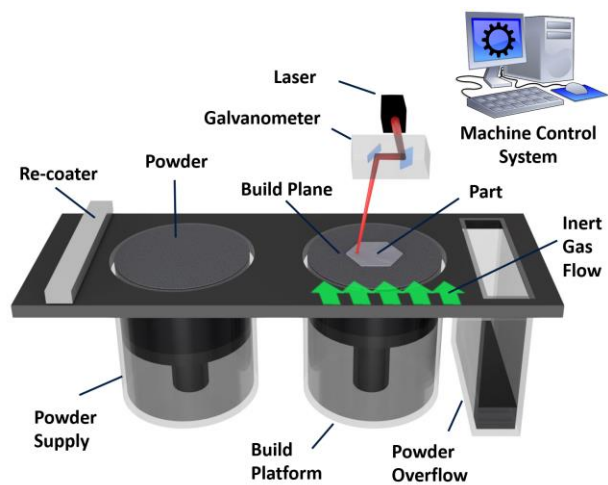
Figure 6 LPBF subsystem schematic

2.4.2 Laser Source

Laser powder bed fusion (LPBF), as the title suggests, is influenced by the laser; however, the laser is frequently overlooked when discussing parameters. The majority of LPBF machines utilize 1070nm Yb-fiber laser ranging from 200-1000w and some research systems operate in the green or blue wavelength spectrum[71]. The laser beam profile is focused to the build plane and typically has a profile similar to that shown in Figure 7. The key characteristics are the focused waist radius and the Rayleigh length. The effect of laser spot size will be discussed in section 2.4.3 Beam Steering System.

$$\omega_0 = Beam\ waist\ radius$$

$$\theta = divergance\ angle$$

$$Z_R = Rayleigh\ Length$$
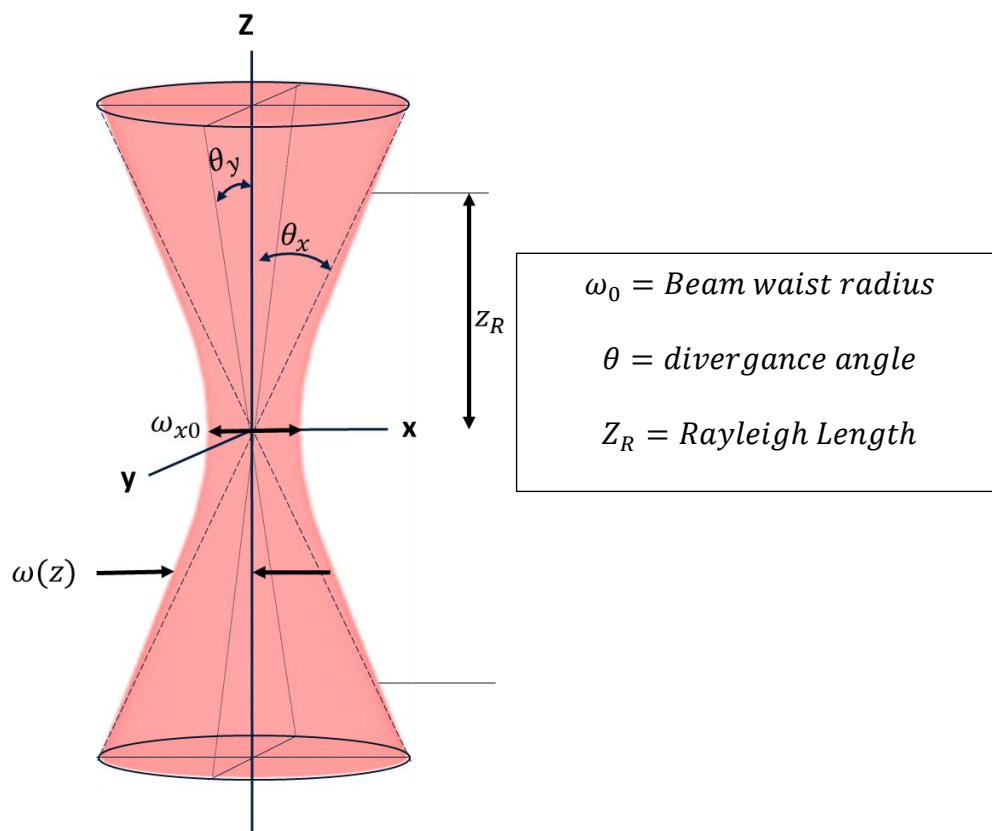
Figure 7 Schematic of the beam profile

2.4.3 Beam Steering System

Apart from some Xact Metal machines, all manufactures utilize a pair of galvanometers to direct the beam to the build surface, but there are two methods available to focus the beam and perform flat field compensation to reduce focal plane variations[72]. The options are a static F-theta lens after the galvo or a dynamic lens pre galvo as depicted in Figure 8.
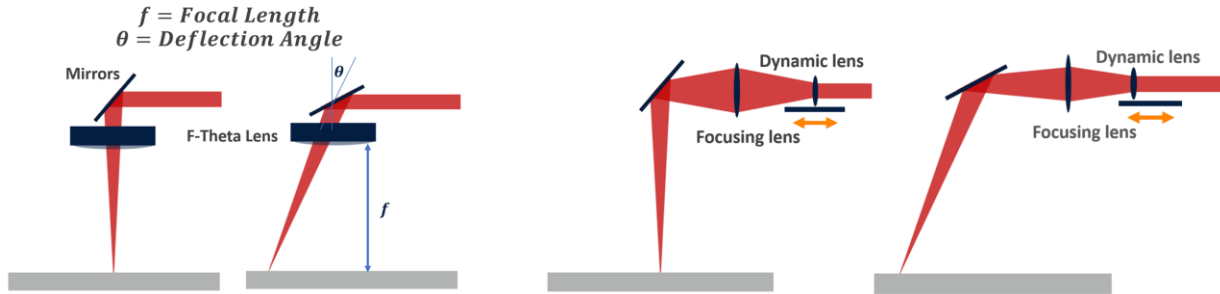
Figure 8 Comparison of F-theta flat field optic vs dynamic lends flat field optic

Goossens et al. investigated the influence of high-power single mode Nd-Yag fiber laser on thermal lensing induced focal shifts and how this can affect the LPBF process [73]. The system used a 3D scanning setup on an in-house developed machine and found that the spot size can change by as much as 75% under 500w power for 40 seconds of exposure. When printing pure copper it was found that the first cube scanned each layer was denser than the 6th cube and the change in density was attributed to the change in spot size cause by thermal lensing. Since this work was performed on a custom LPBF platform it is difficult to utilize these results to help guide this work other than to say beam characterization must be performed and that thermal lensing must be minimized. The work also does not mention F-theta lenses, which are still commonly used in LPBF machines such as the EOS M290.

Only 3D scanning systems enable variable spot size; however, the ability to dynamically adjust the effective spot size creates opportunities to increase build rate and/or alter the microstructure. McLouth et al.(2018) investigated the effect of both convergent and divergent defocus on the microstructure of In718 before and after HIP/heat treatment [46]. Although the authors did not perform beam spot size measurements and utilized the OEM reported spot size, the work identified that larger spot size (lower energy density) produces a stronger epitaxial growth than a focused beam, and that the effect can still be seen after solution heat treatment with evidence of precipitates along the prior columnar grain boundaries.

In addition to the optical effects induced by the beam steering system, there is a mechanical aspect where the beam is controlled by two mirrors attached to galvanometers. Since the galvanometer is moving physical mirrors, changes in direction have an associated acceleration. The scanner control cards have a number of built-in methods to account for the various timing and spatial inaccuracies this causes. Figure 9 is a schematic from the RTC-5 control card manual used to control Scanlabs scan heads[74]. One of the functions developed to improve accuracy in laser marking and adapted to LPBF to improve quality is called "skywriting", which is intended to prevent the scanner from accelerating/ decelerating while the laser is on (see Figure 9 right). The exact time of skywriting is typically hidden to the user.
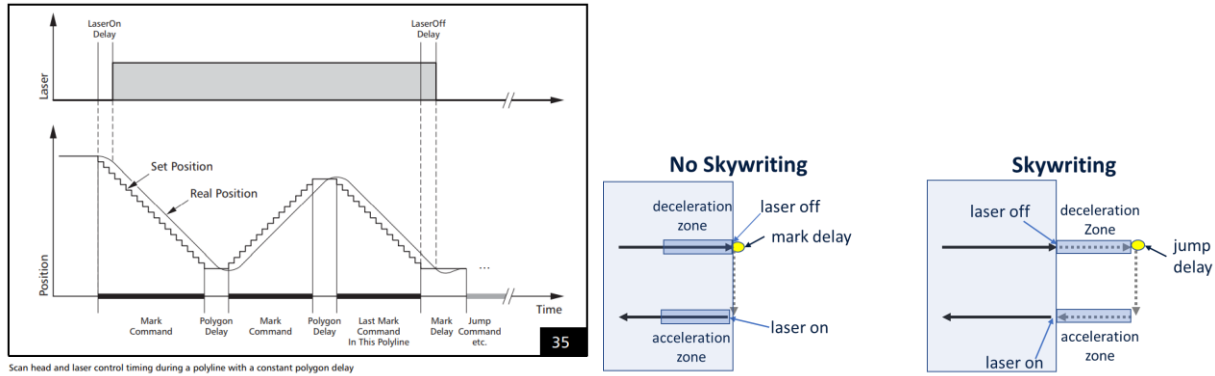
Figure 9 left) Schematic of laser/position timing offsets from RTC-5 manual [74]right) schematic of skywriting

2.4.4 Powder Management and Spreading System

In general, there are two types of powder spreading methods for LPBF;

1. displacement method – where a supply hopper moves powder up and a blade or roller pushes powder onto the print bed. (EOS M 290, DMG MORI systems, Aconity3D systems)
2. gravity fed – where powder comes from above the print bed and is dropped in front of the rake blade or roller. (EOS M400, Renishaw systems, SLM Solutions systems)

In addition to these two common approaches Velo3D has developed a patented non-contact recoater where a thick layer is deposited then subsequently vacuumed up to create a thin layer but no publication with this system exist[75].

Each method can produce a thin layer of powder, however the blade type, geometry, dosing factors, and rake speed all impact the quality and uniformity of the spread layer[76–79]. Utilizing an EOS M 290, Fox et al. (2022) evaluated the OEM supplied high speed steel (HSS), carbon fiber brush, and silicone rubber recoaters against printed part density, tensile properties, and compression of a lattice structure[80]. This work was unable to identify a statistical difference between the strength results. The authors mention concerns about potential contamination from

the recoater but no analysis was performed. This work is an example of research where the impact of on aspect of the LPBF process is interrogated by analyzing a subset of potential results that ultimately result in no applicable knowledge advancement.

Another approach to establishing recoater type effects was presented by Le et al. (2021) where the layer quality was defined by roughness and density as determined by a picture[81]. They were able to show that spreading speeds greater than 80mm/s reduced quality and that the rubber recoater which had a larger contact surface than the steel blade and resulted in improved quality[81]. This approach defined spreading quality independent of printing parts, which has benefits by removing confounding variables from other subsystems.

2.4.5 Environmental Control Chamber

The environmental control chamber serves to create a safe enclosure to prevent safety hazards and to protect the metal from oxidation during melting. Bidare et al. (2018) investigated the effect of chamber pressure on melting single powder layers monitored by high-speed cameras in two separate publications and found that neither produced improved results over ambient pressure[82,83]. LPBF in vacuum (10μbar to 20mbar) caused excessive powder denudation obscuring the beam line of sight and removing all powder from the nearby melt area. LPBF in high pressures (3 & 5 Bar) resulted in increased melt pool temperature and ionized metal vapor reducing melt pool penetration and smoothness due to beam obscuring[82,83].

Dietrick et al. performed an extensive analysis of building Ti-6Al-4V under different chamber oxygen contents from 977ppm down to 2ppm and found that the oxygen content in the

built parts increases from powder under all conditions in a linear fashion and under the lost oxygen content conditions found an increase of 200ppm [84]. The increase in oxygen content also results in an increase in tensile strength of the LPBF built parts. In an oxidation resistant alloy, IN718, Pauzon et al. (2021) showed that the oxygen content of the spatter particles more than doubled from the starting powder ($\sim$270ppm to $\sim$620ppm) [85]. In this work the authors collect $\sim$63g of spatted but did not approximate how much spatter landed in the powder bed that is oxidized and would be reused. This oxidized spatter will lead to the gradual increase of oxygen in the overall feedstock, but the local increase of a single highly oxidized particle may lead to micron scale oxide inclusions, a practically undetectable defect. These works point to the standard control of 1000ppm as potentially inadequate

2.4.6 Gas Flow and Filtration

The primary purpose of the gas flow in LPBF machines is to remove the smoke and vaporized metal soot from the build chamber. Typically, LPBF machines have a nozzle near the print bed and another near the top of the machine to prevent soot from depositing on the optics. Poor gas flow is likely to reduce the delivered beam energy by causing interference resulting in lack of fusion type defects[86–89].

Shen et al. (2020) evaluated the effect of cross flow velocity on porosity and powder particle pick up and found a threshold value of 1.5m/s, below which the likelihood of a lack of fusion pore occurring more than doubled[90]. They also found that alloy density heavily influenced blow off speed with aluminum being blown at speeds above 4m/s and Fe-based/Ni-based alloys not blowing away until above 6m/s establishing an important upper limit to the gas flow velocity [7]. Reijonen

et al. investigated flow in an SLM 125 and used a handheld hotwire anemometer to measure flow velocity at the build plate. This work identified[83] a minimum flow velocity of 2.5m/s below which porosity frequency began to increase and melt pool depth was reduce by more than 50%[91].

In addition to the peer reviewed journal articles the machine builders like Trumpf, Renishaw, Velo 3D, Concept Laser (GE Additive), and Additive Industries have advertised via white papers, blogs, and webinars the improvements or importance of their gas flow with regards to part quality [92–96]. Gas flow has elevated to high importance as other process controls have been improved enabling users to quantify and attribute defects to this subsystem, a trend that will continue as control over the process improves. [21][89]

2.5 POST PROCESSING

2.5.1 Thermal Post-Processing

Heat treatment is a critical aspect of nearly all metal part production from casting to machining and even machining here parts are often annealed for machining then heat-treated post machining to increase hardness. The heat treatment for the traditional manufacturing methods was optimized based on the starting stated of the material which is likely different than the as built state of LPBF parts due to the iterative and rapid heating cycles. Gallmeyer et al. investigated thermal postprocessing of LPBF IN718 and concluded the traditional heat treatment for wrought and cast IN718 is not optimal for LPBF IN718 [97]. They developed an alternative that allows for retention of the beneficial cellular dislocation structure created in LPBF but also eliminated negative delta phase [97]. It was also noticed that performing heat treatment after build plate removal is preferred as it allows for more rapid cooling without the build plate thermal mass. The new heat treatment

of a 1020°C SA 20min followed by water quench then 720°C 24hr age resulted in improvements of ultimate strength, yield strength and elongation over wrought IN718. This example of optimization of heat treatment was extensive, but lacks sufficient detail on the processing condition (scan parameters, chamber oxygen, recoating) to assume this heat treatment is robust enough to ensure complete elimination of delta phase in various part thicknesses and more.

2.5.2 Surface Post-Processing

The as built surface in LPBF typically ranges between 5µm and 40µm Sa which is an order of magnitude rougher than typical for other metal manufacturing methods [45,62,69]. Although the surface roughness arithmetic mean is commonly used in literature, it is not agreed to be the optimal metric to describe the surface integrity in relation to performance [98]. Rott et al. (2020) defined a surface normal angle that accounted for laser beam incident angle relative to the part geometry, and used this angle to improve roughness uniformity across the build plate by tilting parts to normalize the surface normal angle with the laser incident angle [59]. The primary concern with as built surfaces from LPBF is the reduction of fatigue life, which can be as low as half that of a machined sample with all other aspects held constant [6]. There are several approaches being pursued to improve surface integrity of LPBF components to include chemical assisted finishing capable of improving internal passageways, in situ machining or laser polishing, and improvement through parameter optimization. To date, the best solution appears to be application specific with no one size fits all surface finishing option, adding to the cost of LPBF parts.

Chapter 3: Development of the Qualification Test Artifact

Chapter 3.1 contains a peer reviewed publication from the journal of Additive Manufacturing entitled "Toward a Common Laser Powder Bed Fusion Qualification Test Artifact". As an author of the Elsevier article no permissions for use are required. My contribution to the article was substantial from concept to writing and reviewing.

3.1 TOWARD A COMMON LASER POWDER BED FUSION QUALIFICATION TEST ARTIFACT

H. C. Taylor[a, c], E. A. Garibay[a, b], R. B. Wicker[a, b]

[a] W.M. Keck Center for 3D Innovation, The University of Texas at El Paso, El Paso, TX 79968, USA
[b] Department of Mechanical Engineering, The University of Texas at El Paso, TX 79968, USA
[c] Department of Metallurgical, Materials and Biomedical Engineering, The University of Texas at El Paso, TX 79968, USA
Email of corresponding author: hctaylor@miners.utep.edu

Conflict of interest statement

One or more of the authors of this article are a part of the Editorial Board of the journal. To avoid a potential conflict of interest, the responsibility for the editorial and peer-review process of this article lies with a different editor. Furthermore, the authors of this article were removed from the peer review process and had no, and will not have, any access to confidential information related to the editorial process of this article.

3.1.1 Introduction

Additive manufacturing (AM) of metal components via powder bed fusion (PBF) has reached a maturity sufficient for serialized production of components that can achieve Federal Aviation Administration (FAA) and Food and Drug Administration (FDA) certification. In spite of the ability of PBF to produce quality components, there are significant gaps in standardization and a general lack of understanding relating to process sensitivity [1]. In many cases, the existing

standards leave the work to certify a part or qualify a machine up to the supplier/buyer determined criteria or machine manufacturer [1–4]. This must be supported by an extensive testing plan requiring the production of many witness coupons and sacrificial components that must be subjected to destructive testing such as the procedure laid out in NASA MFSC-STD-3716 and MFSC-STD-3717 [3,5]. This approach is costly from both financial and time considerations, preventing wider adoption of metal AM [6]. Since qualification and certification of AM parts are often led and financed by the supplier, suppliers are incentivized to keep any data generated proprietary leaving large gaps in fundamental and practical knowledge across government and industry.

Certification at the part level requires qualification of the multiple inputs or variables affecting the process, which must include feedstock, manufacturing systems, component design, operators, and the overall production facility [7]. Due to limited fundamental understanding between the various factors that can affect a build and the final part performance, the certification process is unique to the part, machine, material, and facility.

To reduce the time to certification, it is important to develop a fundamental understanding of how process variations influence the outcome. To help focus effort on these issues, America Makes and American National Standards Institute (ANSI) created the Additive Manufacturing Standardization Committee AMSC Standardization Roadmap for Additive Manufacturing, identifying 93 gaps with lack of published standards, with over 60 needing further R&D [1]. The National Institute of Standards and Technology (NIST) has multiple ongoing efforts to develop the fundamental understanding in AM as it relates to fatigue, part qualification, and machine

qualification to help fill the R&D needs noted in the Standardization Roadmap [8–11]. The AM Part Qualification project at NIST is intended to address the difficulties in measurement of relevant AM parts that have complex features such as lattice structures and topology optimized designs [9], and to produce curated datasets, measurement tools, and protocols that will enable part qualification. The NIST effort involves the development of test artifacts that enable testing of these features.

A key aspect of all R&D and qualification efforts includes the use of test artifacts that allow for easy and standardized inspection of features relevant to the manufacturing process, but the vast majority of test artifacts used are simple geometries such as density cubes. Test artifacts for AM have been in use since the early 1990s soon after 3D printing was commercialized, and they fall into three basic categories to date: geometric, mechanical, and process artifacts according to Lara et al. [12]. The majority of test artifacts have been designed to be process agnostic with a focus on geometric accuracy leaving gaps in relevant data collection for PBF, which may also be why there is not a widely accepted common test artifact for PBF [12–18]. A frequently cited test artifact was created by NIST in 2012 (Figure 1A) and consists of a large flat plate with a variety of features to quantify geometric accuracy and minimum feature size [19]. Peres et al. produced a similar square artifact to benchmark polymer desktop systems that had a single detachable dogbone tensile bar shown in Figure 1B [20]. In June 2019, ISO/ASTM released "ISO/ASTM 52902:2019(E) Additive manufacturing — Test artifacts — Geometric capability assessment of additive manufacturing systems", which may see wider adoption as it evaluates certain possible machine errors with specific parts and includes a reference part for surface roughness as a function of overhang angle [21].
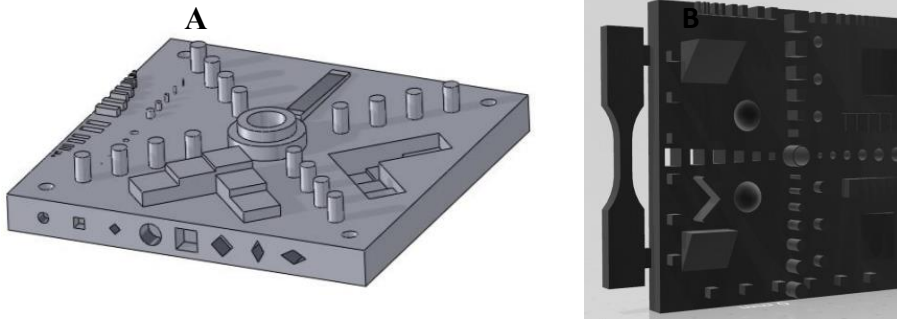
Figure 10 Previously developed test artifact A) Moylan et al. NIST test artifact (metal AM) [19] B) Lopes et al. (2020) desktop benchmarking artifact (polymer AM) [17]

The PBF process and subsequent post processing (thermal and mechanical) dictate both macro and microstructure which control the properties and ultimately the performance of the component. The PBF process allows for increased design freedom and promotes design optimization through material reduction, topology optimization, and more, leading to the creation of features that inherently experience different thermal conditions throughout the building process. These differences help create fabrication-induced anisotropic performance and properties in the manufactured components [22–28].

Several major test artifact design considerations (in addition to geometry and surface roughness) that are not generally quantified in current test artifacts but have been shown to impact performance are:

- Microstructure as a function of part geometry [24,29–33]
- Chemical composition [34]
- Powder removal from internal channels [35–37]
- Pressure drop through printed flow passages [38]
- Residual stress approximations [28,39–49]
- Mechanical properties [25,31,33,50]
- Integrity of various internal and external surfaces [51–56], and
- Distortion analysis [57–59].

A critical barrier preventing wider adoption and implementation of metal additive manufacturing is the lack of anomaly size distribution and frequency of occurrence in terms of AM materials and processes [6,60]. The design freedom of LPBF and known anisotropy associated with geometry and building locations and directions require location specific anomaly distributions be developed which can then be used to create realistic exceedance curves [24,25,31–33]. Southwest Research Institute, for example, developed Design Assessment of Reliability with Inspection (DARWIN) as a probabilistic damage tolerance framework for casting and forging of critical components. DARWIN adopted a zone-based approach to probability of anomaly, residual stress, inspection and facture mechanics to produce the probabilistic damage tolerance framework [61,62]. It would be logical for AM to adopt a similar zone-based methodology. The successful implementation of such an approach requires detailed understanding of material properties and anomaly distribution in terms of specific geometries, feedstock, machines, scan strategy, and numerous other factors. The work contained in this paper is intended to establish a test artifact specific to LPBF that can be effectively used to develop this detailed understanding.

In light of the above, the current research explores the development of an LPBF-specific test artifact that addresses multiple standards gaps and research needs. Additionally, the artifact was designed to fulfil several functional constraints to aid in global adoption including low production cost and designed for ease of use, compact size, and functionality. The artifact's functionality is intended to help establish zone specific anomaly distributions ultimately reducing risk in adoption of LPBF for critical applications. Details of this development are described below.

29

3.1.2. Test Artifact Design Considerations

The test artifact was designed to directly or indirectly address needs noted in 13 AMSC standards gaps as highlighted in Table 3. Table 1 includes 13 specific AMSC standards gaps that can be addressed through use of a test artifact along with the specific needs within the gap that can be addressed and the feature(s) to be included in the test artifact to address those needs. The physical constraints used to design the artifact are listed in Table 4 and were determined based on experience in sample preparation for metallographic analysis with ease of use, compact size, and experimental repeatability and reproducibility as criteria. Finally, additional features are included in Table 5 that the authors deem important to include based on literature review.

Table 3 AMSC Gaps

AMSC Gap	Need	Features to Address Need
Gap P4: Surface Finish	Standards for measurement of surface characteristics, specifically on lattice structures and internal channels	Overhang(s), lattice(s), internal channel(s)
Gap FMP1: Material Properties	Develop standards to establish minimum mechanical properties	ASTM E8 subsize tensile bars
Gap FMP3: Cleanliness of Medical AM Parts	Test methods, metrics, and acceptance criteria to establish cleanliness of complex 3D objects	Lattice(s) and internal channel(s)
Gap FMP4: Design Allowables	Test methods to support development of design allowables to include new coupons if necessary	ASTM E8 subsize tensile bars
Gap FMP5 Finished Material Properties: Microstructure	Microstructure, anomaly type and frequency as a function of geometry	Cross section in XY, XZ and YZ planes
Gap PC4: Machine Qualification	Development of machine qualification standards beyond fit and form to include chemical composition, residual stress, microstructure, surface integrity, and fine features.	Lattice(s), overhang(s), bulk areas, residual stress overhang, chemical test coupons, ASTM E8 tensile bars
Gap PC5: Parameter Control	Demonstrate process parameters can produce repeatable results	Overall Part
Gap PC16: In-Process Monitoring	Standardize the approach to turn in-process monitoring into an accurate 3D representation of the part.	Overall Part

Gap D5: Support for Customizable Guidelines	Customizable guidelines for a machine, alloy chemistry or application	Overall Part
Gap D7: Design Guide for Post Processing	Standards for heat treatment and surface finishing techniques on internal and external features	Overall Part (specific features: internal channel, lattice(s) and overhang(s)
Gap D8: Machine Input and Capability Report	For a given material and machine, what is achievable in terms of quality.	Overall Part
Gap D9: AM Simulation Benchmark Model/Part Requirement	A standard for a process-specific AM benchmark model/part is needed to enable verification and validation of applicable process simulation tools	Overall Part (specific features: Island arches and residual stress overhang)
Gap D28: Specification of Surface Finish	Specify what the relevant surface characteristic can be quantified to effectively make associations to performance	Internal channel and overhang(s).

Table 4 Test Artifact Constraints

Feature	Constraint	Reason
Artifact Size	Must fit in 50mm metallographic mount	50mm is the largest standard metallographic mount
Artifact Shape	Must contain a flat area on all sides to allow for easy gripping, increasing cross-section accuracy	Allows for accurate and repeatable cross sectioning.
Sectioning Guides	Indicate where to section part	Measurement repeatability across all users
Interior Locator Marking	Must include three features to quantify location of cross-section	Quantify location of analysis within cross section
Go/No-Go Dimensional Check	Include a feature that allows for quick dimensional check without physically using measuring device	Provides a rapid part check that can also be used between builds

Table 5 Additional features determined necessary from literature review

Feature	Reason
Residual Stress Overhang [40,41,45,63]	Allow for residual stress approximation
Straight Through-Holes [38]	Horizontal channels to conduct pressure drop testing
Chemical Analysis Coupons [34]	Easily detachable coupons for chemical analysis
Complex Internal Channel [38,64,65]	Powder removal testing and internal channel surface finish testing

3.1.2.1 Geometric Features

Dimensional accuracy in LPBF is principally controlled by the laser beam quality, galvanometric scan head, shrinkage and build platform displacement [19]. Large scale distortion due to residual stresses can also impact the dimensional accuracy of LPBF built components[45,57]. The LPBF user can compensate for dimensional error by adjusting a scaling factor to account for shrinkage and beam compensation to account for melt pool width [66]. The galvanometric scan head for each machine has a calibration file to account for image field distortions that may lead to dimensional inaccuracy but is typically verified by markings on a flat plate during machine maintenance [67–69]. The primary function of the geometric features on a test artifact is to ensure the scanner system is operating as expected and that the selected scanning strategy produces a component that is geometrically accurate.

The test artifact was designed with an overall consideration that virtually any commercial LPBF system could produce it. The recommendation based on machine manufacturers, literature, and standards included a minimum unsupported overhang of 40° and minimum feature of 200µm [70–72]. With these constraints, features were included to quantify errors in scaling factors, beam compensations, and scanner calibration. Detailed descriptions of features to quantify errors in scaling factors, beam compensations, and scanner drift can be found in several test artifact articles such as Moylan et al. [19]. The features used in the current artifact include: thin walls, pins, holes, rectangular extrusions, lattices, and overhangs.

3.1.2.2 Chemical Analysis

Chemical analysis is an important aspect of LPBF AM not only in characterizing and documenting feedstock chemistry but also in establishing the final chemistry in the fabricated components [73]. Dietrich *et al.* showed that building titanium under 1000ppm O_2 in the chamber can still increase oxygen content from 0.13% in the powder to 0.18% in the as-built part [34]. As a result, a design requirement for the artifact was incorporation of a detachable feature for chemical analysis with a total volume sufficient (determined to be $1cm^3$) for inert gas fusion analysis (typically OHN) and inductively coupled plasma - optical emission spectroscopy (ICP-OES) analysis. These analyses are commonly performed on LPBF materials that include Al-base, Fe-Base, Ni-base, and Ti-base alloys.

3.1.2.3 Microstructure

NASA MSFC-SPEC-3717 requires that a qualified metallurgical process evaluate the as-built microstructure across relevant interfaces and aspects of a machine's parameters to include downskins, contours, stripe overlap interface, and more [3,36]. Deviation in thermal history induced by geometry of the part is known to alter microstructure and impact anomaly generation [24,25,29,31–33]. As a result, over ten specific elements (to be discussed in more detail in Section 3.4) were designed for microstructure evaluation throughout the part that allowed for correlation of the location in the 2D cross-section with the overall 3D part. Location indicators (reference marks) were also included to assist with specific location determination for sectioning. The designed test artifact can be used for microstructure characterization including anomaly

quantification such as size and frequency of porosity, directly addressing AMSC Gap FMP5 and indirectly addressing gaps FMP1 and FMP4 [1].

3.1.2.4 Surface Integrity

The aspects affecting performance of the LPBF-fabricated surface must be evaluated and quantified to address AMSC Gap P4, FMP5, and D28[1]. Component geometry is known to affect surface integrity, and it is well known that overhanging and downfacing surfaces result in higher roughness values [51,53,54,74,75]. The test artifact was designed to allow for characterization of bulk 40° and 60° downfacing surfaces (located at the base of the artifact) using contact and/or non-contact surface roughness measurement techniques. Additionally, the artifact was designed to be sectioned through these surfaces so that examination of surface integrity in the cross-section can be made using the same surfaces as the external measurements, allowing for further investigation of surface integrity in terms of voids, microstructure, and microcracks that may not be observable with traditional surface inspection tools. The artifact also includes thin-walled 40° and 60° structures in the cross-section that can be included in these analyses to examine potential surface integrity differences between bulk and thin-walled features.

3.1.2.5 Internal Channel

Two issues commonly encountered when fabricating internal channels include (1) removal of powder from the channels post-fabrication, and (2) measuring and modifying (finishing) the surface of internal channels. The importance of powder removal is emphasized by Gradl et al. (2018) in which the authors mentioned scrapping multiple rocket nozzle components

due to trapped powder that could not be removed after LPBF manufacturing [35]. To address development of powder removal techniques along with subsequent verification of powder removal, the test artifact includes a complex (helical) internal channel as well as two lattice structures. Hunter et al. (2020) examined ultrasonic powder removal techniques on LPBF and EB-PBF manufactured parts with complex internal channels and found as channels become tortuous and their diameter is reduced to 1mm, powder removal becomes ineffective for LPBF parts[76]. For EB-PBF, powder could not be cleared successfully due to inherent sintering of the powder during manufacturing. Hunter further evaluated weight loss and X-ray computed tomography (XCT) as means to verify powder removal concluding that only XCT was sufficient to confidently claim powder had been cleared from internal channels [76]. In the evaluation of the test artifact, it is anticipated that XCT will prove to be a very effective measurement means for evaluating powder removal, surface integrity, and porosity throughout the artifact.

In addition to powder removal, the test artifact internal channels and lattice features can be used to examine surface integrity and effectiveness of surface finishing techniques in a similar manner to the work done by Hamidi et al. and Hooreweder et al. [64,65]. Specifically, Hamidi et al. (2017) examined sand blasting, vibro-finishing, and chemically assisted vibro-finishing on complex internal channels by cross-sectioning through the channel and performing surface roughness measurements[65]. In the event that surface integrity and/or surface finishing techniques on internal channels are explored but cross sectioning is not viable, four horizontal straight channels (0.25, 0.5, 1, 2mm in diameter) were included to allow for pressure drop testing, for example, following the approach implemented by Kolb et al. [38]. Currently, there is no LPBF

standard for evaluating the effectiveness of non-contact surface finishing techniques but the authors view cross-sectioned channels and pressure drop testing as viable methods.

3.1.2.6 Distortion Compensation and Residual Stress

Due to the thermal cycling inherent in LPBF fabrication, residual stress and warpage become significant contributions to build failures, tolerance discrepancies, and mechanical properties [77,78]. To minimize the effect of residual stress and thermal-induced warpage, many strategies have been employed that include: scanning strategy control, increased build platform temperatures, and post processing stress relief [28,42,44,46–49]. Alternatively, it has become possible to simulate the build with commercial software available from Velo3D, ANSYS, and Autodesk Netfabb, as examples, and preemptively distort the build file to accommodate for warpage so that the as-built component matches the desired product [57–59,79]. AMSC Gap D9 requires the development of a representative test artifact to verify and validate the effectiveness of distortion simulation or residual stress reduction scan strategy [1].

To evaluate simulation of distortion, an "island" according the ISO/ASTM 52911-1-19 was designed [80]. An island refers to a feature that grows from a starting location surrounded by powder and later connects to another feature being built in the same build. These island features are susceptible to warpage and facilitate evaluation, even by eye, of distortion as a horizontal "step" will appear where the island merges with the main artifact body as seen in Figure 11c.

Residual stress must be examined separately from distortion and can be utilized to evaluate support structures in addition to residual stress. To quantify residual stress, a flat overhang was created with wall supports that can be cut post-print to allow for the overhang to curl as it deforms under the residual stress, similar to the approach used by Roehling et al. and Kruth et al. [41,48]. The proposed artifact uses a similar support type to those used by Chen et al. (2019) but the intent is to allow for user defined supports to evaluate the effect of support structure on stress and to determine if a selected support is sufficient to prevent failure during a build [63]. The island and overhang features allow for data and feedback to be provided for verification and validation of simulation tools as well as providing useful build data for each build, machine, and material.
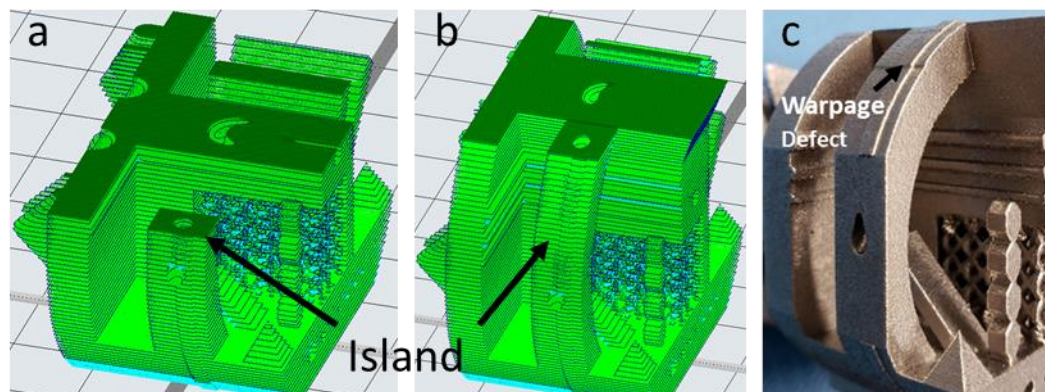
Figure 11 Island feature showing the effect of distortion. The horizontal "warpage" defect is only visible in the feature that grew as an island and re connected to the part, creating a "step". The wall adjacent to the feature shows no step, highlighting the utility of the technique.

3.1.2.7 Mechanical Properties

Comprehensive understanding of mechanical performance for specific, complex components is a major roadblock in adoption of LPBF, due to the many influencing fabrication

parameters and geometry-specific properties that impact ultimate part performance [6,81,82]. As a result, it is often required to include test coupons in every build, such as mentioned in NASA-MFSC-SPEC-3716, which specifies four tensile witness specimens to be included in every build of Class A or B components that are in continuous production [5]. Seifi et al. (2017) discuss the utility of witness coupons but note the similitude between witness coupons and real parts may vary due to the many variables affecting local thermal history during fabrication of actual components [81]. Dzugan et al. (2018) attempted to favorably address the additional cost and effort added by printing witness coupons through an investigation of small scale (18mm tall) flat tensile coupons. The smaller coupons showed promising results comparable to full size tensile bars, although this approach is not yet an accepted standard [31].

Based on the need to relate process, microstructure, properties, and performance, mechanical testing coupons were included as a part of the test artifact. Similar to Dzugan et al. (2018), the authors chose to use subsize specimens in the test artifact as full-size standard specimens were simply too large to maintain the artifact small and compact. The ASTM E8 subsize round specimen with a gauge diameter of 4mm and 2.5mm were chosen, and although ASTM E8 does not recommend utilizing subsize specimen (mainly due to difficulty in manufacturing small specimen as well as more stringent requirements to obtain reliable data during testing), this recommendation is not necessarily for AM-fabricated components [83]. In fact, it is common to produce AM parts with thicknesses and features comparable to the subsize standards. Further, it is also desirable to include the mechanical test coupons in the artifact to ensure a singular scan strategy is utilized to address potential issues related to the test artifact properties matching the mechanical test coupons. In the end, the authors believed including the ability to measure

mechanical performance in this single, compact test artifact, along with all of the other features, will provide an important all-in-one source for data leading to widespread adoption of the artifact, and ultimately, LPBF in production. Using the comprehensive list of design considerations outlined in this section, the following section describes the final design of the LPBF test artifact in more detail.

3.1.3. LPBF Test Artifact

Based on the needs established and described above in Section 2, an iterative design, build, test approach was used to develop a single, compact LPBF test artifact with the following features:

- Detachable chemical test coupons (providing sufficient volume for routine OHN and ICP chemical analyses)
- 40° and 60° overhangs (in bulk material on each of four faces transitioning from bottom face to side faces)
- Thin (1mm thick) 40° and 60° overhangs in three directions on mid-height shelf
- Residual stress test overhang
- Straight internal channels (Eight horizontal circular channels, two each of four different diameters)
- Complex internal channels (one vertical helical 1mm diameter, two curved 1mm diameter, and one curved 2mm diameter)
- Octet (0.5mm strut thickness) and gyroid type lattice features
- Internal and external locating features in cross section (triangles for position determination)
- External indicators (raised profile) for sectioning locations in xy, xz, and yz planes
- 16 positioning pins (four positioned radially along each of four directions on top shelf)
- Two concentric cylinders on centerline of top shelf
- Beam compensation features on all four faces in build direction and top shelf
- Shrinking vector triangle feature for microstructure analysis
- Five vertical thin wall features of different thicknesses
- Island features
- Go/No-Go Check
- ASTM E8 Tensile bars (four specimen size four and three specimen size five)

The design of the final test artifact with the above features is described in more detail below.

3.1.3.1 Isometric Views with Labeled Features

The design of the LPBF test artifact is shown in Figure 2. The artifact was designed in CAD (NX10 and lattices were created in nTopology). The overall bounding box dimensions are 40x39x40mm(x,y,z) and the total volume of material used to print the artifact is $25cm^3$, which is similar in volume to three round ASTM E8 small-size tensile bars built as solid cylinders [83]. Assuming the artifact is manufactured in Grade 5 Titanium at ~$200 USD per kg, the test artifact uses ~$22USD in powder. The final design allows the artifact to fit compactly within virtually any LPBF machine, providing ease of use and functionality within and across platforms. For example, the size enables the artifact to be printed in multiple locations within many commonly used machines to provide location-specific comparisons within a single machine as well as to possibly be included within production builds and used as part of the qualification process. It is the intention of the authors to release the digital (CAD) file of this artifact to the AM community through a new initiative called the LPBF Global Test Artifact Data Exchange Program (GTADExP). To assist with rapid adoption of this test artifact, the authors are committed to performing measurements through the program on artifacts produced by various organizations (with results available through GTADExP from test artifacts manufactured in different machines and organizations around the world). More details of this program including how to participate can be found at keck.utep.edu/GTADExP, and it is the goal of the program to provide results from at least 100 different test artifacts over the next year. Subsequent publications will provide updates on the program, including comprehensive analyses from the many LPBF-manufactured artifacts produced through this program.
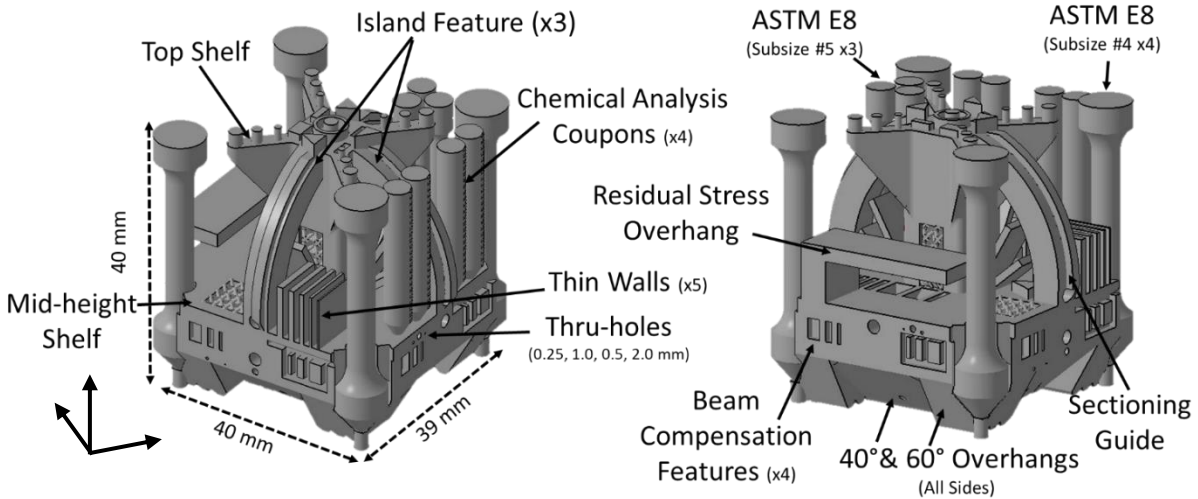
Figure 12 Labeled isometric CAD views of the LPBF test artifact.

3.1.3.2 Geometric Feature

The artifact shown in Figure 12 allows for quantification of dimensional accuracy measurements on all four vertically built faces and the top face. To assist with identifying minimum feature size manufacturability, the test artifact includes (1) the thin walls (0.2, 0.4, 0.6, 0.8, and 1mm thick) and (2) the small horizontal holes with diameters (0.25, 0.5, 1 and 2mm diameters) selected based on manufacturer recommended minimums discussed in Section 2.1. The top level (top shelf) of the test artifact is primarily designed for dimensional analysis and is shown in Figure 13. The measurement methods and specific allowable tolerances can be specified by specific qualification/certification entities.

The artifact is to be built at a 45° angle of inclination to the raking direction to minimize contact length as recommend by ISO/ASTM 52911-1[80], as depicted in Figure 13. The 45° rotation also aligns the positioning pins and tensile bars along the X and Y coordinate directions of most machines which aids in quantification of scaling factors. The artifact has the addition of

16 positioning pins located along four radial positions separated by 90° along the top shelf, similar to the NIST test artifact proposed by Moylan et al. to quantify beam compensation and scaling errors [19].

The mid-height shelf of the artifact has a 45-degree angled hole through the base that enables dual use functionality of the 4mm chemical test coupons to act as go/no-go dimensional checks. This hole has a step diameter change from 4.15mm down to 3.90mm at 0.05mm increments. The chemical test coupon includes small witness lines every millimeter. By sliding the chemical test coupon into the holes, the user can quickly check for dimensional accuracy, which may provide utility for a simple comparison between builds.
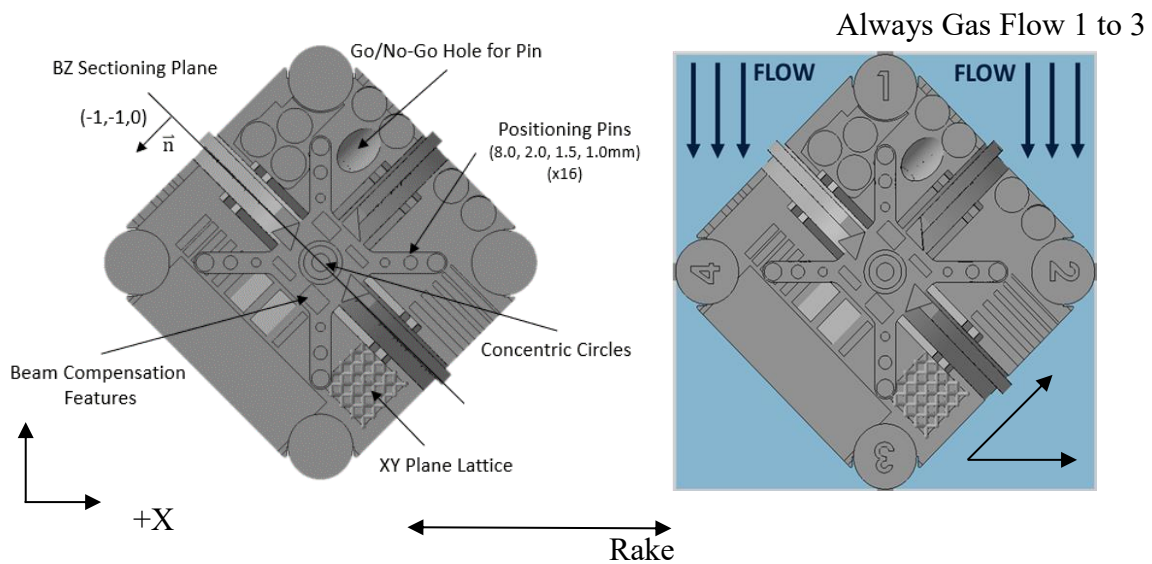
Figure 13 (left) Top view of test artifact with major features indicated along with the sectioning plane used for metallography with normal vector, $\vec{n}$, in (-1,-1,0) direction – referred to as BZ plane; (right) positioning on build plate with flow from tensile bar 1 to bar 3

42

3.1.3.3 Chemical Analysis

Four, 21mm tall, 4mm diameter cylinders (chemical analysis coupons) were designed to be built with the artifact and attached with a 1mm diameter base to allow the user to easily break the coupons off the artifact after fabrication. The volume of the cylinders was determined by materials needs for chemical analysis by ICP-OES and inert gas fusion methods suggested in ASTM F3302-18 and ASTM F3055 for titanium and nickel alloys [84–88]. Figure 12 illustrates the locations of the four test coupons.

3.1.3.4 Microstructure

The artifact cross section was designed by combining specific qualification guidelines set forth in NASA MSFC-STD-3717 section A 4.2.3.1 and common metallographic limitations [3]. The artifact was designed to create a wide range of thermal histories by including overhangs, islands, thin features, channels, lattice structures and bulk areas to determine microstructure and anomaly population effects as a function of geometry. The maximum width of the cross section in XY, XZ, and YZ planes is 40mm to allow the artifact to comfortably fit (determined through experience) inside a 50mm metallographic mount, reducing likelihood for errors in polishing. Each one of the cross-section faces reveals a surface area greater than 6cm^2 which is the minimum area of measurement recommended in NASA MSFC-STD-3717 [3]. Figure 14a depicts the sectioning plane used for metallography with normal vector, $\vec{n}$, in (-1,-1,0) direction, hereafter referred to as the BZ plane, while Figure 14b depicts the cross-section in the xy plane. Figure 15 further indicates the hypothesized "zones" for anomaly probability. Zones will ultimately be determined from detailed analysis of the entire cross-section and creating an anomaly population map.

Top Locating Triangles

BCC Lattice & TPMS Gyroid Block

1mm Internal Curved Channel (x2)

Shrinking Vector Triangle (x2)

40° Bulk Overhangs

Bulk Area

z

40 mm

40 mm

Helical Internal Channel (1mm)

40° & 60° 1mm Thick Overhangs

2mm Internal Curved Channel

Thru-holes (0.25, 1.0, 0.5, 2.0mm)

Bottom Locating Triangles

XY Plane Gyroid Block

XY Plane Thin Wall (x5)

XY Plane 40° & 60° 1mm Thick Overhangs

XY Plane Locating Triangles (x2)

y

x

XY Plane BCC Lattice

Figure 14 Cross section view of artifact (top) BZ plane with major features indicated, (bottom) XY plane cross section.

ZONE	Description
1	Lower Bulk Infill
2	Upper Bulk Infill
3	Over Lattice Poor Thermal Conductivity
4	40° Bulk Overhang
5	Shrinking Vector Triangle
6	Unsupported Overhang
7	Over Thru-hole
8	1mm Thick 40° Overhang
9	1mm Thick 60° Overhang
10	TPMS Gyroid Block
11	BCC Lattice Block
12	Upskin/Top Surface
13	All Areas Within 500µm Of Edge
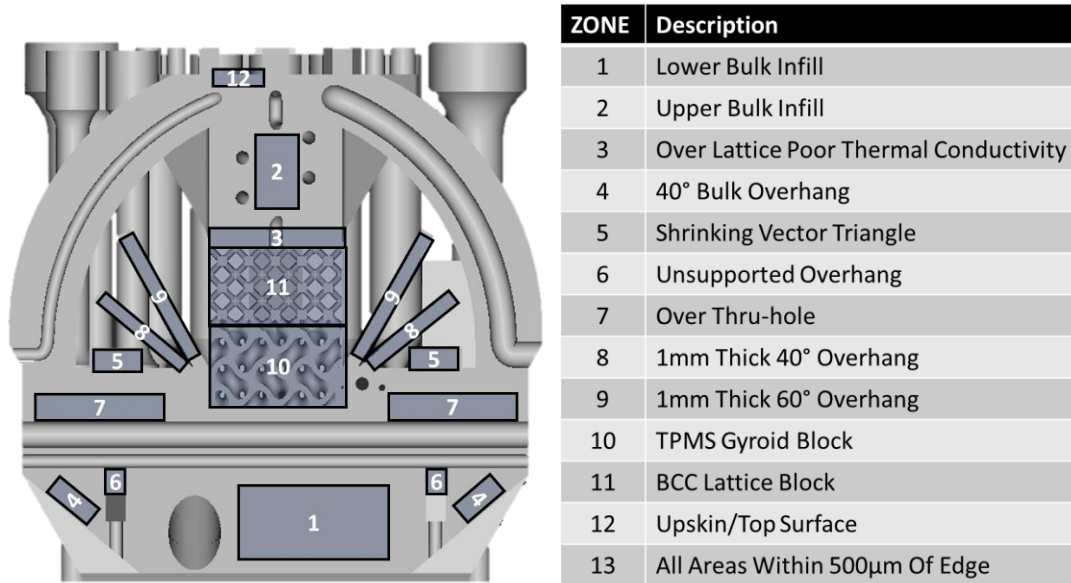
Figure 15 Hypothesized "zones" in BZ Plane of test artifact

3.1.3.5 Surface Integrity

DIN ISO 4288 was used to establish the minimum measuring conditions for the commonly reported surface roughness ranges seen in LPBF of Ra 5µm-60µm [89]. For a traditional contact stylus, the minimum recommended travel length is 8 mm for Ra values larger than 10 µm [90]. The lower section of the test artifact includes 40° and 60° bulk overhang surfaces on all four faces shown in Figure 16. Each of these overhanging surfaces has a measurable area >1.2cm^2 and total length > 8mm along the overhang surface in the build direction.
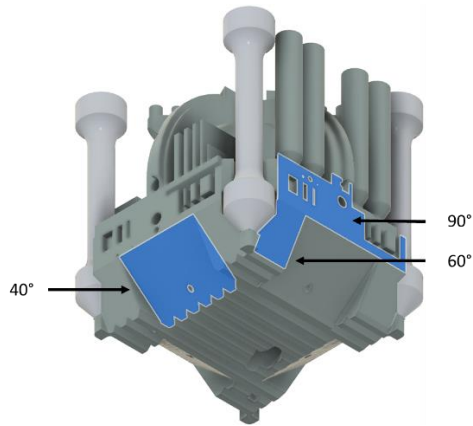
Figure 16 Surface integrity features

3.1.3.6 Internal Channels

A complex helical internal channel, with inner diameter of 1mm, was included in the final design with the purpose of studying powder removal and internal surface finishing techniques as discussed in section 2.5. Figure 17 highlights the path of the complex internal channel through the test artifact. Additionally, straight holes in each face with diameters of 0.25, 0.5, 1, and 2mm are available for pressure drop testing and manufacturability based on work done by Kolb et. al. [38]. The straight thru-holes are depicted in Figure 2, while Figure 4 illustrates sectioning the part in the xz plane and exposing the internal helical channel as well as one 2mm diameter thru-hole to allow for surface integrity analyses.

Figure 17 Wire view of test artifact highlighting the internal passageway utilized to test powder removal and surface finish/finishing of internal features.

3.1.3.7 Residual Stress/Distortion Validation

Current and future simulation software programs allow users to predict distortion induced by residual stress, and in some cases, auto-distort the geometry to accommodate the predicted distortion, increasing as-printed accuracy [57,79]. The test artifact includes three islands that later reconnect to the center of the artifact as suggested in ISO/ASTM 52911-1-19 [80] shown in Figure 18. The island is analyzed for any ridge or visible layer line (i.e., "step") at the point of merging with the main body of the artifact. This feature can be used as a go/no-go check or can be quantified to provide data for the simulation software, modify scan strategy, increase platform temperature, and more.
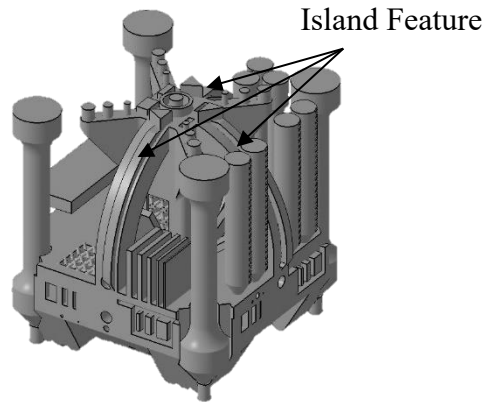
Island Feature

Figure 18 Island features in test artifact

Additionally, a simple residual stress overhang with dimensions of 8x20x2mm was included to characterize released residual as shown in Figure 19 with simple thin wall support (see Figure 21 for actual part with support structure after fabrication and after sectioning to reveal residual stress). The feature allows for; quantification of residual stress minimization strategies, support structure optimization, residual stress simulation vs actual comparisons and evaluation of stress relief schedules using the curvature method [39–41].
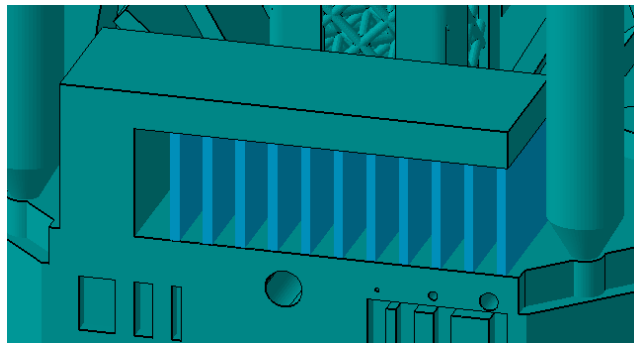
Figure 19 Residual stress overhang with a standard support structure

3.1.3.8 Mechanical Testing

Using currently available standards for mechanical testing limits the testing to tensile measurements. As discussed above, ASTM E8 specimens were selected and the dimensions of the subsize specimens are shown in Figure 20. The available locations for the tensile specimens were limited due to the allowable height of the artifact, and ultimately, an ASTM E8 subsize specimen 4 was added to the four corners of the artifact (4 specimens) and subsize specimen 5 (3 specimens) were included in a group on one quadrant (see Figure 3). Similar to the detachable chemical test coupons, each of the subsize tensile specimens are attached to the base structure through a 1.5-mm diameter cylinder, making them easily detachable by hand from the artifact after fabrication. Other standards, such as ISO 6892-1, were reviewed but did not have a prescribed dimension that suited the needs of the subsize specimen, and therefore, ASTM E8 was selected[91].
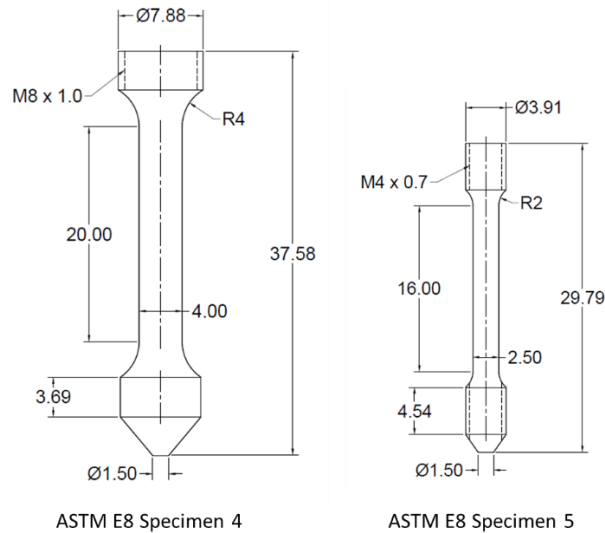
Figure 20 Dimensions for ASTM E8 Subsize specimens

3.1.4 Example Artifact Demonstrations

The test artifact described above was a result of a series of design, build, and test iterations. This artifact was designed specifically for use with LPBF to help develop detailed understanding of material properties and anomaly distribution in terms of multiple geometries, feedstock, machines, scan strategies, and a variety of other factors. To illustrate the use and overall utility of the artifact, several artifacts were built in Ti64 on two commercial LPBF systems (EOS M290 and AconityONE), and the following sections include results from these fabrication demonstrations.

3.1.4.1 General Overview of Manufactured Artifact

Figure 21 depicts two iterations of the artifact highlighting its ability to be sectioned, the ease of coupon removal, and emphasizes the small overall size of the artifact. Included in Figure 21a are the indication marks (highlighted) used to maintain consistent sectioning practices. The sectioned example in Figure 21c reveals the location of four triangular indicators utilized to quantify the plane where analysis is to take place. The residual stress overhang was cut from its supports with hand tools allowing for low-cost residual stress inspection. The chemical and mechanical testing coupons were able to be snapped off the part by hand reducing post process equipment needs and minimizing analysis costs.
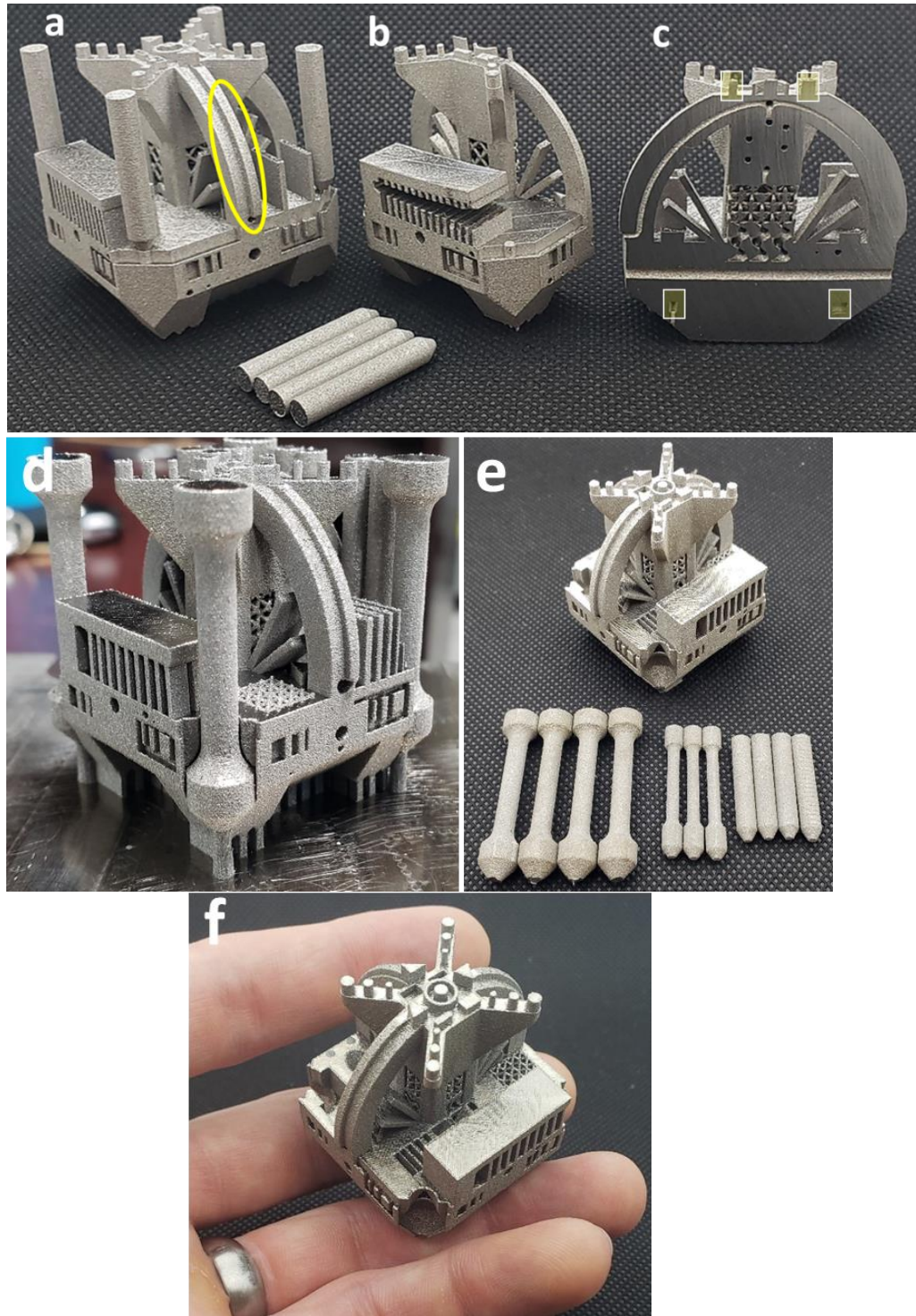
Figure 21 Trial print using Ti-6Al-4V on AconityONE (a) as-built prior to preparation for analysis (b and c) sample prepared for analysis with chemical test coupons removed, residual stress overhang supports cut and cross-sectioned. Additional trial print on EOS M290 (with Ti-6Al-4V) (d) with the inclusion of mechanical test specimen (e) with mechanical and chemical specimen broken off artifact (f) in the fingers of a hand to emphasize the small footprint of the artifact.

There are two lattice structures fabricated along a central vertical section as highlighted most prominently in Figure 14. In the current version of the artifact, BCC and gyroid lattices are used as they are commonly seen in literature and encompass two main lattice types, strut and triply periodic minimal surfaces (TPMS) [92–94]. These can be changed depending on the needs of the user. The ability to quantify microstructure and surface integrity of lattice features helps to address gaps P4, FMP5, and PC4 from the AMSC roadmap [1].

Figure 22 highlights that the entirety of the part is available for holistic microstructure analysis, examining microstructure architectures resulting from widely varying thermal histories. Section 2.3 and 3.4 describe the need for microstructure evaluation resulting from thermal history extremes experienced during fabrication. A particular emphasis of the overall test artifact is to allow research activity to move away from microstructure investigation on simple cubes and

toward more realistic geometries, adding significant value to qualification efforts and advancing efforts in zone-based defect detection approaches.
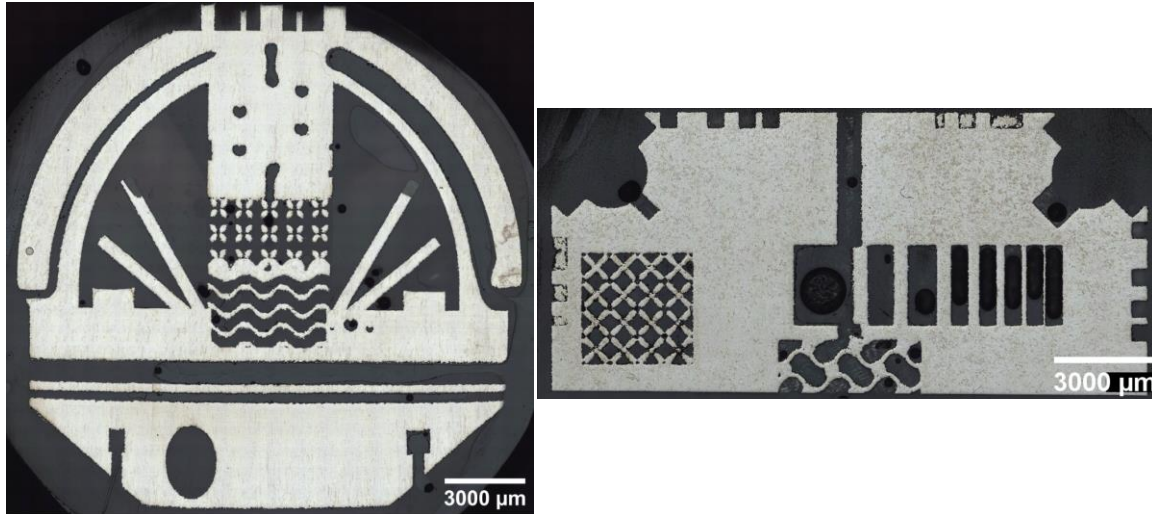
Figure 22 Sectioned and mounted Ti64 test artifact TA01.02 built on EOS M290 using Ti64 Performance Parameters

3.1.4.2 Fabrication Methods

As demonstrations, the following describes two builds performed on different LPBF machines using the same feedstock. Build TA01 was performed on an AconityONE machine and Build TA04 was performed on an EOS M290 machine. Details of each machine are described elsewhere [95,96], although necessary build-specific details are provided here. TA01 consisted of three artifacts and TA04 consisted of three artifacts with 10 additional fatigue bars included in the build for a separate project. Only one artifact from each build (TA01.02 and TA04.03) will be discussed in detail. Since most of the following sections include demonstrations and comparisons of the two artifacts built on the two different LPBF machines, each artifact will be referenced from this point forward as TA01.02(Aconity) and TA04.03(EOS) so that the reader can more easily determine the machine from which the sample was manufactured. The full list of print parameters

for each build is available as supplementary data. The support structure for each build was identical and provided as a separate .stl file. For file preparation, the test artifact was generated as a slice stack (.cli file) in nTopology at 30μm layer thickness. The .cli file was loaded into EOSPRINT v2.5 for the EOS M290 and Netfabb Ultimate 2020.3 to prepare the prints for the EOS and Aconity machines, respectively. EOS Ti64 performance parameters were used for the EOS print and a custom slicing script created in the Netfabb Advanced Toolpath Utility (ATU) was used to prepare the part for printing on the Aconity machine.

Grade 5 Ti-6Al-4V ASTM F2924 powder supplied by AP&C with nominal particle size 20-63μm (AP&C, a GE Additive Company, Boisbriand, Quebec, Canada) was used for the builds with chemistry as supplied by the manufacturer provided in Table 6. The feedstock was further characterized for size and shape, bulk density, and tap density by the authors and results are shown in

Table 7. Size and shape analyses was performed on a CamsizerX2 (Microtrac Retsch GmbH, Haan, Germany) from powder sampled immediately prior to printing from the supply hopper. Bulk and Tap Densities were measured according to ASTM B212 and ASTM B527[97,98]. Oxygen and nitrogen were also characterized from this feedstock sample collected immediately prior to printing the artifacts. Oxygen and nitrogen were measured according to ASTM 1409 using an Eltra ONHp (Eltra Haan, Germany) [85].

Table 6 Chemical *composition of Ti64 feedstock for test artifact builds (AP&C Material Certificate MC-19-1296)*

Element	Al	V	Fe	O	H	N	Other
Wt%	6.39	3.81	0.21	0.14	0.002	0.01	<0.4

Table 7 Particle size and shape, bulk density, and tap density measurements.

Number of Particles Imaged	Mean Particle Size	Size (By Volume)			Shape		Bulk Density	Tap Density
		d10	d50	d90			ASTM B212	ASTM B527
	μm	μm	μm	μm	compactness	roundness	g/cc	g/cc
3614	43.4	22.3	47.3	58.4	0.929	0.622	2.61	2.9

3.1.4.3 Surface Roughness

The average roughness of the 40°, 60°, 90° faces (highlighted in Figure 23) from all four sides of both TA01.02(Aconity) and TA04.03(EOS) were measured on a Keyence VR-5000 Wide-Area 3D Measurement System. The measurements, comparing Sa, are depicted in a bar graph in Figure 23. Examination of the figure shows varying downskin surface roughness as a function of LPBF machine manufacturer.   TA01.02(Aconity) illustrates a lower measured Sa surface roughness than TA04.03(EOS) for the 40º overhang with surface roughnesses approaching more similar values as the overhang becomes vertical, reaching nearly the same value at 90º (vertical wall). The similarity in average roughness of vertical roughness with different contour approaches implies other factors like feedstock may control vertical wall roughness.

Figure 24 provides an equivalent layer view of the scan vectors for a slice that intersects the artifact's 40º and 60º overhangs from two file preparation software packages. As illustrated in Figure 14, the average Sa for TA01.02(Aconity) along the 40º overhang is ~23μm while ~38 μm for TA04.03(EOS). The differences may be explained through the significant differences in scan strategies (Figure 15) for the 40° overhang where the TA04.03(EOS) regular infill intersects the part contour and has a downskin melt resulting in excess energy, assisting with dross formation on the downfacing surface. It is also noteworthy that TA01.02(Aconity) uses a single contour while TA04.03(EOS) uses two contours. Four reference layers are used to define the downskin region for both file preparation methods; however, Netfabb also defines a downskin angle for when to

consider a region for downskin whereas EOS defines a downskin ridge value for the same function. The interpretation of these parameters results in potential scan strategy differences. There was no identifiable reason in EOSPRINT to describe why TA04.03(EOS) would overlap the infill into the downskin region as shown in Figure 15 likely leading to the increased roughness.

There is yet to be a universal strategy to optimize as built surface roughness despite the understanding of the negative effects of surface roughness on fatigue performance [99]. As an example, two industry leading LPBF manufacturers, EOS and SLM Solutions, each use dissimilar approaches for contour parameters – in which EOS performs infill first followed by two contours (innermost contour first) while SLM Solutions scans contours first (outermost first, 2 contours called borders by SLM Solutions, followed by a third contour called fill contour) and then infill. The scan strategy used on TA01.02(Aconity) utilizes a single contour scanned before infill resulting in lower roughness and less contour passes should result in less contour scan time. The investigation possibilities go beyond this brief demonstration to include, as examples, the effect of laser incident angle and alternative roughness parameters such as Sv, comparison of contact and non-contact measurement techniques as well as comparison to and investigation of near surface integrity through cross section examination, which to date collectively has not been achievable through a single, compact test artifact.
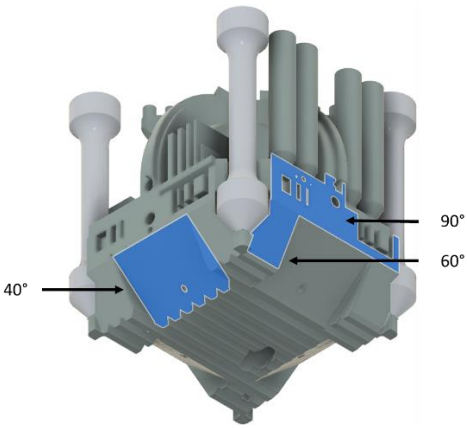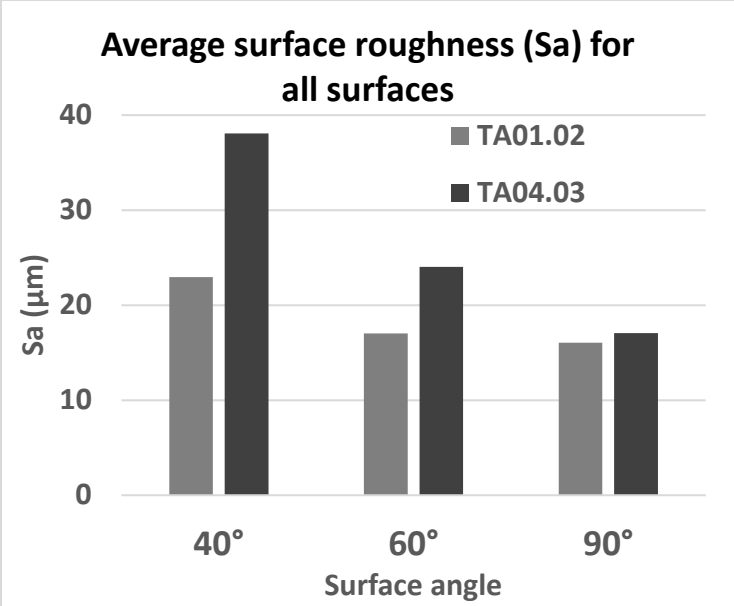
Figure 23, Surface roughness (Sa) values measured for all 40°, 60° and 90° surfaces, for both TA01.02 (Aconity ONE) and TA04.03 (EOS M290) test artifacts.

TA01.02 Netfabb ATU

TA04.03 EOS Print 2.5
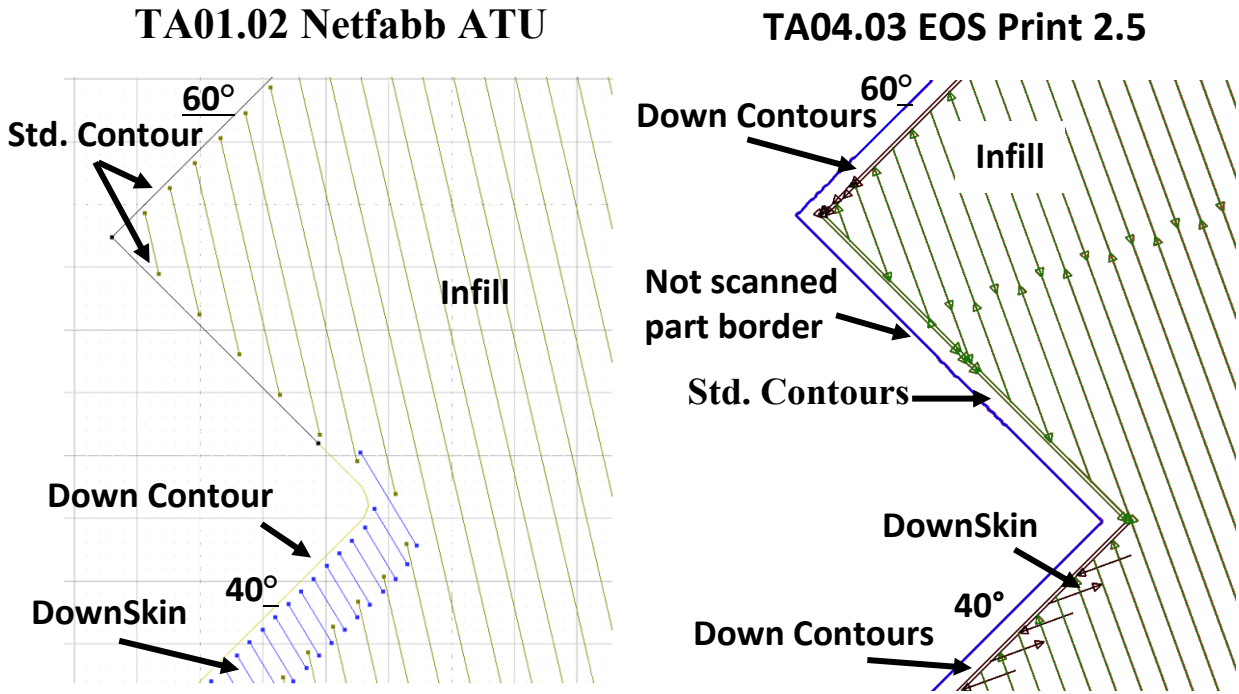
Figure 24 Slice from build file intersecting artifact's 40° and 60° overhang from two file preparation software packages: Left) Slice from Netfabb 2020.3 build preparation software for TA01.02(Aconity). Right) Slice from EOS Print 2.5 software for similar layer of test artifact, TA04.03(EOS), comparing differences in scan strategies.

3.1.4.4 Residual Stress Estimation

As a demonstration of the residual stress overhang to estimate residual stress was performed using the approach described in Roehling et al. [47]. For both TA01.02(Aconity) and TA04.03(EOS) in the as-built condition, the residual stress overhang's z-height as a function of length was measured prior to and after being cut from supports. The z-height was recorded at

$$\sigma = Et\frac{\partial^2 h}{\partial x^2}$$ **Equation 1**

7.5μm increments along the beam length for 50 profile lines using the Keyence VR5000 and the average height from all 50 lines was fit using a parabolic least squares regression and a y intercept of 0. Similar to Roehling et al. (2019), the approximate released residual stress is calculated based

58

on where E is elastic modulus of Ti64 (115GPa), t is the half thickness of the bridge (1mm), and

$\frac{\partial^2 h}{\partial x^2}$ is the second derivative of the best fit polynomial [47].

The results using the above analysis for each artifact are shown in Figure 25, and these results highlight potential differences between the best fit polynomial approach and maximum deflection. In this case, TA04.03(EOS) had a larger maximum deflection yet lower overall curvature than TA01.02(Aconity) as depicted in Figure 25. Using Eq. 1, the calculated released residual stress for TA04.03(EOS) is 408MPa (with 0.97mm deflection) while TA01.02(Aconity) is 456 MPa (with deflection of 0.88mm). Review of prior work using cantilever beam style residual stress approximations did not identify detailed discussions on measurement errors or reproducibility[40,41,46,47]. As a result, the artifact along with the extensive data to be generated through its use can be used to develop a robust method for residual stress measurement as well as establishing comprehensive understanding of the effects of materials, scan strategies, postprocessing conditions, and more on residual stress.
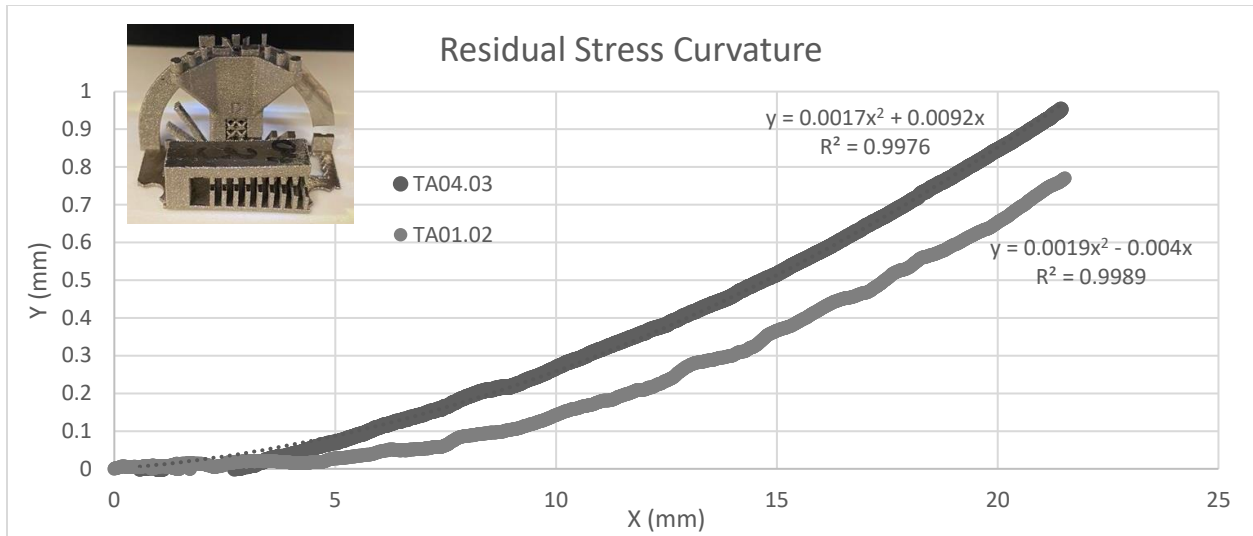
Figure 25 Residual stress beam curvature comparison between TA01.02(Aconity) and TA04.03(EOS)

3.1.4.5 Defect and Microstructure Analysis

To demonstrate the ability of the artifact to capture porosity and microstructures in complex geometries beyond the use of cubes that are commonly used today, the following describes metallography results from the two artifacts, TA01.02(Aconity) and TA04.03(EOS). Samples were prepared using standard metallography techniques and etched with Krolls reagent (see [96] as example for sample preparation). Microscopy was performed on a Keyence VHX 7000 (Keyence Corporation, Osaka, Japan) using the 3D auto stitching function. Calibration was performed the day of imaging and determined to be 1.034µm/pixel. Porosity analysis was performed using the Keyence VHX7000 software and every pore was manually verified. The total surface area analyzed from the BZ plane and the XY plane was 20.9cm^2 for TA01.02(Aconity) and 21cm^2 TA04.03(EOS). The BZ plane metallographic image and a section from the thin-walled 40° overhang with a characteristic pore are shown in Figure 27. For this analysis, a defect was defined as a pore with an equivalent diameter for a circle of greater than 25µm. Figure 28 represents all counted pores (sum of XY plane and BZ plane) in a histogram with the largest pore

between the two artifacts having an equivalent circle diameter <85µm, which is notably below the

NASA MSFC-SPEC-3717 call for rejection.
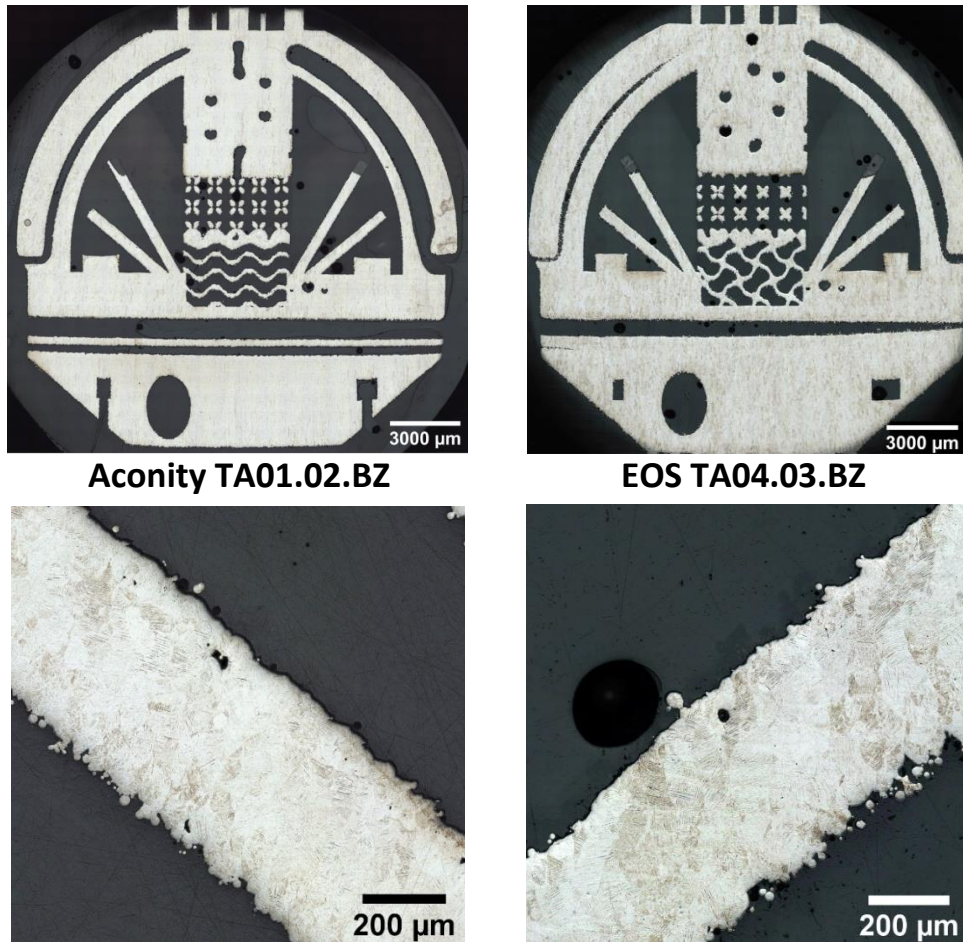
Figure 27 BZ plane metallography of (left) TA01.02 (Aconity) and (right) TA04.03(EOS)

Since both TA01.01(Aconity) and TA04.03(EOS) have less than 0.014% porosity as determined by optical microscopy, the authors believe the LPBF community should move beyond density as a singular quality metric for qualification and more toward defect population quantification. Furthermore, greater than 85% of the pores in both the EOS and Aconity built test artifacts were within 500µm of the part edge, which likely means even at this low defect level, these pores are not stochastic but instead could potentially be eliminated if the source can be

identified and controlled. The prominence of near edge porosity is not new but its source is not well understood. Ertay et al. (2018) found that as the hatch vectors become near parallel to the contour, porosity increased [100]. Mancisidor et al. (2016) found laser deceleration at the ends of vectors to be a key contributor to porosity and went on to show a density increase of 0.46% by implementing "skywriting", which is now an industry standard [101]. Yu et al. (2019) showed that surface remelting did not eliminate the existent of near edge porosity in Al10SiMg concluding that the porosity must be keyholing [102]. Other causes of porosity such as contour gap and short vectors in small geometries have all been shown to increase edge porosity [103–106]. The authors believe the artifact provides a powerful and cost-effective tool that can be used to identify the actual sources of porosity through testing and subsequent data analysis, and ultimately, used to demonstrate elimination of systematic sources of porosity through process modification and control.
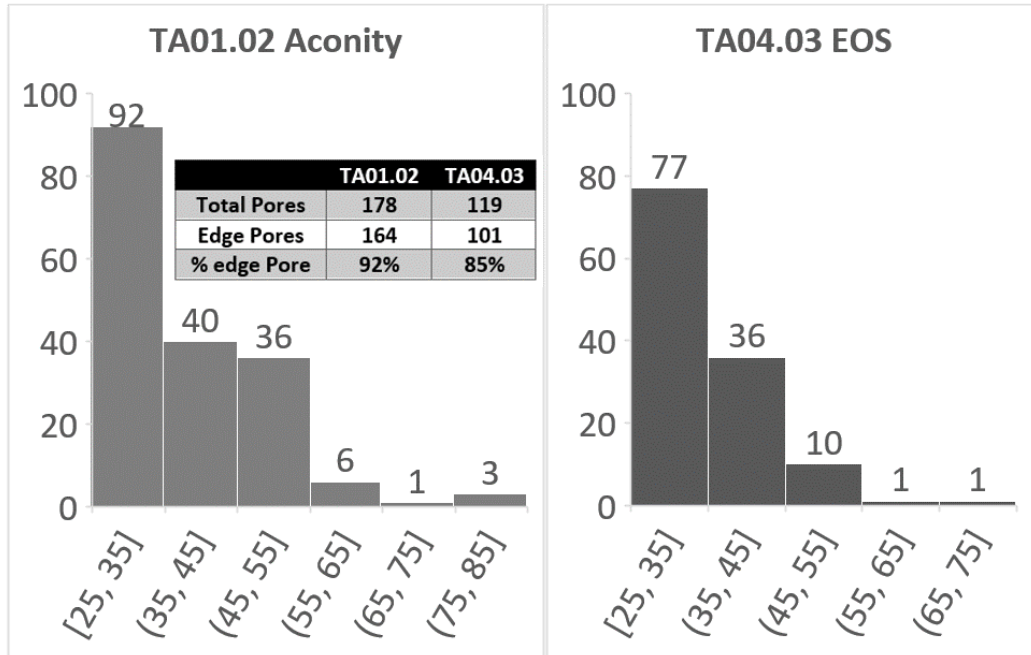
Figure 28 Porosity histograms (sum of XY plane and BZ plane) from TA01.02(Aconity) and TA04.03(EOS)

A key element in the design of the artifact is the use of the predetermined sectioning planes, which enables the ability to correlate defects with scan strategy (particularly in the XY plane). Figure 29 highlights this utilty in the XY plane of TA01.02(Aconity) in which a series of near-edge pores are linked with bulk porosity through the scan strategy for that layer, which is highlighted by overlaying the scanning vectors for this plane. The figure indicates the bulk and near-edge pores seem to coincide with a stripe overlap, leading one to conclude that this porosity is associated with the beginning and/or end of vectors. Combining this knowlelge and the previously determined >85% of identified pores are near a part edge suggests that the stripe overlaps combined with and/or in addition to part boundries may increase the probability of defect formation. Additionally, this example serves to demonstrate the correlation of scan strategy with defect type allowing for the quantification of the probability of defect formation from vector

length, vector start/end points, and geometry providing a basis for scan strategy optimization beyond object geometry alone, which is arguably the current state-of-the-art in LPBF.
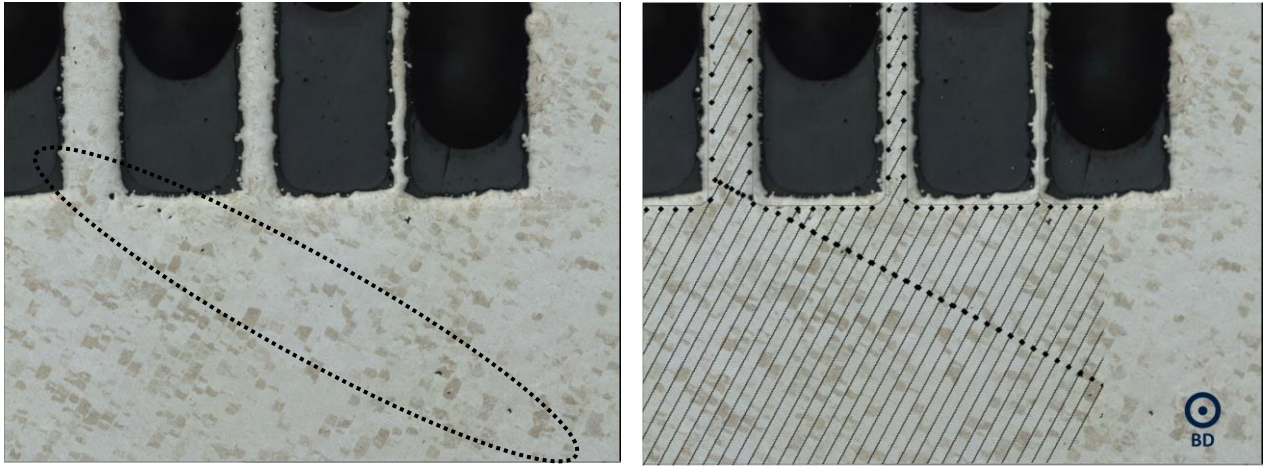
Figure 29 XY plane micrograph with slice file overlay describing the stripe overlap porosity in TA01.02(Aconity)

Additionally, the microstructure in the lower bulk region (highlighted as zone 1 in Figure 6) for TA01.02(Aconity) and TA04.03(EOS) was investigated by stitching 25, 500x magnification images together as shown in Figure 22. The figure illustrates that both artifacts consisted of a fine basket weave alpha in columnar prior beta grains. TA01.02(Aconity) has a uniform vertical columnar prior beta grain growth while TA04.03(EOS) still consists of columnar yet less regular prior beta grains.

TA01.02 Lower Bulk   **Build Direction**   **TA04.03 Lower Bulk**
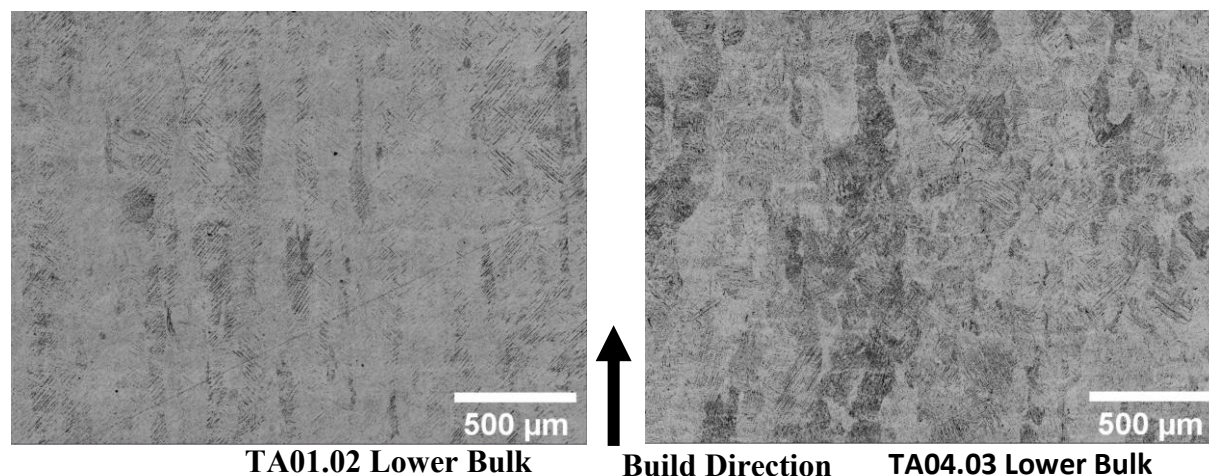
Figure 30 Lower bulk 500x images from TA01.02(Aconity) and TA04.03(EOS)

The orientation of the alpha lath was measured in each artifact using MIPAR image analysis software (MIPAR, Worthington, OH, USA) as a means to quantify the microstructural differences between TA01.02(Aconity) and TA04.03(EOS). Prior beta grain size analysis was not possible due to lack of contrast variation. The alpha lath orientation from over 10,000 individual laths from each artifact was compiled and plotted in a histogram (Figure 31). TA01.02(Aconity) alpha laths formed predominately at ~45° angle to the building direction and therefore a 45° angle inside the prior beta columnar grains. It is believed that the variation in lath orientation is likely proportional to texture evolution and therefore a surrogate to describe the microstructural variation between TA04.03(EOS) and TA01.02(Aconity). Although the authors have not been able to identify relating lath orientation to prior beta grain orientation or prior beta grain size in the literature, lath orientation is clearly different in these two artifacts. For these two artifacts, lath orientation is the largest quantifiable microstructural difference identified using the current analysis, and thus, additional studies and comparisons will be used to determine quantifiable characteristics that explain process variability.

65
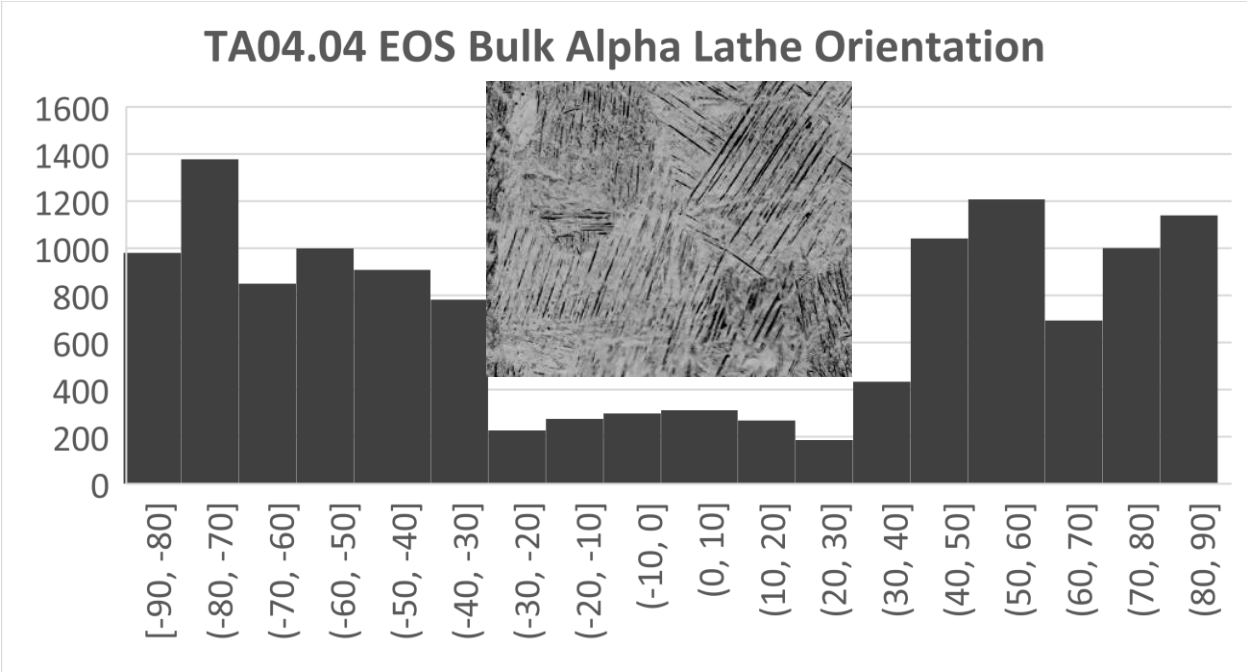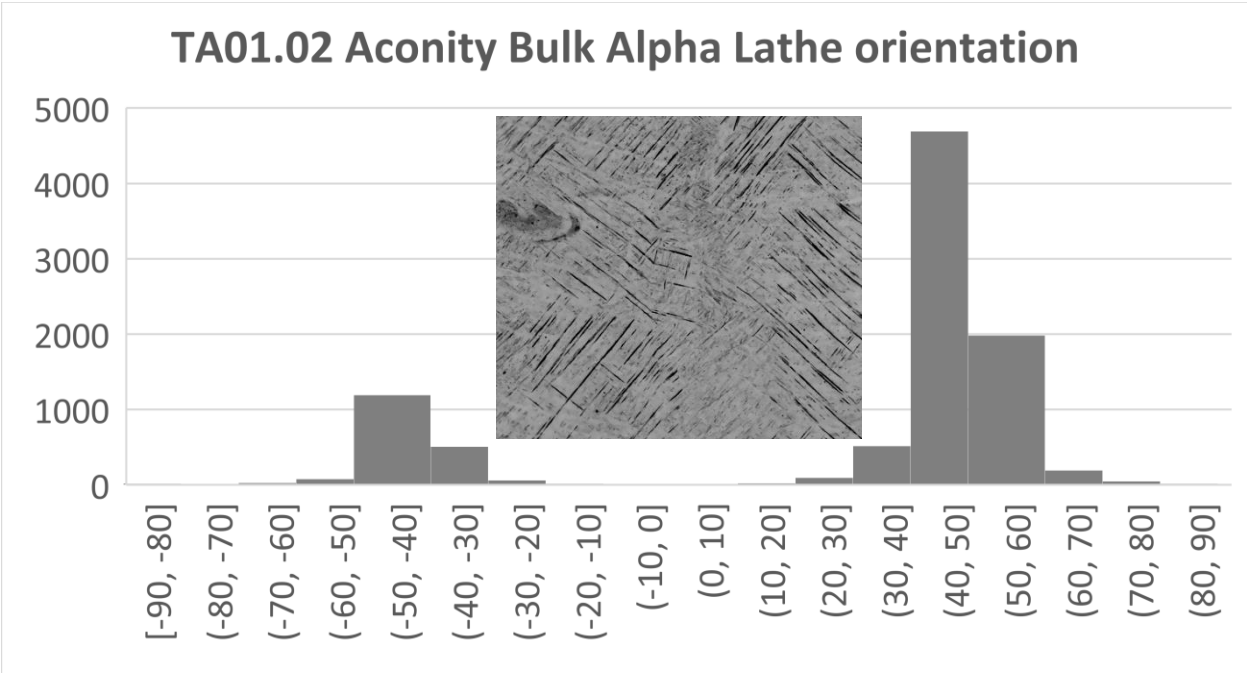
Figure 31 Acicular alpha orientation histogram from bulk area of TA01.02(Aconity) and TA04.03(EOS)

3.1.4.6 Chemical Analysis

A single chemical analysis coupon (Figure 3) was used to quantify oxygen and nitrogen content of the TA01.02(Aconity) and TA04.04(EOS) fabricated artifacts. Analysis was conducted according to ASTM E1409 using an Eltra ONHp (Eltra Haan, Germany) [85]. The coupon was sectioned into disks weighing approximately 0.12g in order to match the standards used to calibrate the Eltra ONHp. The analysis was conducted on three disks from each coupon and the average oxygen and nitrogen for each artifact are presented in Figure 32. The TA04.03(EOS) had a maximum chamber O_2 set at 0.1% while TA01.02(Aconity) was kept below 0.04% O_2. The ON analysis results show that this difference in chamber atmosphere can be measured in the as-built material, which directly affects mechanical properties of Ti64 as reported by Dietrich et al. [34]. Dietrich et al. (2020) performed a series of builds at controlled chamber oxygen levels in an EOSM290 with Ti64 powder and measured oxygen pickup in small cylinders with similar dimensions to the chemical coupons used in test artifact. The powder had a starting O_2 of 0.135% and Dietrich et al. reported a pickup of 0.02% O_2 when building at 68ppm and 0.04% O_2 when building at 1003ppm where as TA01.02(Aconity, 400ppm) and TA04.03(EOS, 1000ppm) had O_2 pickup of 0.015% and 0.02%, respectively [34]. The nitrogen content in TA04.03(EOS) nearly doubled from powder to part (although this is still within ASTM F3302-18 $N_2 < 0.05\%$), which is not proportional to the oxygen uptake nor, to the authors' knowledge, been reported as a common occurrence or investigated in detail. This is only a partial demonstration of the utility of the chemical test coupons that, as a reminder, were sized to include sufficient material for both inert gas fusion as well as inductively coupled plasma - optical emission spectroscopy.
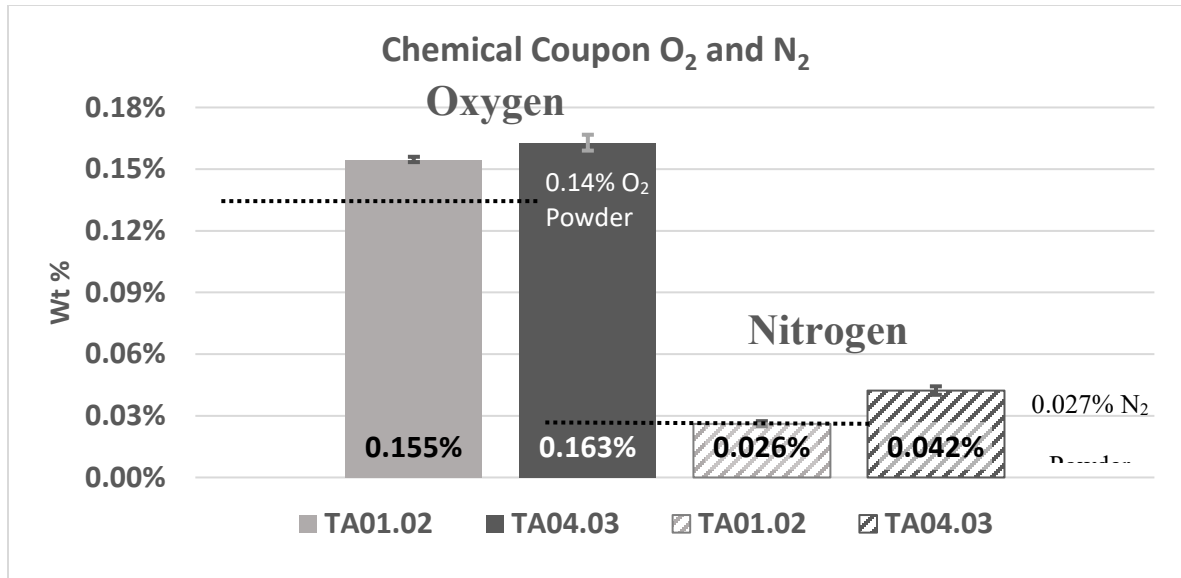
Figure 32 Oxygen and nitrogen analysis of as built test artifacts

3.1.4.7 Tensile Test Results

The ability to rapidly determine mechanical properties from the test artifact without post build machining was another key design feature of the artifact. This required the custom manufacturing of split grips to hold the sample around the radius of the button heads. These grips are shown in Figure 33 A&B while in use and in the open condition to illustrate the design, respectively. Tensile testing was performed on an MTS Landmark (MTS Systems Corporation, Eden Prairie, MN, USA) with a 100kN load cell and crosshead displacement setting of 0.3 mm/min. It should be noted that an extensometer was not available during testing, so only crosshead displacement is reported here. Future work will include measured strain. The ultimate strength and crosshead displacement from all eight ASTM E8 Size 4 bars is reported in Figure 34. TA04.03(EOS) outperformed TA01.02(Aconity) in both ultimate tensile strength and crosshead displacement to failure (proportional to strain) for all samples, except TA04.03(EOS) where there was a clear print defect (Figure 25D). The standard deviation within an artifact for ultimate strength was under 12MPa, which is surprisingly lower than most literature reports for build

direction tensile strength [107]. The ultimate strength of these samples is consistent with as-built

Ti-6Al-4V values reported for LPBF tensile results in literature[107]. Analysis cost represents a

significant obstacle to global adoption of LPBF, and these results help demonstrate as-built

samples can be used to provide, and this case, saving nearly $200 (USD) to machine the tensile

test specimen. For users interested in exploring effects of machining, other surface finishing

techniques such as chemical and laser finishing, post-process heat treatment and hot isostatic

pressing, among numerous other factors that will impact performance, the authors believe the

artifact provides a very efficient and cost-effective platform for these studies.
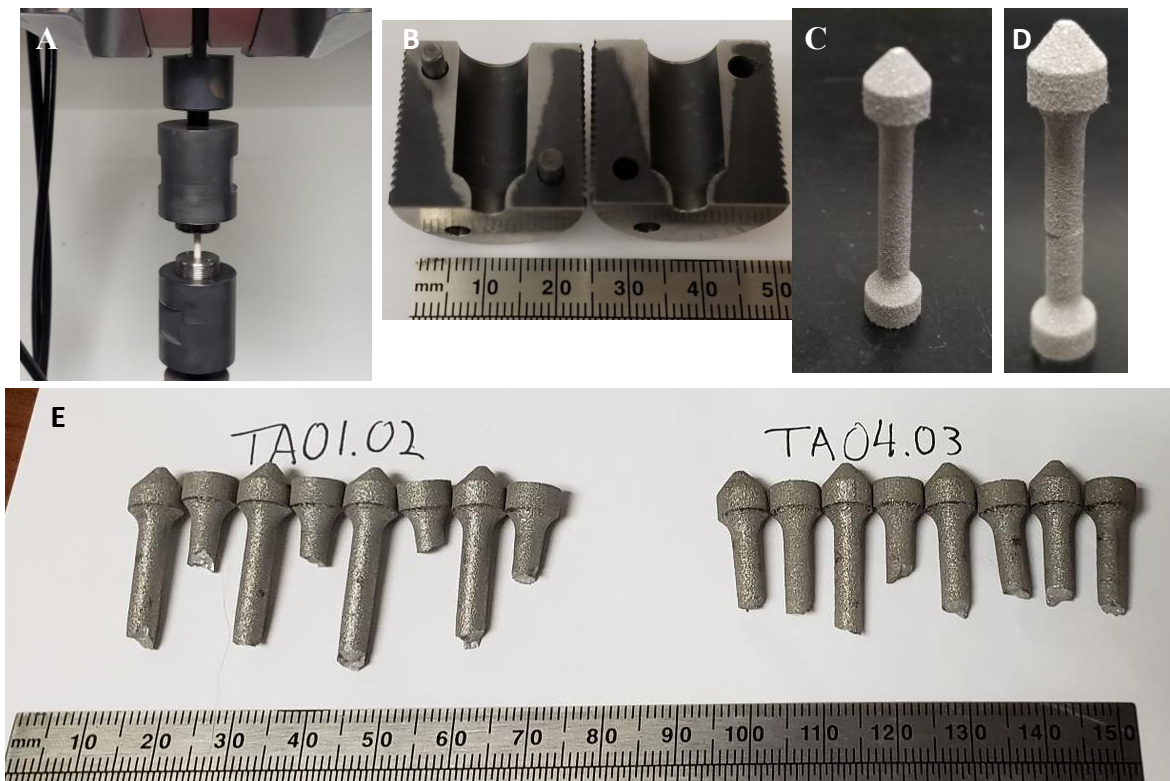
Figure 33 A) Tensile bar testing setup B) split grip design for subsize samples C) normal tensile sample D) TA04.03(EOS) sample with clear defect due to part warpage during build E) Post fracture image of all eight tensile bars.
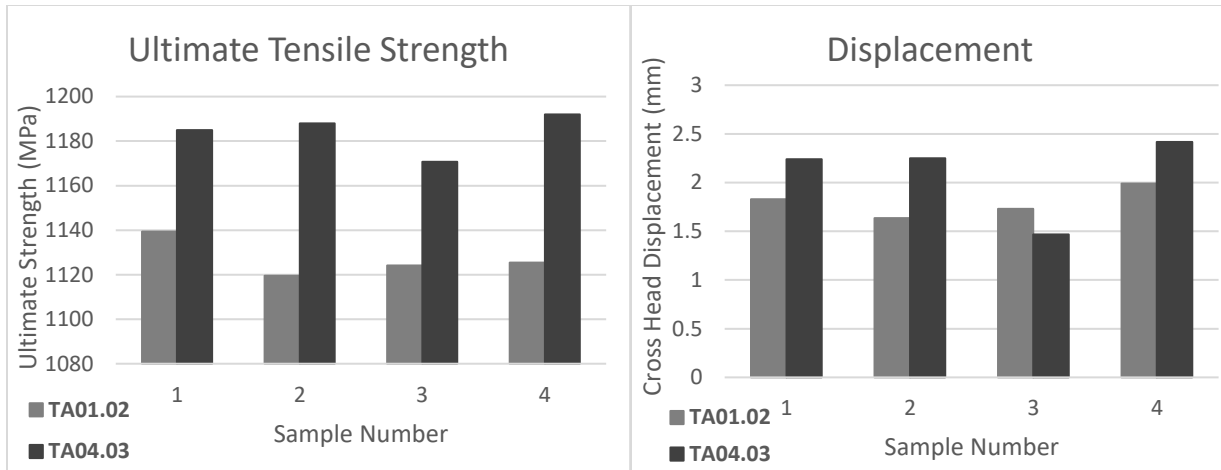
Figure 34 Tensile Ultimate strength and displacement results from TA01.02(Aconity) and TA04.03(EOS)

In summary, the analyses described above compare TA01.02(Aconity) and TA04.03(EOS) with results summarized in Table *8*. It should be emphasized that the results provided in Table 6 were measured using an artifact with an overall bounding box of $64cm^3$ representing $25cm^3$ of solid material. In terms of material, this artifact uses less than 0.11kg and $22USD (assuming $200USD/kg) of Ti64. The summarized data reveals TA01.02(Aconity) and TA04.03(EOS) only have a 5% variation in ultimate tensile strength. The ultimate strength variability is likely not due to the 0.01% difference in density as porosity levels below 1% have been shown to have no measurable effect on ultimate strength but can affect ductility [108,109]. The oxygen content of TA01.02(Aconity) is ~80ppm lower than TA04.03(EOS), and is also not sufficiently different to account for the ultimate strength differences shown in Figure 32 according to Dietrich et al. [34]. The most notable difference between the TA01.02(Aconity) and TA04.03(EOS) is the microstructural variation (highlighted in Figures 30 and 31), which is linked with thermal history, and therefore, scan strategy, laser beam size and shape, build chamber gas cross flow, build time and preheat differences [33,110]. It is concluded that thermal history is the major contributor to the difference in ultimate strength between TA01.02(Aconity) and TA04.03(EOS), but the results

provided in this section are only a demonstration, and further analysis is required to determine the individual contributions, for example, of each factor to the variations in performance – ultimately using this process to predict and optimize performance for qualification. In further support of the thermal history difference conclusion, the build time for TA01 (Aconity 3 artifacts) was ~24hrs and TA04 (EOS 3 artifacts) was only ~12hours. The detailed contributions of different factors on build time are difficult to determine due to the proprietary nature of, in this case, the EOS build parameters. However, every scan vector in a build has laser delays associated with it, which will contribute to thermal history variation and therefore microstructure evolution[33,110,111]. In the end, the immense number of artifacts to be produced and evaluated will produce large curated datasets and data science opportunities to advance LPBF in production using techniques such as those described in the recent review of Johnson et al. (2020).

Table 8 Comparison between TA01.02(Aconity) and TA04.03(EOS). $\% \, Difference = \frac{Aconity-EOS}{EOS} * 100$

TA01.02(Aconity)		TA01.02(Aconity)			TA04.03(EOS)			% Difference		
Digital File	nTopology	Same Slice File						Equivalent		
Scan Strategy	--	Netfabb Custom			EOSPRINT Ti64 Performance			--		
Machine	--	AconityONE			EOS M 290			--		
Layer Thickness	--	30µm						Equivalent		
Feedstock	AP&C Ti64	Equivalent (D10=23µm D50=47µm D90=59µm)						Equivalent		
Residual Stress	Curvature	456MPa			408MPa			+12%		
	Displacement	0.88mm			0.97mm			-9%		
Oxygen Content	Inert Gas Fusion	0.155±0.002%			0.163±0.006%			-5%		
Defects	Optical (Count)	178			119			+50%		
% Density	1-%porosity	99.986%			99.993%			-0.01%		
Microstructure	Optical	Columnar Basket Weave			Stochastic Basket Weave			Dissimilar		
Roughness	Fringe Projection (Sa)	40°	60°	90°	40°	60°	90°	40°	60°	90°
		23±1µm	17±1µm	16±1µm	38±2µm	24±2µm	17±2µm	-40%	-29%	-6%
Ultimate Strength	4 Samples Ea.	1117±14MPa			1171±6MPa			-5%		

3.1.5 Conclusions

This paper described the design and development of a single, compact test artifact for LPBF that only occupies a solid volume of 25cm^3 (within a 64 cm^3 bounding box) and comfortably fits within a standard 50mm metallographic mount, yet creates a holistic view of process health by allowing for analysis of the following:

- Microstructure,
- Residual stress,
- Chemical composition,
- Surface integrity,
- Distortion,
- Internal channel integrity,
- Powder removal testing,
- Geometric accuracy, and
- Mechanical properties.

At a minimum, the authors believe this artifact provides a much improved, small-size complex geometry demonstration for others to use in addition to the more commonly used density cubes seen in LPBF parameter development studies. Overall, implementation of the test artifact will directly address the needs established in 13 AMSC standards gaps and can be used in process qualification under the guidelines provided in NASA MFSC-SPEC-3717. Widespread adoption along with standardized data collection methods will accelerate the development of zone-specific anomaly size and frequency distribution for a given machine, feedstock and process parameter set. Quantitative knowledge of LPBF anisotropy in terms of anomalies can then be used to intelligently develop representative mechanical property testing. Ultimately, this can lead to establishing exceedance curves, a prerequisite to development of a probabilistic damage tolerance framework.

In conclusion, the authors intend to use the artifact described in this paper as the basis for a LPBF Global Test Artifact Data Exchange Program (GTADExP), described in more detail at

keck.utep.edu/GTADExP. For rapid adoption and implementation, LPBF test artifact data manufactured from different machines and organizations around the world will be stored and accessed through the program website. After registration (which includes program details such as providing specific build parameters and other build data for each artifact), test artifacts manufactured externally can also be sent to the program for analysis along with ~50g of the feedstock used for the build. The program is intended to produce and analyze at least 100 test artifacts from a single material system by the end of 2021, providing unprecedented performance data for LPBF, and the program will continue until the LPBF test artifact is no longer used or as long as program resources remain available. It is expected that many future publications will provide results from this program. The approach of this artifact with some process-specific modifications can also be extended to other powder bed-based processes such as electron beam PBF and binder jetting.

3.1.5.1 Acknowledgements

3.1.6 References

[1]   America Makes, AMSC, Standardization Roadmap for Additive Manufacturing - Version 2.0, 2018.

[2]   S. Requirements, M. Containing, L. Than, T. Percent, C. Titanium, Astm 2924, 2019. https://doi.org/10.1520/F2924-14.2.

[3]   MSFC-SPEC-3717, SPECIFICATION FOR CONTROL AND QUALIFICATION OF LASER POWDER BED FUSION METALLURGICAL PROCESSES, 2017.

[4]   ASTM F3049 – 14, Standard Guide for Characterizing Properties of Metal Powders Used for Additive Manufacturing Processes, West Conshohocken, PA, 2014. https://doi.org/10.1520/F3049-14.

[5]   MSFC-SPEC-3716, STANDARD FOR ADDITIVELY MANUFACTURED SPACEFLIGHT HARDWARE BY LASER POWDER BED FUSION IN METALS, 2017.

[6]   M. Gorelik, Additive manufacturing in the context of structural integrity, Int. J. Fatigue. 94 (2017) 168–177. https://doi.org/10.1016/j.ijfatigue.2016.07.005.

[7]   R. Russell, D. Wells, J. Waller, B. Poorganji, E. Ott, T. Nakagawa, H. Sandoval, N. Shamsaei, M. Seifi, Qualification and certification of metal additive manufactured hardware for aerospace applications, in: Addit. Manuf. Aerosp. Ind., Elsevier, 2019: pp. 33–66. https://doi.org/10.1016/b978-0-12-814062-8.00003-0.

[8]   J. Waller, New Guide for Nondestructive Testing of Additive Manufactured Metal Parts

Used in Aerospace Applications, (2014).

[9]   Additive Manufacturing Part Qualification | NIST, (n.d.). https://www.nist.gov/programs-projects/additive-manufacturing-part-qualification (accessed February 4, 2020).

[10]   AM Machine and Process Qualification | NIST, (n.d.). https://www.nist.gov/programs-projects/am-machine-and-process-qualification (accessed February 4, 2020).

[11]   Qualification for Additive Manufacturing Materials, Processes, and Parts | NIST, (n.d.). https://www.nist.gov/programs-projects/qualification-additive-manufacturing-materials-processes-and-parts (accessed February 4, 2020).

[12]   L. Rebaioli, I. Fassi, A review on benchmark artifacts for evaluating the geometrical performance of additive manufacturing processes, Int. J. Adv. Manuf. Technol. 93 (2017) 2571–2598. https://doi.org/10.1007/s00170-017-0570-0.

[13]   D. Dimitrov, W. Van Wijck, K. Schreve, N. De Beer, J. Meijer, An investigation of the capability profile of the three dimensional printing process with an emphasis on the achievable accuracy, CIRP Ann. - Manuf. Technol. 52 (2003) 189–192. https://doi.org/10.1016/S0007-8506(07)60562-9.

[14]   D. Scaravetti, P. Dubois, R. Duchamp, Qualification of rapid prototyping tools: Proposition of a procedure and a test part, Int. J. Adv. Manuf. Technol. 38 (2008) 683–690. https://doi.org/10.1007/s00170-007-1129-2.

[15]   T. Brajlih, B. Valentan, J. Balic, I. Drstvensek, Speed and accuracy evaluation of additive manufacturing machines, Rapid Prototyp. J. 17 (2011) 64–75. https://doi.org/10.1108/13552541111098644.

[16]   M. Mahesh, Y.S. Wong, J.Y.H. Fuh, H.T. Loh, Benchmarking for comparative evaluation of

RP systems and processes, Rapid Prototyp. J. 10 (2004) 123–135. https://doi.org/10.1108/13552540410526999.

[17]	A.J. Lopes, M.A. Perez, D. Espalin, R.B. Wicker, Comparison of ranking models to evaluate desktop 3D printers in a growing market, Addit. Manuf. 35 (2020) 101291. https://doi.org/10.1016/j.addma.2020.101291.

[18]	K.A. Ghany, S.F. Moustafa, Comparison between the products of four RPM systems for metals, Rapid Prototyp. J. 12 (2006) 86–94. https://doi.org/10.1108/13552540610652429.

[19]	S. Moylan, J. Slotwinski, M. Cooke, K. Jurrens, M. Alkan Donme, Proposal for a Standardized Test Artifact for Additive, in: Solid Free. Fabr. Symp., 2012: pp. 902–920. https://ws680.nist.gov/publication/get_pdf.cfm?pub_id=911953.

[20]	P. Mireya, R. Jorge, E. David, H. Mohammad, W. Ryan, Ranking models for 3D printers, in: Proc. 2013 Annu. Int. Solid Free. Fabr. Symp., 2013.

[21]	ISO/ASTM 52902, Additive manufacturing - test artifact - geometric capability assessment of additive manufacturing systems, (2019). https://doi.org/10.1520/52902-19.

[22]	E. Bassoli, A. Sola, M. Celesti, S. Calcagnile, C. Cavallini, Development of laser-based powder bed fusion process parameters and scanning strategy for new metal alloy grades: A holistic method formulation, Materials (Basel). 11 (2018). https://doi.org/10.3390/ma11122356.

[23]	N.C. Levkulich, S.L. Semiatin, J.E. Gockel, J.R. Middendorf, A.T. DeWald, N.W. Klingbeil, The effect of process parameters on residual stress evolution and distortion in the laser powder bed fusion of Ti-6Al-4V, Addit. Manuf. 28 (2019) 475–484. https://doi.org/10.1016/j.addma.2019.05.015.

[24] C. Li, M.F. Gouge, E.R. Denlinger, J.E. Irwin, P. Michaleris, Estimation of part-to-powder heat losses as surface convection in laser powder bed fusion, Addit. Manuf. 26 (2019) 258–269. https://doi.org/10.1016/j.addma.2019.02.006.

[25] Z. Dong, X. Zhang, W. Shi, H. Zhou, H. Lei, J. Liang, Study of size effect on microstructure and mechanical properties of AlSi10Mg samples made by selective laser melting, Materials (Basel). 11 (2018). https://doi.org/10.3390/ma11122463.

[26] Y. Kok, X.P. Tan, P. Wang, M.L.S. Nai, N.H. Loh, E. Liu, S.B. Tor, Anisotropy and heterogeneity of microstructure and mechanical properties in metal additive manufacturing: A critical review, Mater. Des. 139 (2018) 565–586. https://doi.org/10.1016/j.matdes.2017.11.021.

[27] D. Wang, S. Mai, D. Xiao, Y. Yang, Surface quality of the curved overhanging structure manufactured from 316-L stainless steel by SLM, Int. J. Adv. Manuf. Technol. 86 (2016) 781–792. https://doi.org/10.1007/s00170-015-8216-6.

[28] L. Parry, I.A. Ashcroft, R.D. Wildman, Understanding the effect of laser scan strategy on residual stress in selective laser melting through thermo-mechanical simulation, Addit. Manuf. 12 (2016) 1–15. https://doi.org/10.1016/j.addma.2016.05.014.

[29] X. Tan, Y. Kok, Y.J. Tan, G. Vastola, Q.X. Pei, G. Zhang, Y.W. Zhang, S.B. Tor, K.F. Leong, C.K. Chua, An experimental and simulation study on build thickness dependent microstructure for electron beam melted Ti-6Al-4V, J. Alloys Compd. 646 (2015) 303–309. https://doi.org/10.1016/j.jallcom.2015.05.178.

[30] H. Yeung, B. Lane, J. Fox, Part geometry and conduction-based laser power control for powder bed fusion additive manufacturing, Addit. Manuf. 30 (2019) 100844.

https://doi.org/10.1016/j.addma.2019.100844.

[31]   J. Dzugan, M. Seifi, R. Prochazka, M. Rund, P. Podany, P. Konopik, J.J. Lewandowski, Effects
        of thickness and orientation on the small scale fracture behaviour of additively
        manufactured   Ti-6Al-4V,   Mater.   Charact.   143   (2018)   94–109.
        https://doi.org/10.1016/j.matchar.2018.04.003.

[32]   H. Salem, L.N. Carter, M.M. Attallah, H.G. Salem, Influence of processing parameters on
        internal porosity and types of defects formed in Ti6Al4V lattice structure fabricated by
        selective   laser   melting,   Mater.   Sci.   Eng.   A.   767   (2019).
        https://doi.org/10.1016/j.msea.2019.138387.

[33]   C. Phutela, N.T. Aboulkhair, C.J. Tuck, I. Ashcroft, The effects of feature sizes in selectively
        laser melted Ti-6Al-4V parts on the validity of optimised process parameters, Materials
        (Basel). 13 (2020) 117. https://doi.org/10.3390/ma13010117.

[34]   K. Dietrich, J. Diller, S. Dubiez-Le Goff, D. Bauer, P. Forêt, G. Witt, The influence of oxygen
        on the chemical composition and mechanical properties of Ti-6Al-4V during laser powder
        bed   fusion   (L-PBF),   Addit.   Manuf.   32   (2020).
        https://doi.org/10.1016/j.addma.2019.100980.

[35]   P. Gradl, O. Mireles, N. Andrews, Intro to Additive Manufacturing for Propulsion Systems,
        2018. https://ntrs.nasa.gov/search.jsp?R=20180006357 (accessed February 14, 2020).

[36]   P.R. Gradl, S.E. Greene, C. Protz, B. Bullard, J. Buzzell, C. Garcia, J. Wood, K. Cooper, J.
        Hulka, R. Osborne, Additive manufacturing of liquid rocket engine combustion devices: A
        summary of process developments and hot-fire testing results, in: 2018 Jt. Propuls. Conf.,
        American   Institute   of   Aeronautics   and   Astronautics   Inc,   AIAA,   2018.

78

https://doi.org/10.2514/6.2018-4625.

[37]   M.A. Mitchell, R.E. Raley, K.E. Jacobs, E./ Em50, Cleaning and Cleanliness Measurement of Additive Manufactured Parts Materials & Processes/EM50 Jacobs ESSSA/EM50 NASA Marshall Space Flight Center NASA Marshall Space Flight Center, n.d. https://ntrs.nasa.gov/search.jsp?R=20160008863 (accessed April 3, 2020).

[38]   T. Kolb, A. Mahr, F. Huber, J. Tremel, M. Schmidt, Qualification of channels produced by laser powder bed fusion: Analysis of cleaning methods, flow rate and melt pool monitoring data, Addit. Manuf. 25 (2019) 430–436. https://doi.org/10.1016/j.addma.2018.11.026.

[39]   P. Promoppatum, S.-C. Yao, Influence of scanning length and energy input on residual stress reduction in metal additive manufacturing: Numerical and experimental studies, J. Manuf. Process. 49 (2020) 247–259. https://doi.org/10.1016/j.jmapro.2019.11.020.

[40]   S. Le Roux, M. Salem, A. Hor, Improvement of the bridge curvature method to assess residual stresses in selective laser melting, Addit. Manuf. 22 (2018) 320–329. https://doi.org/10.1016/j.addma.2018.05.025.

[41]   J.-P. Kruth, J. Deckers, E. Yasa, R. Wauthlé, Assessing and comparing influencing factors of residual stresses in selective laser melting using a novel analysis method, Proc. Inst. Mech. Eng. Part B J. Eng. Manuf. 226 (2012) 980–991. https://doi.org/10.1177/0954405412437085.

[42]   J. Robinson, I. Ashton, P. Fox, E. Jones, C. Sutcliffe, Determination of the effect of scan strategy on residual stress in laser powder bed fusion additive manufacturing, Addit. Manuf. 23 (2018) 13–24. https://doi.org/10.1016/j.addma.2018.07.001.

[43]   F. Schmeiser, E. Krohmer, N. Schell, E. Uhlmann, W. Reimers, Experimental observation of

stress formation during selective laser melting using in situ X-ray diffraction, Addit. Manuf. 32 (2020). https://doi.org/10.1016/j.addma.2019.101028.

[44]   H. Ali, L. Ma, H. Ghadbeigi, K. Mumtaz, In-situ residual stress reduction, martensitic decomposition and mechanical properties enhancement through high temperature powder bed pre-heating of Selective Laser Melted Ti6Al4V, Mater. Sci. Eng. A. 695 (2017) 211–220. https://doi.org/10.1016/j.msea.2017.04.033.

[45]   J.L. Bartlett, X. Li, An overview of residual stresses in metal powder bed fusion, Addit. Manuf. 27 (2019) 131–149. https://doi.org/10.1016/j.addma.2019.02.020.

[46]   L. Cheng, A. To, Part-scale build orientation optimization for minimizing residual stress and support volume for metal additive manufacturing: Theory and experimental validation, CAD Comput. Aided Des. 113 (2019) 1–23. https://doi.org/10.1016/j.cad.2019.03.004.

[47]   J.D. Roehling, W.L. Smith, T.T. Roehling, B. Vrancken, G.M. Guss, J.T. McKeown, M.R. Hill, M.J. Matthews, Reducing residual stress by selective large-area diode surface heating during laser powder bed fusion additive manufacturing, Addit. Manuf. 28 (2019) 228–235. https://doi.org/10.1016/j.addma.2019.05.009.

[48]   D. Buchbinder, W. Meiners, N. Pirch, K. Wissenbach, J. Schrage, Investigation on reducing distortion by preheating during manufacture of aluminum components using selective laser melting, J. Laser Appl. 26 (2014) 012004. https://doi.org/10.2351/1.4828755.

[49]   N.C. Levkulich, S.L. Semiatin, J.E. Gockel, J.R. Middendorf, A.T. DeWald, N.W. Klingbeil, The effect of process parameters on residual stress evolution and distortion in the laser powder bed fusion of Ti-6Al-4V, Addit. Manuf. 28 (2019) 475–484. https://doi.org/10.1016/j.addma.2019.05.015.

[50]   J. Dzugan, M. Sibr, P. Konopík, R. Procházka, M. Rund, Mechanical properties determination of AM components, in: IOP Conf. Ser. Mater. Sci. Eng., 2017. https://doi.org/10.1088/1757-899X/179/1/012019.

[51]   Z. Chen, X. Wu, D. Tomus, C.H.J. Davies, Surface roughness of Selective Laser Melted Ti-6Al-4V alloy components, Addit. Manuf. 21 (2018) 91–103. https://doi.org/10.1016/j.addma.2018.02.009.

[52]   I. Koutiri, E. Pessard, P. Peyre, O. Amlou, T. De Terris, Influence of SLM process parameters on the surface finish, porosity rate and fatigue behavior of as-built Inconel 625 parts, J. Mater. Process. Technol. 255 (2018) 536–546. https://doi.org/10.1016/j.jmatprotec.2017.12.043.

[53]   Y. Tian, D. Tomus, P. Rometsch, X. Wu, Influences of processing parameters on surface roughness of Hastelloy X produced by selective laser melting, Addit. Manuf. 13 (2017) 103–112. https://doi.org/10.1016/j.addma.2016.10.010.

[54]   A. Charles, A. Elkaseer, L. Thijs, V. Hagenmeyer, S. Scholz, Effect of process parameters on the generated surface roughness of down-facing surfaces in selective laser melting, Appl. Sci. 9 (2019) 1–13. https://doi.org/10.3390/app9061256.

[55]   B.R. Whip, Effect of Process Parameters on the Surface Roughness and Mechanical Performance of Additively Manufactured Alloy 718, (2018). http://rave.ohiolink.edu/etdc/view?acc_num=wright1526993831680976.

[56]   G.E. Bean, D.B. Witkin, T.D. McLouth, D.N. Patel, R.J. Zaldivar, Effect of laser focus shift on surface quality and density of Inconel 718 parts produced via selective laser melting, Addit. Manuf. 22 (2018) 207–215. https://doi.org/10.1016/j.addma.2018.04.024.

[57] Distortion Compensation for Additive Manufacturing, 2018. www.ansys.com/additive (accessed February 3, 2020).

[58] S. Afazov, W.A.D. Denmark, B. Lazaro Toralles, A. Holloway, A. Yaghi, Distortion prediction and compensation in selective laser melting, Addit. Manuf. 17 (2017) 15–22. https://doi.org/10.1016/j.addma.2017.07.005.

[59] J. Francis, L. Bian, Deep Learning for Distortion Prediction in Laser-Based Additive Manufacturing using Big Data, Manuf. Lett. 20 (2019) 10–14. https://doi.org/10.1016/j.mfglet.2019.02.001.

[60] M. Seifi, M. Gorelik, J. Waller, N. Hrabe, N. Shamsaei, S. Daniewicz, J.J. Lewandowski, Progress Towards Metal Additive Manufacturing Standardization to Support Qualification and Certification, Jom. 69 (2017) 439–455. https://doi.org/10.1007/s11837-017-2265-2.

[61] H. Millwater, J. Wu, M. Enright, D. Riha, G. Leverant, C. McClung, G. Chell, C. Kuhlman, S. Fitch, M.D. Gorelik -AlliedSignal Herrman -Rolls Royce Allison, USAF Aircraft Structural Integrity Program Conference, 1999.

[62] R.C. Mcclung, M.P. Enright, Current Trends in Probabilistic Damage Tolerance with DARWIN Current Trends in Probabilistic Damage Tolerance, 2015.

[63] Q. Chen, X. Liang, D. Hayduke, J. Liu, L. Cheng, J. Oskin, R. Whitmore, A.C. To, An inherent strain based multiscale modeling framework for simulating part-scale residual deformation for direct metal laser sintering, Addit. Manuf. 28 (2019) 406–418. https://doi.org/10.1016/j.addma.2019.05.021.

[64] B. Van Hooreweder, K. Lietaert, B. Neirinck, N. Lippiatt, M. Wevers, CoCr F75 scaffolds produced by additive manufacturing: Influence of chemical etching on powder removal

and mechanical performance, J. Mech. Behav. Biomed. Mater. 70 (2017) 60–67. https://doi.org/10.1016/j.jmbbm.2017.03.017.

[65]   M. Hamidi, A. Falzetti, A. Redaelli, N. Lecis, A. Giussani, L. Sala, M. Vedani, Finishing of internal and external surfaces produced by Powder Bed Fusion, n.d. www.euspen.eu (accessed January 29, 2020).

[66]   J. Kozak, T. Zakrzewski, Accuracy problems of additive manufacturing using SLS/SLM processes, in: AIP Conf. Proc., 2018: p. 160009. https://doi.org/10.1063/1.5056273.

[67]   Calibration Solutions, (n.d.). www.scanlab.de (accessed November 13, 2020).

[68]   M.A. Ortega Delgado, A.F. Lasagni, Reducing field distortion for galvanometer scanning system using a vision system, Opt. Lasers Eng. 86 (2016) 106–114. https://doi.org/10.1016/j.optlaseng.2016.05.016.

[69]   Scanlabs, Installation and Operation The RTC ® 5 PC Interface Board and RTC ® 5 PC / 104-Plus Board, (2010) 1–467.

[70]   How to design parts for Metal 3D printing | 3D Hubs, (n.d.). https://www.3dhubs.com/knowledge-base/how-design-parts-metal-3d-printing/#rules (accessed February 13, 2020).

[71]   J. Kranz, D. Herzog, C. Emmelmann, Design guidelines for laser additive manufacturing of lightweight structures in TiAl6V4, J. Laser Appl. 27 (2015) S14001. https://doi.org/10.2351/1.4885235.

[72]   Renishaw, Design for metal AM - a beginner's guide, 2017. https://www.renishaw.com/en/design-for-metal-am-a-beginners-guide--42652.

[73]   C. Pauzon, E. Hryha, P. Forêt, L. Nyborg, Effect of argon and nitrogen atmospheres on the

properties of stainless steel 316 L parts produced by laser-powder bed fusion, Mater. Des. 179 (2019) 107873. https://doi.org/10.1016/j.matdes.2019.107873.

[74]   F. Cabanettes, A. Joubert, G. Chardon, V. Dumas, J. Rech, C. Grosjean, Z. Dimkovski, Topography of as built surfaces generated in metal additive manufacturing: A multi scale analysis from form to roughness, Precis. Eng. 52 (2018) 249–265. https://doi.org/10.1016/j.precisioneng.2018.01.002.

[75]   Y. Zhou, F. Ning, Build Orientation Effect on Geometric Performance of Curved-Surface 316L Stainless Steel Parts Fabricated by Selective Laser Melting, J. Manuf. Sci. Eng. 142 (2020). https://doi.org/10.1115/1.4047624.

[76]   L.W. Hunter, D. Brackett, N. Brierley, J. Yang, M.M. Attallah, Assessment of trapped powder removal and inspection strategies for powder bed fusion techniques, (n.d.). https://doi.org/10.1007/s00170-020-04930-w.

[77]   P. Mercelis, J.P. Kruth, Residual stresses in selective laser sintering and selective laser melting, Rapid Prototyp. J. 12 (2006) 254–265. https://doi.org/10.1108/13552540610707013.

[78]   K. Cooper, P. Steele, B. Cheng, K. Chou, Contact-Free Support Structures for Part Overhangs in Powder-Bed Metal Additive Manufacturing, Inventions. 3 (2017) 2. https://doi.org/10.3390/inventions3010002.

[79]   Deformation Correction and First Print Yield, (n.d.). https://blog.velo3d.com/blog/deformation-correction-and-first-print-yield (accessed February 4, 2020).

[80]   ISO/ASTM 52911-1:2019, Additive manufacturing — Design — Part 1 : Laser-based powder

bed fusion of metals 1, 2019. https://doi.org/10.1520/52911-1-19.2.

[81]   M. Seifi, M. Gorelik, J. Waller, N. Hrabe, N. Shamsaei, S. Daniewicz, J.J. Lewandowski, Progress Towards Metal Additive Manufacturing Standardization to Support Qualification and Certification, JOM. 69 (2017) 439–455. https://doi.org/10.1007/s11837-017-2265-2.

[82]   M.J. O'Brien, Development and qualification of additively manufactured parts for space, Opt. Eng. 58 (2019) 1. https://doi.org/10.1117/1.oe.58.1.010801.

[83]   ASTM E8, Standard Test Methods for Tension Testing of Metallic Materials, Annu. B. ASTM Stand. 4. (2010) 1–27. https://doi.org/10.1520/E0008.

[84]   ASTM F3302, Standard for Additive Manufacturing – Finished Part Properties – Standard Specification for Titanium Alloys via Powder Bed Fusion, West Conshohocken, PA, 2018. https://doi.org/10.1520/F3302-18.Copyright.

[85]   ASTM E1409-13, Standard Test Method for Determination of Oxygen and Nitrogen in Titanium and Titanium Alloys by Inert Gas Fusion, (2013). https://doi.org/10.1520/E1409.

[86]   ASTM E2371, Standard Test Method for Analysis of Titanium and Titanium Alloys by Direct Current Plasma and Inductively Coupled Plasma Atomic Emission Spectrometry (Performance-Based Test Methodology) Coupled Plasma Atomic Emission Spectrometry (ICP-AES), West Conshohocken, PA, 2013. https://doi.org/10.1520/E2371-13.2.

[87]   ASTM E354, Test Methods for Chemical Analysis of High-Temperature , Electrical , Magnetic , and Other Similar Iron , Nickel , and Cobalt Alloys, West Conshohocken, PA, 2014. https://doi.org/10.1520/E0354-14.Copyright.

[88]   ASTM F3055, Standard Specification for Additive Manufacturing Nickel Alloy (UNS N07718) with Powder Bed Fusion, West Conshohocken, PA, 2014. https://doi.org/10.1520/F3055-

14A.Copyright.

[89]   ISO 4288, Specification (GPS) Surface Texture Profile Method: Rules and Procedures for the Assessment of Surface Texture, 1998.

[90]   Brian Griffiths, Surface Finish Measuring Methods, in: Manuf. Surf. Technol. Surf. Integr. Funct. Perform., 1st ed., Penton Press, London, 2001: pp. 70–107.

[91]   ISO6892-1:2009, Metallic materials — Tensile testing — Part 1: Method of test at room temperature, (2009).

[92]   D. Kang, S. Park, Y. Son, S. Yeon, S.H. Kim, I. Kim, Multi-lattice inner structures for high-strength and light-weight in metal selective laser melting process, Mater. Des. 175 (2019) 107786. https://doi.org/10.1016/j.matdes.2019.107786.

[93]   C. Yan, L. Hao, A. Hussein, P. Young, Ti-6Al-4V triply periodic minimal surface structures for bone implants fabricated via selective laser melting, J. Mech. Behav. Biomed. Mater. 51 (2015) 61–73. https://doi.org/10.1016/j.jmbbm.2015.06.024.

[94]   T. Maconachie, M. Leary, B. Lozanovski, X. Zhang, M. Qian, O. Faruque, M. Brandt, SLM lattice structures: Properties, performance, applications and challenges, Mater. Des. 183 (2019) 108137. https://doi.org/10.1016/j.matdes.2019.108137.

[95]   EOS, EOS M 290 produces highest quality metal parts in additive manufacturing, (2019). www.eos.info (accessed November 12, 2020).

[96]   P.A. Morton, H.C. Taylor, L.E. Murr, O.G. Delgado, C.A. Terrazas, R.B. Wicker, In situ selective laser gas nitriding for composite TiN/Ti-6Al-4V fabrication via laser powder bed fusion, J. Mater. Sci. Technol. 45 (2020) 98–107. https://doi.org/10.1016/j.jmst.2019.11.009.

[97]   ASTM B527-20, Standard Test Method for Tap Density of Metal Powders and Compounds, (n.d.). https://doi.org/10.1520/B0527-20.

[98]   ASTM B212-17, Standard Test Method for Apparent Density of Free-Flowing Metal Powders Using the Hall Flowmeter Funnel , (n.d.). https://doi.org/10.1520/B0212-17.

[99]   N. Sanaei, A. Fatemi, Defects in Additive Manufactured Metals and Their Effect on Fatigue Performance: A State-of-the-Art Review, Prog. Mater. Sci. (2020) 100724. https://doi.org/10.1016/j.pmatsci.2020.100724.

[100] D. Sera Ertay, H. Ma, M. Vlasea, Correlative Beam Path and Pore Defect Space Analysis for Modulated Powder Bed Laser Fusion Process, in: Solid Free. Fabr. 2018 Proc. 29th Annu. Int., 2018: pp. 272–284. http://sffsymposium.engr.utexas.edu/sites/default/files/2018/021 CorrelativeBeamPathandPoreDefectSpaceAnalys.pdf.

[101] A.M. Mancisidor, F. Garciandia, M.S. Sebastian, P. Álvarez, J. Díaz, I. Unanue, Reduction of the residual porosity in parts manufactured by selective laser melting using skywriting and high focus offset strategies, in: Phys. Procedia, 2016: pp. 864–873. https://doi.org/10.1016/j.phpro.2016.08.090.

[102] W. Yu, S.L. Sing, C.K. Chua, X. Tian, Influence of re-melting on surface roughness and porosity of AlSi10Mg parts fabricated by selective laser melting, J. Alloys Compd. 792 (2019) 574–581. https://doi.org/10.1016/j.jallcom.2019.04.017.

[103] D.B. Witkin, D. Patel, T. V. Albright, G.E. Bean, T. McLouth, Influence of surface conditions and specimen orientation on high cycle fatigue properties of Inconel 718 prepared by laser powder bed fusion, Int. J. Fatigue. 132 (2020) 105392.

https://doi.org/10.1016/j.ijfatigue.2019.105392.

[104] B. Lane, H. Yeung, Process Monitoring Dataset from the Additive Manufacturing Metrology Testbed (AMMT): "Three-Dimensional Scan Strategies," J Res Natl Inst Stan. 124 (2019) 124033. https://doi.org/10.6028/jres.124.033.

[105] S.A. Khairallah, A.T. Anderson, A. Rubenchik, W.E. King, Laser powder-bed fusion additive manufacturing: Physics of complex melt flow and formation mechanisms of pores, spatter, and denudation zones, Acta Mater. 108 (2016) 36–45. https://doi.org/10.1016/j.actamat.2016.02.014.

[106] T. Fiegl, M. Franke, C. Körner, Impact of build envelope on the properties of additive manufactured parts from AlSi10Mg, Opt. Laser Technol. 111 (2019) 51–57. https://doi.org/10.1016/j.optlastec.2018.08.050.

[107] S. Liu, Y.C. Shin, Additive manufacturing of Ti6Al4V alloy: A review, Mater. Des. 164 (2019) 107552. https://doi.org/10.1016/j.matdes.2018.107552.

[108] H. Gong, K. Rafi, H. Gu, G.D. Janaki Ram, T. Starr, B. Stucker, Influence of defects on mechanical properties of Ti-6Al-4V components produced by selective laser melting and electron beam melting, Mater. Des. 86 (2015) 545–554. https://doi.org/10.1016/j.matdes.2015.07.147.

[109] T. Voisin, N.P. Calta, S.A. Khairallah, J.B. Forien, L. Balogh, R.W. Cunningham, A.D. Rollett, Y.M. Wang, Defects-dictated tensile properties of selective laser melted Ti-6Al-4V, Mater. Des. 158 (2018) 113–126. https://doi.org/10.1016/j.matdes.2018.08.004.

[110] W. Xu, E.W. Lui, A. Pateras, M. Qian, M. Brandt, In situ tailoring microstructure in additively manufactured Ti-6Al-4V for superior mechanical performance, Acta Mater. 125 (2017)

390–400. https://doi.org/10.1016/j.actamat.2016.12.027.

[111] G. Mohr, S.J. Altenburg, K. Hilgenberg, Effects of inter layer time and build height on resulting properties of 316L stainless steel processed by laser powder bed fusion, Addit. Manuf. 32 (2020) 101080. https://doi.org/10.1016/j.addma.2020.101080.

3.2 CREATING THE GLOBAL TEST ARTIFACT DATA EXCHANGE PROGRAM

3.2.1 Data Infrastructure development beyond a "database"

Engineering data has little value if it is not FAIR; Findable, Accessible, Interoperable, and Reusable. For this reason, the primary effort in developing holistic understanding of LPBF has been data curation. In parallel with artifact design, measurement, and analysis, a database management system (DBMS) and analysis framework has been developed as part of this research leveraging the entire Keck Center and DRIVE AM team. LPBF challenges the traditional DBMS solutions for the same reasons it challenges qualification; that is, the heterogeneous nature of the process creates heterogeneous data. Big data refers to the 4 V's of data that includes Velocity, Volume, Veracity, and Variety.

- Volume – the amount of data cumulative and within a single file. Handling thousands of 100MB files vs a single TB file pose different challenges and the need to store greater than 1PB of data creates yet another challenge
- Velocity – the speed at which new data is created
- Variety – structured data like excel files and unstructured data like images
- Veracity – data quality and trustworthiness to include accuracy of meta data detail of the data context and chain of custody, how/when/why is the data altered

The 4 V's are used to help identify an appropriate DBMS; however, AM data creates data that is low volume and velocity from one instrument and high volume and velocity from another source for the same part. Variety creates significant challenges, and no one-size-fits-all solution

exists to date. Commercial solutions to include Citrine, MaterialCenter by Hexagon, and Ansys Granta were evaluated against the following requirements: have a rest API, enable the construction of custom scripts to guide data capture, handle one petabyte of data over next 3 years, be flexible in that the structure can be updated overtime, and handle multiple users from different locations globally. The estimated costs were similar across commercial prospects at roughly $150,000+/yr when balancing the upfront engineering cost and the growing amount of stored data over the lifetime of the project. In addition to the commercial solutions, an AFRL funded and developed DBMS called HyperThought was evaluated. This no-SQL solution does not enable the direct development of data collection scripts to reduce data upload burden however this DBMS checked the remaining requirements. Through collaboration with Contextualize, the W.M. Keck Center for 3D Innovation, and HyperThought a custom data infrastructure solution has been developed that serves as the basis of a yet to be published report titled "Constructing and AM data Infrastructure".

The DBMS is only one aspect of the data infrastructure required to effectively curate data for the GTADExP. The data infrastructure had to meet the following criteria:

- Isolate equipment that creates data from the outside internet
- Reduce burden of data collection to an absolute minimum
- Maximize data veracity creating consistent detailed metadate using data collection templates
- Enable automatic and semi-automatic data quality checks
- Be able to grow to data collection volume exceeding 1 petabyte a year
- Enable version control
- Enable with no programming experience to query data quickly
- Integrate high compute resource data analysis/scrapers/parsers prior to upload to DBMS
- Multi-level user roles

Isolating the physical equipment (LPBF machines, Mechanical testing equipment XCT, and more) from the internet is important to prevent system updates and improve data security however the data must be transferred from the equipment to the DBMS which is not deployed on premises. This challenge was solved by implementing a proxy server that is physically connected to the equipment through a 48-port network switch. Each piece of equipment is maintained offline while the proxy server can be online. By utilizing a 10gbps port the data velocity challenges are minimized. In addition to providing a solution to isolating equipment, the integration of the proxy server provides a centralized compute resource for data parsing, quality checking, and meta data curating. Figure 35 described the data flow from source of creation to labeling/contextualizing though custom application, to on premises parsing to data upload to HyperThought were it can be accessed by 3rd party software such as Carta to enable easy analysis by GTADExP members.
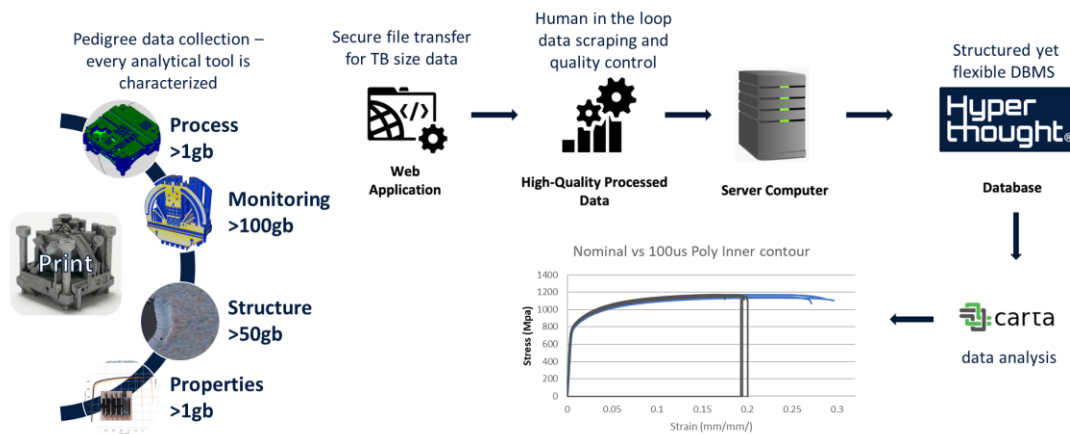
Figure 35 GTADExP data flow schematic

3.2.2 GTADExP Workflow

The data curation workflow required substantial parallelized testing and data collection to ensure that data was not only being collected but that data quality was well understood and repeatable. To ensure data quality and repeatability, the effort has taken steps towards achieving ISO 9001. Although ISO 9001 certification has, at the time of this writing, not yet been achieved, the steps taken have laid the groundwork of data quality. Each step of the process has an active work instruction and an associated GAGE R&R, if applicable. This means the data generated by technicians have measurement uncertainty values that captures equipment, users, and part induced variation. The work instructions are living documents that allow for adjustments to improve quality over time. Improvements in analysis are tracked by re-performing the GAGE R&R studies at specified time intervals based on the specific equipment.

The data collection begins with the digital file preparation and ends with micro hardness analysis as detailed in Figure 36. Each green box links to a sub flow that includes work instructions, data types generated, anticipated unique ID, and an associated web application. The blue boxes indicate a step with work instructions but no data generation. Figure 37 opens the tensile testing sub workflow and details the different steps of data collection related to tensile testing for the artifact.
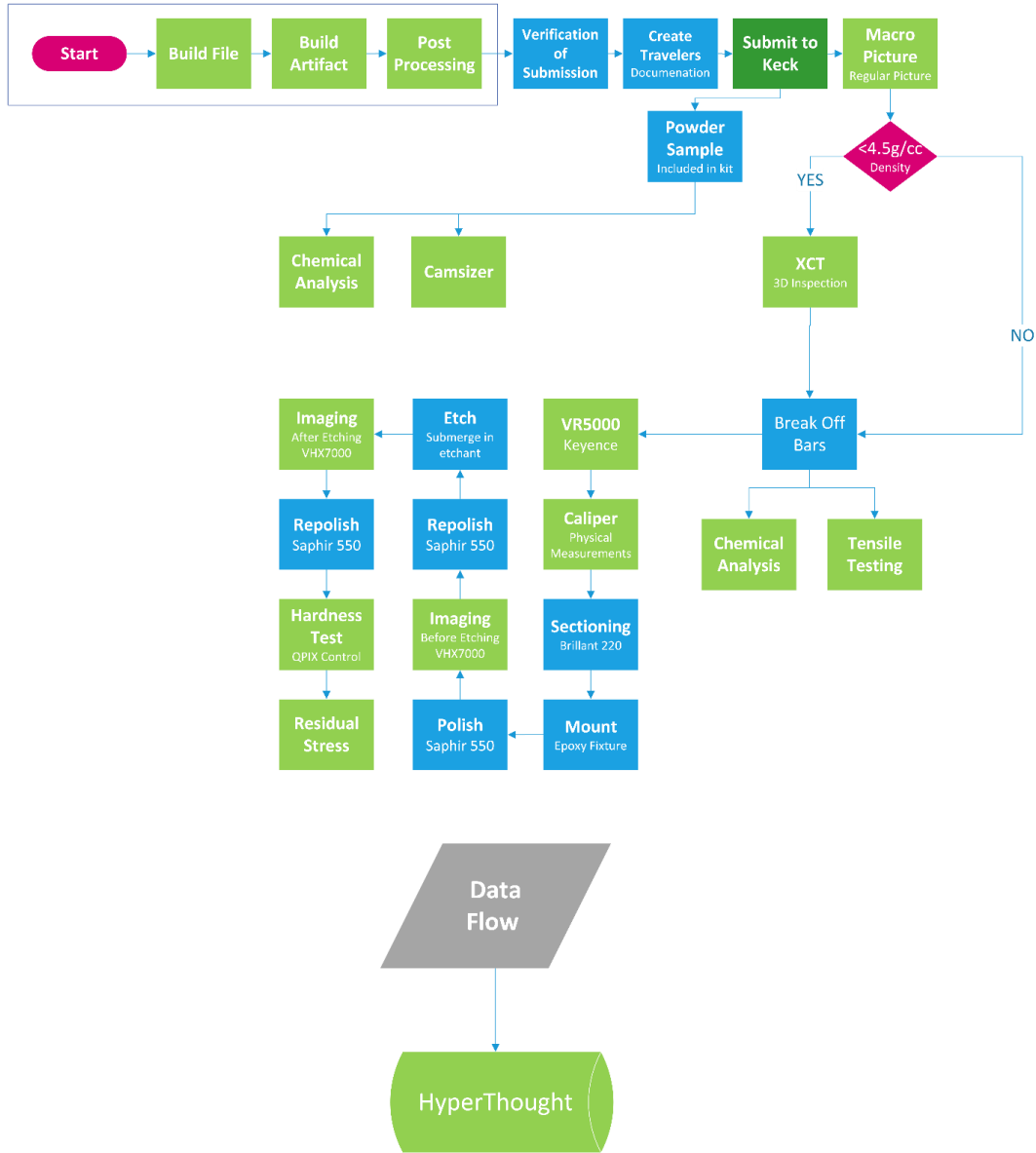
Figure 36 GTADExP analysis workflow from digital file to microhardness
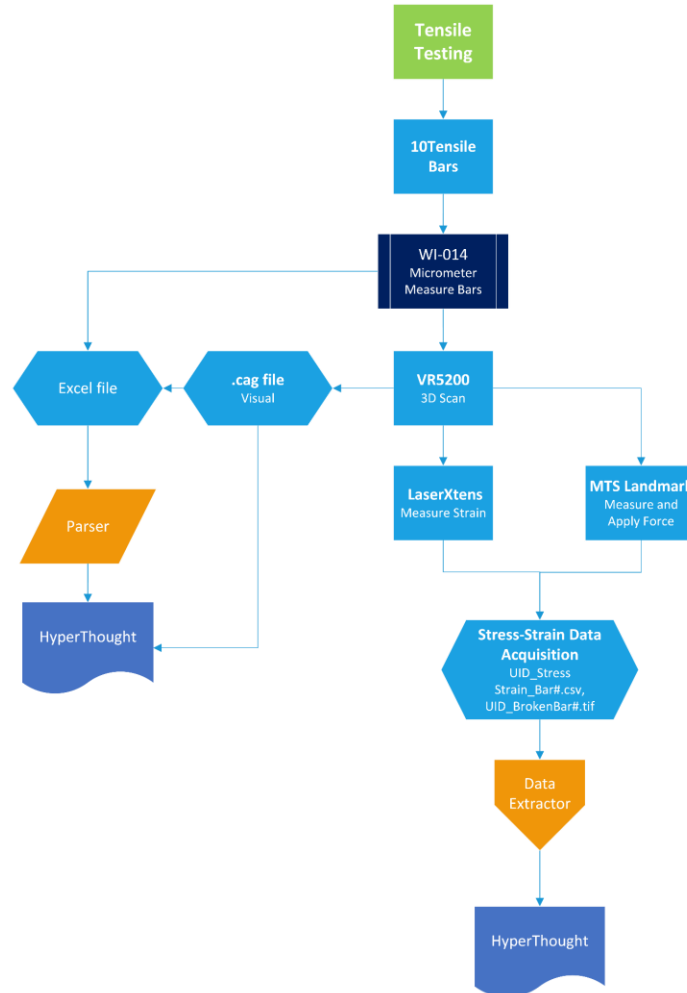
Figure 37 subset of GTADExP workflow detailing the tensile testing sub workflow

As discussed in the DBMS section, easing the burden of data collection while improving data quality required the implementation of templates for students to capture data in a consistent manner. The solution to this came in the form of custom web applications installed on the data collecting equipment. For example, a student performing the polished image XY plane capture can open the web application home page, shown in Figure 38 (which is run offline through the browser and directly linked to the proxy server via static IP address control), and select XY optical cross section. The student can then key in the required fields as well as attach the raw files for that

analysis. In addition to easy-to-use prepopulated fields, the web app page can be programmed to include links to the appropriate work instructions, or pictorials of what is required, shown in Figure 39. The web apps can handle data files exceeding 100GB via direct ethernet port to the proxy server where further parsing or data extraction can be employed.
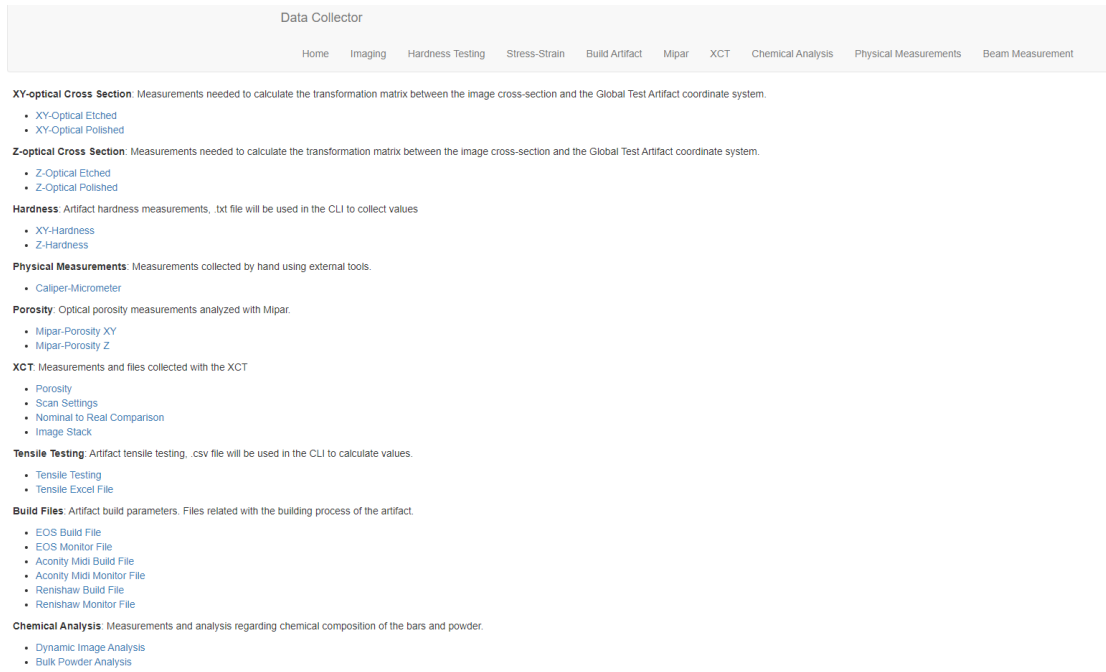
Figure 38 Screen shot of the GTADExP web app data collection page for each process step

Member ID

Build ID

Part #

lower-left width

lower-right width

upper-left width

upper-right width

rotation

distance from left edge

distance from top edge

User Initials

XY cross-section polished:
Choose File No file chosen
Submit

XY OPTICAL **POLISHED**

Follow this link for references and examples of the measurements reque

Figure 39 Screen capture of the XY optical polished cross section data collector web app

The search for a DBMS solution began in August 2020 and the selection of HyperThought was made in January 2021. It was not until October 2021 that the proxy server install was complete as several components were delayed due to the chip shortage, at a cost of $23,347 for hardware and labor to install. Beginning in October 2021 a team of 2-4 computer science Keck Center students plus the Contextualize and Tailored Alloys teams have met weekly to create solutions to the data ingestion, parsing, and upload. As of October 2022, the team has created the data schema for all aspects of artifact creation and analysis to include over 3,000 individual key/value pairs from each artifact. In addition to the schema, 20 web apps have been developed, plus 11 data parsers with 4 more in development. It must also be noted that all code development is hosted in GitLab to ensure traceability and prevent loss of functionality when students graduate and to quickly integrate new team members safely. The effort to create the pedigree holistic data infrastructure that enables the community to remove "it depends" has been immense. **If adopted successfully, it is anticipated that the global test artifact data exchange program could serve as the method to define LPBF process quality and could potentially be adapted beyond**

artifacts and AM to serve as guide to creating the links between process and the resulting structure-properties-performance for any manufacturing method.

3.3 QUALIFICATION TEST ARTIFACT REDESIGN

As the workflow for GTADExP was finalized and artifact analysis matured and several potential improvements to the test artifact design were identified.   Table 3, 4 and 5 in section 3.1 were used as the basis for the redesign. New criteria determined through testing include:

1. Design must be performed from start to finish in one software
2. Remove residual stress overhang
3. Add tensile bars at second orientation
4. Additional flat surfaces for improved geometric analysis by a micrometer
5. Reduction in through thickness solid material distance for improved XCT penetration in Ti64
6. Center hole in bottom to act as fixture point for post processing
7. Features to reduce user error during sectioning

Completing the design within one software without removing the lattice and gyroid features narrowed the option to utilizing traditional CAD software such as NX, SolidWorks, or Inventor with a list of criteria shown in Figure 40. Unfortunately, the traditional cad solutions do not enable the automatic generation of the complex structures and therefore required significant manual work to create the artifact. The need for a single cad file is from the need to have a single source of truth for the design intent without potential loss traceability of dimensional quality. The redesign was completed entirely in SolidWorks by Briana Ugarte.

Top CAD Software contenders:

	SolidWorks	3DXpert	Fusion360	Creo Parametric	nTopology
Create needed geometry	✓	✗	✓	✓	✗
Apply lattices to geometry	✓	✓	✓	✓	✓
Auto-generate **gyroid** lattice	✗	✓	✓	✓	✓
Auto-generate **octet** lattice	✗	✓	✓	✓	✓
Control Perimeter Wall Thickness	✗	✓	✗	✓	✓
Export lattice to solid body/STEP	✓	✗	✗	✗	✗

Manual CADing needed

Figure 40 selection criteria for artifact redesign in one software

Unpublished analysis of the geometry where 48 bridges were built revealed that the uncertainty in calculating the released residual stress exceeded the variation produced by different scanning methods (stripe, checkerboard, and meander). Additionally, literate review was unable to produce a single study of the bridge curvature methods accuracy or uncertainty with nearly all published work based on comparison of one sample to another with no sensitivity or measurement uncertainty analysis. Since the bridge did not provide quantitative data, it was removed from the design.

The removal of the bridge created an opportunity for a new feature. Anisotropy in LPBF (and other manufacturing methods such as forging) has been identified in several alloys. The available space only enabled the use of the ASTM EB # 5 bar dimensions, and the angle selection was limited by build orientation limitations. It would have been optimal to build horizontal bars, however, supports on the gauge area of the bar are not permitted eliminating this possibility. To minimize additional cost, the same ASTM E8 #5 bar used for the vertical bar was reused. To prevent any free-floating melts during the processing the steepest orientation of the tensile bar was

identified as 55°. Bars shown in Figure 41 were at a 54.74° highlighting a potential for free floating material.
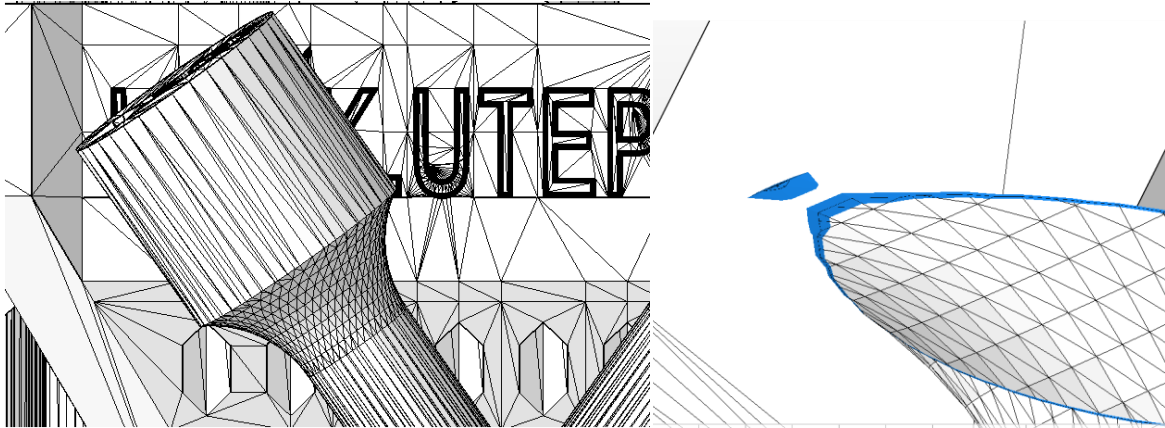
Figure 41 tensile bar at 54.74° showing the free-floating overhanging region

A major improvement was based on extensive work to establish measurement uncertainty for geometric dimensioning and tolerancing with a publication entitled "Measurement systems analysis for Beam Compensation, Scaling factors and Geometric Dimensioning for a metallic additively manufactured test artifact" still under review. The work identified that calipers provided lower measurement uncertainty on several features than the non-contact inspection by Keyence VR-5000. A caliper or micrometer cost $100-$500 and takes less than 1 hour to train a student to operate while the VR-5000 cost roughly $75,000 and takes multiple days of training to be proficient. To better accommodate the use of micrometers and calipers the QTA was redesigned to include larger flat surface that were parallel to each other as shown in Figure 42. The redesigned features enable micrometer measurements from 0.2mm feature to 40mm. The redesigned features still maintain the ability to check scaling factors and beam compensation factors at the lower bulk region and upper region of the artifact.

Figure 36 also shows an isometric view of the artifact with an indication of one of the sectioning grip features designed to reduce human errors during sectioning. The size of the feature is designed for a v-notch vice utilized on a precision section saw. Thus far the feature has been beneficial.
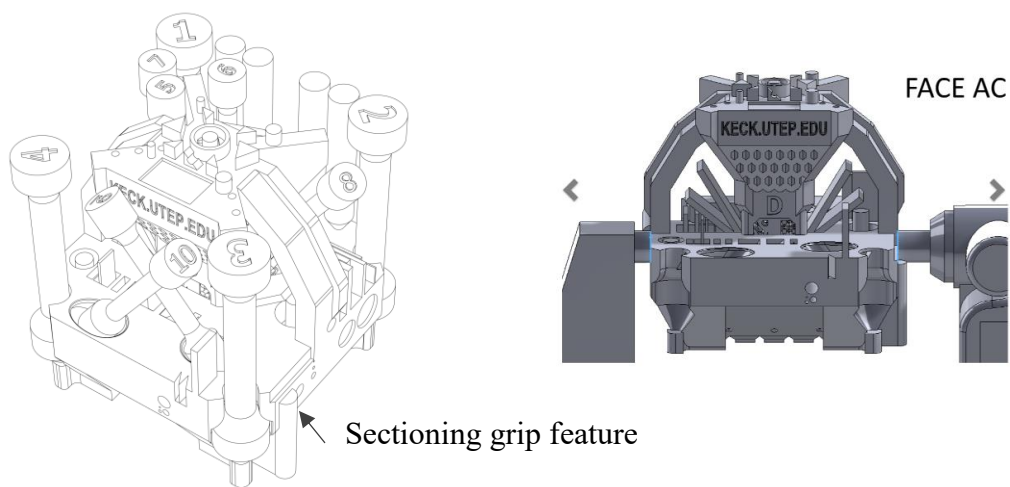
Figure 42 Features improved for micrometer measurements

To reduce total thickness the base of the artifact was shelled and latticed as much as reasonably possible to reduce max x-ray path to below 40mm with tensile bars still attached. In addition, a centered threaded hole was added to the bottom of the artifact. This threaded hole serves three functions: central location to picture artifact in XCT, threading test, location to attached potential channel finishing testing as seen in Figure 43.

Build Direction Cross section

Perpendicular to Build Direction
Cross section

Increased lattice
zone

Threaded fixture hole
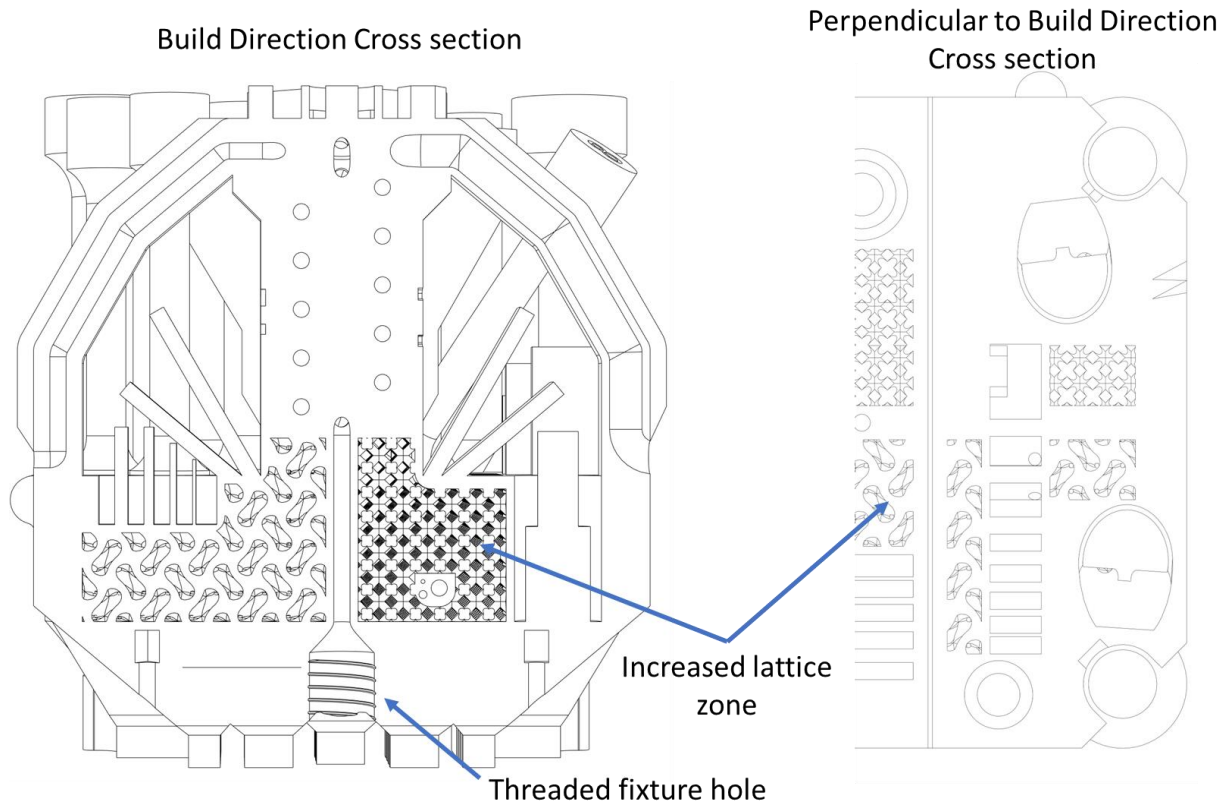
Figure 43 Redesigned cross section indicating larger lattice region for reduced through thickness and threaded hole for fixturing

Chapter 4: Microsecond Impacts in Laser Powder Bed Fusion

Chapter 4 contains a peer reviewed publication from the journal of Additive Manufacturing entitled "Microsecond impacts in laser powder bed fusion". As an author of the Elsevier article no permissions for use are required. My contribution to the article was substantial from concept to writing and reviewing.

H. C. Taylor[a, c, d], R. B. Wicker[a, b]

[a] *W.M. Keck Center for 3D Innovation, The University of Texas at El Paso, El Paso, TX 79968, USA*
[b] *Department of Aerospace and Mechanical Engineering, The University of Texas at El Paso, El Paso, TX 79968, USA*
[c] *Department of Metallurgical, Materials and Biomedical Engineering, The University of Texas at El Paso, El Paso, TX 79968, USA*
[d] *Tailored Alloys LLC, Horizon City, TX 79928, USA*
Email of corresponding author: htaylor@tailoredalloys.com; rwicker@utep.edu

Conflict of interest statement

4.1 INTRODUCTION

The laser powder bed fusion (LPBF) process is strongly influenced by the scanning strategy that determines the laser beam path along with its speed and power. However, each LPBF Original Equipment Manufacturer (OEM) handles, among other things, scanning strategies differently making equivalency across platforms difficult to impossible, and thus, preventing a common material data sheet to exist[4,42,56,99,100]. It has been shown that parameters beyond what most machine manufacturers' allow for user access can affect the process quality, including such parameters as the effect of skywriting angle, laser delays, and more advanced functions like laser power ramping[5].

The current approach to scanning strategy is limited to a handful of zones where different geometric features such as downskins, thin walls, part borders and bulk areas are exposed with different powers, speeds, offsets and overlaps. The user control is typically limited to commands that apply when the laser is on, while the parameters that dictate how and when the laser turns on/off and jumps from one vector to the next such as skywriting time and laser delays are commonly hidden. Although hidden, these parameters can have significant impact on the build quality, significantly affecting porosity and surface integrity.

A typical LPBF part is composed of millions of single melts or vectors and every vector has three distinct phases: the start, the middle, and the end. Khairallah et al. investigated the melt

pool with high-speed in situ x-ray imaging and identified that the high recoil pressures generated during the first 10's of microseconds of a melt can produce a "back spatter" of high velocity molten metal from the interaction zone and also identified the laser off region results in a "frozen depression"[2]. Furthermore, they were able to eliminate both back spatter and frozen depressions by simultaneously controlling the laser power and scan speed. If the laser power and scan speed are set below known keyholing parameters, Zhao et al. showed that it is unlikely for a stochastic keyhole to form[101]. Similarly, lack of fusion defects are unlikely to form if the hatch spacing to melt depth does not exceed 1, and laser energy is not scattered/absorbed prior to reaching the build plate(Gordon et al., 2020; Moran et al., 2021). Assuming a reasonable hatch spacing, and in-chamber gas flow sufficiently removes the products of the laser/powder interaction from the region so the laser reaching the build plate is not obstructed, our hypothesis is that most defects occur at the start or end of the vector during continuous wave laser operation. Although some manufacturers employ pulsed wave and modulated continuous wave lasers, this work is focused solely on the effects of continuous wave laser operation. A lengthwise cross section of a melt pool in IN718 is shown in Figure 44 and indicates the back spatter and frozen depression typically visible from the top view of a melt pool.
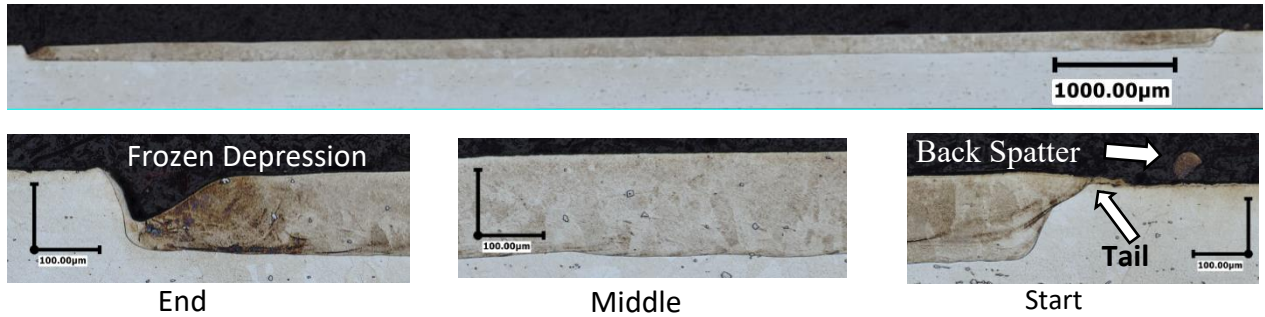
Figure 44 a) Lengthwise cross section of LPBF melt pool in IN718 b) start region with indication of frozen back spatter c) middle stable region d) laser off region with characteristic frozen depression.

Diehl et al. determined that interhatch travel time <4,000μs can increase the likelihood of porosity by 4-8x due to insufficient cooling time between adjacent melts and Mancisidor et al. determined the application of skywriting to ensure constant laser travel speed when the laser is on reduced near edge porosity [47,56]. Martin et al. was able to eliminate end of vector porosity by implementing a custom laser power control strategy based on the beams true speed and reducing the laser power as the galvanometer decelerated at hatch turning points, although sending this type of data to the scanner is not, at least presently, commercially available[15]. Although insightful, these works focus on a specific issue relating one aspect of machine control to one outcome and do not address impacts on the holistic part properties such as surface finish, microstructure effects, or mechanical properties.

Both surface integrity and near surface porosity have been identified as critical performance issues requiring improvements to eliminate gaps in LPBF. As-built LPBF surfaces have fatigue performance less than half of fully machined samples, as shown in [12] for both Ti64 and IN718. In some cases, near surface pores become surface pores during machining. The surface of a part has the most laser on/off interaction and typically the highest concentration of

defects or life limiting flaws [102–106]. Part location on the build plate is also known to affect surface quality. Rott et al. investigated the impact of incident angle relative to the overhang angle in LPBF of IN718 and found increased roughness on faces pointing away from the build plate center [59]. Others investigated the effect of laser incident angle on surface roughness concluding the greater the incident angle the higher the surface roughness due to over penetration or beam shape effects [58,67]. None of these works discuss back spatter or recoil pressure induced meltpool effects and none include significant detail on LPBF processing conditions reducing broad applicability, a common theme in LPBF research.

Commercial LPBF machines typically take a vector file (in CLI, SLI, MTT, or SLM format) that contains vector start/end positions and then divides each vector into micro vectors with individual lengths based on set scan speed and a 10μs clock rate. This means the laser and galvanometer (or galvo) are controlled at 100kHz, which can require specialized and costly research tools to investigate. For example, many publications examining processing in LPBF utilize in situ x-ray imaging from a high energy synchrotron source, high-speed cameras that can cost ~$100k US or more, X-ray computed tomography for post fabrication analysis, and an LPBF platform to conduct the experiments. To complicate these challenges further, the typical LPBF OEM platform does not provide user access to pertinent variables required for scanner control. While not frequently discussed, reducing the cost of investigation is an important aspect necessary for broader access and adoption, which is why many researchers utilize low-cost experiments such as single melt tracks on plates[43,107,108]. Lower-cost tests enable a larger community to participate in research and contribute to knowledge creation. In addition to broadening

participation, low-cost analytical methods are critical for industrial adoption and help enable monitoring of key machine performance variables at a reasonable cost.

In response to the issues highlighted above, particularly focused on laser control, this work investigates the formation of back spatter in IN718 to identify laser control parameters that can prevent its formation. Upon identifying appropriate laser ramping parameters, a complex qualification test artifact (QTA) described previously [109] is fabricated with and without laser power ramping to quantify the effect of laser control on spatter generation and material properties. It should be emphasized that this investigation reveals the effects of laser power ramping on a complex, real part, and highlights the complexity of the LPBF process requiring "intelligent" microsecond control to effectively implement. It further highlights those actions taken to improve particular outcomes can have unexpected consequences, and the holistic approach described here can be used to quantify the outcomes. The results indicate that laser ramping must be coordinated with scanning velocity to implement effectively, and that vector start spatter only accounts for a small portion of total spatter. Finally, results here demonstrated that for a complex part, the QTA, the spatter generated during fabrication totals over 50% of the total part mass, which is much higher than reported previously in literature. The following describes the experimental details and results from this research in more complete detail, although the specific prior work that motivated the current research is described next.

4.1.1 Motivation

The current work was specifically motivated by unpublished research that revealed build location and incident angle effects on surface roughness. The preliminary research was performed

on a commercial system that did not allow access to (or even knowledge of) control information required to perform a repeatable and reproducible experiment (a common problem with almost all commercially available LPBF systems today), and as such, served to motivate a more complete study on an open architecture machine. The authors believe it is important to include the following preliminary work, because (1) it served to motivate the more complete study described in the following, and (2) it describes a possible practical engineering solution (or workaround) that others may employ (and investigate further) using commercial systems. For the surface roughness study, Ti-6Al-4V 4-point bend fatigue samples with nominal dimensions of 5x5x70mm were fabricated on an EOS M 290 with EOS nominal "Ti64_PerfomancM291 1.10" parameter set (typical layout included 84 bars located throughout the build platform). The surfaces at the extents of the build plate facing the center had higher roughness (S_a=22) than the faces which pointed away from the center (S_a=19) as depicted in Figure 45a. This finding was contrary to Kleszczynski et al. where the surface roughness was shown to be greater in regions facing away from the center of the plate [58]. To investigate this effect, a single layer of the build was scanned directly on the surface of a plate and then imaged. The images revealed the beginning (or start) of hatch vectors protruding through the contours (hereafter referred to as "tails") on faces directed at the center of the build plate as seen in Figure 45b. In all incident angles (i.e., all build plane locations), including plate center, tails were identified; however, tails were less frequent and shorter when vectors started at the edge of the plate and scanned to plate center (Figure 47 right). As a preliminary solution to improve surface roughness on the EOS M290, the hatch offset was increased from 20μm to 240μm, and two additional contours were scanned (four total - 60μm apart). This was intended for the tails to be consumed with contour vectors depicted in Figure 45c.
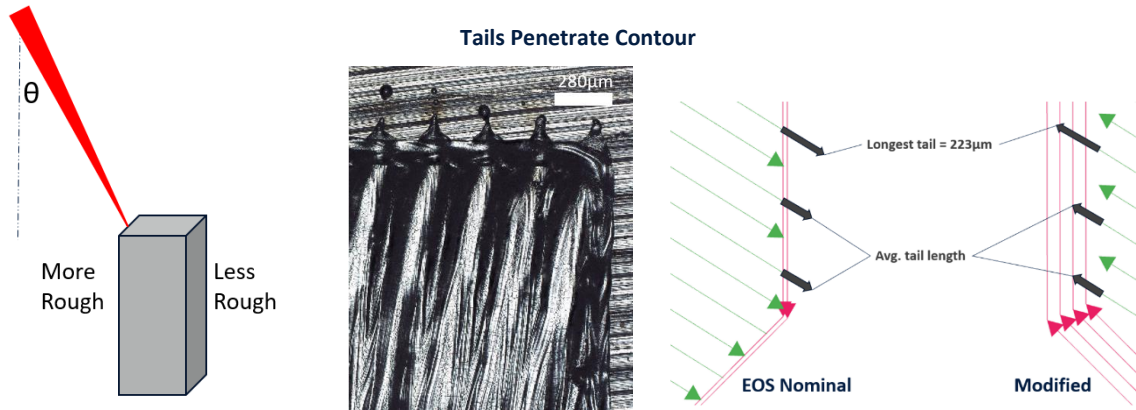
Figure 45 a) Incident angle definition diagram b) melts on Ti64 plate in EOS M 290 using OEM recommended Ti64 parameters showing tails protruding through contours c) depiction of results when hatch distance to parts edge was increased to account for tails (essentially to ensure a contour scans over the tails).

The mitigation strategy (Figure 46c) reduced roughness S_a and S_{vk} by $\approx 50\%$ with surface images shown in Figure 46a. 4-point bend fatigue testing was conducted on the as-built bars with nominal and improved roughness parameters to determine the effect of the surface improvement. However, the fatigue life, as seen in the S-N curves in Figure 46b, does not show appreciable difference between the roughness conditions. This result indicates that the observable roughness does not serve as a relevant indication of fatigue life for roughness values in the range of 5-20μm S_a, at least as measured through 4-point bend testing. Further details on the fatigue testing with more significant results will be published elsewhere.
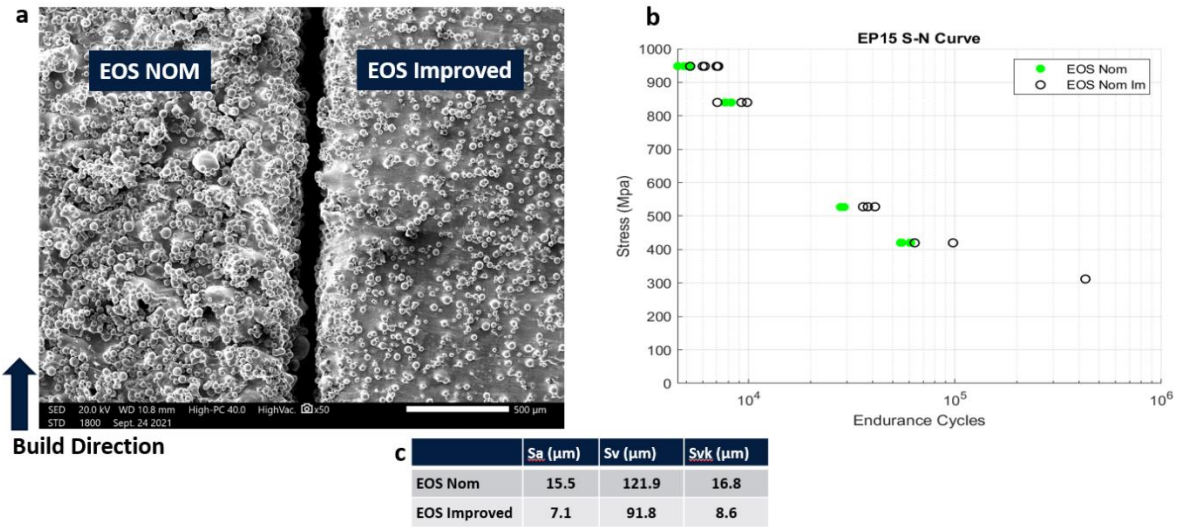
Figure 46 (a) SEM of surfaces with EOS nominal and improved contours removing effect of tails (b) S-N curve from 4-point bend fatigue of as built samples (c) surface roughness of the two parameters

What the above served to motivate was both the desire to eliminate the tails entirely and the realization that plate scans were able to identify the source of the roughness. Plate scans have subsequently been used to diagnose and evaluate enumerable effects in LPBF by our group. In the following, the plate scan method served as the experimental method for eradicating the occurrence of "tails", instead of mitigating their development by using, for example, "extra" offset contours as described above. It should be noted, however, that oftentimes in LBPF, the "band-aid" (practical engineering) solution described above is the only (or at least one of only a few limited) solutions available to the user, since many of the control variables required to modify are not available to the user by the LPBF OEM.

4.2 METHODOLOGY

4.2.1 Materials

Annealed 3.175mm thick plate of IN718 (compliant with AMS 5596) material was sourced from McMaster-Carr for laser melt testing, whereby the laser scanned the plate (called plate scans) without powder. Prior to performing the plate scans, the plates were prepared by abrasive media blasting with SiC media (<100mesh) @6.89kPa with 6.35 mm nozzle until finish was uniformly matte as measured by eye. After media blasting, plates were cleaned in an ultrasonic isopropyl alcohol bath to remove debris, and then washed with soap and water to remove oils.

IN718 powder with nominal particle size 15-53μm (AP&C, a GE Additive Company, Boisbriand, Quebec, Canada) and chemistry as supplied by the manufacturer (Table 10) was used for LPBF builds.

Table 9 Chemical *c*omposition of IN718 feedstock for test artifact builds *(AP&C Material Certificate MC-19-1296)*

Element	Ni	Fe	Al	Mo	Nb/Ta	Cr	Ti	S	P	O	N	Si
Wt%	53.31	18.54	0.53	2.99	5.07	18.4	0.96	0.002	0.003	0.006	0.005	0.05

4.2.2 Processing

4.2.2.1 LPBF Equipment

All plate scanning and part fabrication presented in the results were performed on an AconityMIDI+ (Aconity3D GmbH, Herzongenrath, Germany) equipped with dual lasers. In this work only one laser was used, a 500W continuous wave, water-cooled Yb-fiber laser (CFL-500, nLIGHT, Washington, USA) connected to a scanner head made by Aconity3D in collaboration with Raylase GMBH. The beam was characterized by a Cinogy FBP-2KF (CINOGY

Technologies GmbH, Duderstadt, Germany) to have a Gaussian astigmatic beam at the build platform with D4σ_x= 74µm and D4σ_y= 81µm.

The AconityStudio software unlocks all aspects of control of the LPBF machine including all scanner control card functions. This enables the user to leverage all laser/scanner control parameters available through the control card software. The scanner is controlled by a SP-ICE-3 control card (Raylase, Wessling, Germany) with built-in functions for laser power ramping, dynamic delay times, and dynamic power. These functions and more are not unique to Aconity3D or Raylase and can be performed on other systems; however, other OEM's do not typically allow users to access these commands. AconityMIDI+ laser ramp time was characterized by an oscilloscope (PicoScope 3000, Cambridgeshire, United Kingdom) by monitoring the analog voltage sent to the laser at a frequency of 1MHz. The ramp rate of the laser power was measured to be linear by monitoring the analog voltage command sent to the laser from the scanner control card.

4.2.2.2 Plate Scanning Tests

Plate scanning tests were conducted to identify processing conditions that reduce and eliminate the formation of back spatter and tails. All plate scans were conducted with vectors traveling perpendicular to the gas flow direction and hatching propagating towards the gas flow (flow optimized) as depicted in Figure 47. Plate scan .cli files for the AcoityMIDI+ were prepared in Autodesk Netfabb Ultimate 2022.1. Chamber conditions were set equal to a nominal build for gas flow, pressure, and oxygen (<1000ppm). Plates were set level to the recoater prior to scanning. For the AconityMIDI+, the center of the galvo scan field is at -82mm x, -40.5mm y relative to the

build plate center. The scans performed on the AconityMIDI+ accounted for the scan field offset by positioning the zero degree incident angle scans at -82mm x , -40.5mm y.
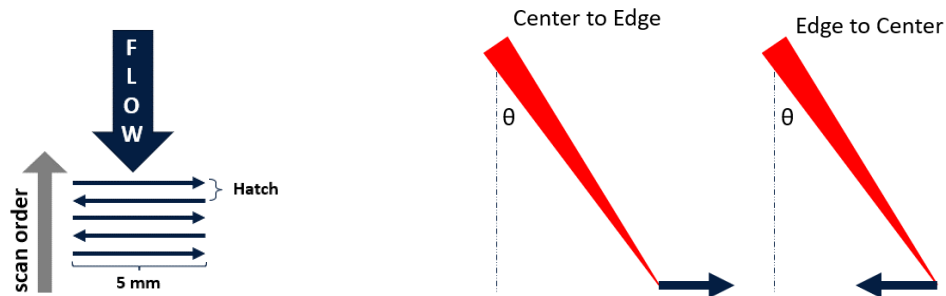
Figure 47 (left) Plate scan vector propagation relative to gas flow (right) definition of incident angle and vector scan direction relative to scan field center

Utilizing the above conditions, two experiments were conducted. First, a screening experiment for ramp rates was conducted testing 50µs, 100µs, 200µs, 300µs, and 400µs with 20 hatch vectors quantified for each ramp rate. A second full factorial experiment was conducted to evaluate other parameters such as laser speed at a constant power/velocity ratio, laser incident angle, and scan direction relative to scanner. Each experiment included four vectors or laser on events. A vector was then classified to have produced spatter, a tail or neither. The experimental factors and levels are described in Table 10.

Table 10 Full-factorial experimental design with 4 vectors for each combination

Factors	Levels	Units
Ramp rate	0, 100, 200, 300, 400	µs
Scan speed @constant 0.28 P/V ratio	1000, 750, 500	mm/s
Incident Angle	vertical, mid plate, extent	
Scan direction relative to scanner 0,0	center to edge, edge to center	

4.2.2.3 Qualification Test Artifact Builds

Builds of a complex Qualification Test Artifact (QTA) (described in [109]) were conducted with laser power ramp (referred to as build, UTEP18/ramp) and without laser power ramping (UTEP19/no ramp) to investigate the holistic impact of back spatter elimination on total spatter produced, porosity, and mechanical properties. Only the laser ramp function was adjusted between builds with all other parameters held constant. Artifacts (UTEP18/ramp and UTEP19/no ramp) are shown in Figure 49 after heat treatment. As described in more detail in [23], the QTA is a compact (40mm x 40mm x 40mm) and complicated artifact that is used to test metal LPBF system performance using a variety of metrics. In this case, only a single artifact was fabricated in each build with laser power ramp settings described in Table 11. The general print parameters for the build were 10mm stripes with a hatch spacing of 0.12mm, 280W laser power, and 1000mm/s scan speed. The parameters included 3 contours at similar P/v as the infill, but at 50% power (so 140W, 500 mm/s for contours). Full parameters are attached in Appendix A as a .json file which can be opened with Mozilla Firefox browser.

To quantify spatter generated during fabrication of a complicated part, the following method was employed. Prior to fabrication, all powder was removed from the system and sieved through a 230-mesh sieve then placed back in the machine. After plate leveling and prior to the build, the area around the print bed and supply hopper was vacuumed. After the build completed, spatter particles blown into the area between the built plate and the exhaust were separated with a metal scraper and collected. This powder is classified as "spatter behind platform". All remaining powder in the build platform, supply hopper, and overflow was collected and sieved with a 230-

mesh sieve and the captured +230 powder was classified at "oversized spatter in powder bed". All spatter captured was weighed to compare the difference in total spatter generation between UTEP18/ramp and UTEP 19/no ramp. The *spatter behind platform* was sieved through a -230 mesh sieve and divided in to +230 and -230 lots and weighed individually. Figure 48 depicts the amount of spatter generated from the build of each artifact. It should be noted that the spatter is visually apparent to the operator to be >10% of the small QTA. It should further be noted that the collection of spatter represents one build versus another and a statistical analysis of error has not been conducted.   However, the amount of spatter collected behind the build platform is representative based on prior experience. A statistical study of spatter for the QTA is the subject of ongoing investigations.
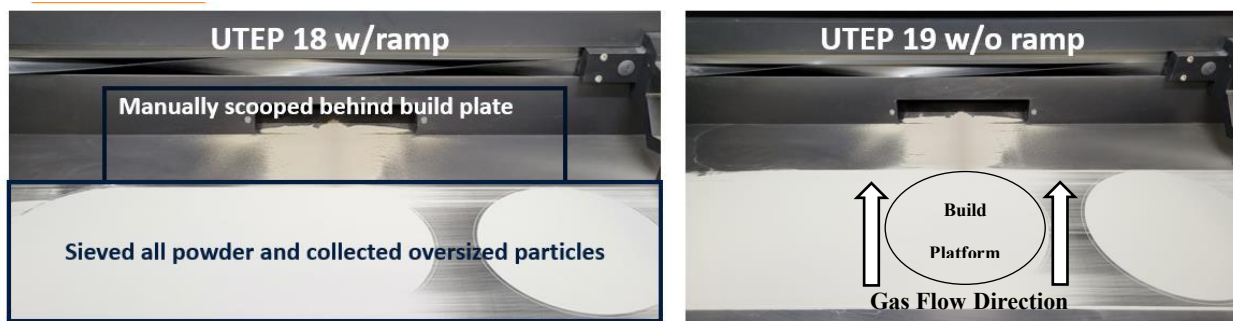
Figure 48 description of spatter collection regions in the AconityMIDI+ build chamber

Artifacts were heat treated together in a Carbolite-Gero tube furnace under vacuum. Samples were intended to be heat-treated at 1020°C for 20 min then quenched in water followed by aging under vacuum for 8hr at 720°C following a suggested optimal heat treatment by Gallmeyer et al. [17]. However, analysis of the heat treatment schedule revealed the internal thermocouple was not utilized to maintain the specified set point, and the actual temperature was roughly 100°C lower than the set point. As a result, the heat treatment schedule used here was ~920°C for 20 min, followed by rapid water quench, and a final aging under vacuum for 8hr at

620°C [19]. The lower solution temperature will not fully eradicate the presence of delta phase in the material, potentially reducing ductility, while the lower temperature aging is likely insufficient to fully develop the strengthening γ', γ'' precipitates. The combination of these two effects will result in lower yield, ultimate strength and ductility; however, both artifacts were heat treated at the same time and can be expected to have the same performance.

Table 11 Build ID and Laser Ramp Settings

Build ID	Laser Ramp Setting	Laser Ramp Time
UTEP19/no ramp	N/A	$< 5\mu s$
UTEP18/ramp	0.00175 $\%/\mu s$	$\approx 300\mu s$
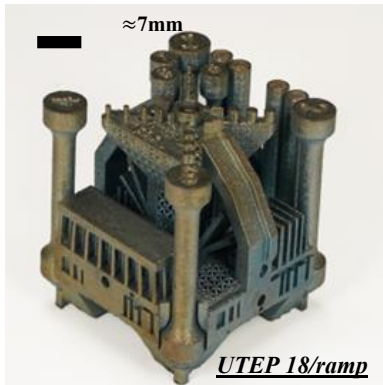
Figure 49 AconityMIDI+ fabricated UTEP18/ramp and UTEP 19/no ramp macro images post heat treatment

4.2.3 Analysis

4.2.3.1 Back Spatter and Tail Analysis

Video recording was performed during plate scans and QTA builds to identify the formation of back spatter and help to optimize the laser power ramp setting. High speed imaging was performed with a FASTCAM SA-Z (Photron USA, Inc. , California, USA) equipped with an Infinity K2 DistaMax with CF-1 objective (Infinity Photo-Optical, Colorado, USA) and no

additional illumination. Frame rate was set at 20,000fps with an exposure time of 48.39μs. As part of the effort to develop a low-cost analysis tool, a Samsung Galaxy S21 smartphone (Samsung, Suwon-si, South Korea) was used to identify the generation of back spatter vs no back spatter at a frame rate of 30fps, with camera resolution 1920x1080. Post plate scan imaging was performed to determine if the parameters created tails. Imaging was performed on a Keyence VHX-7000 (Keyence Corporation, Osaka, Japan) digital microscope at 100x magnification with ring lighting mode and 3D image stitching function to obtain one in focus image.

4.2.3.2 Feedstock and Spatter Analysis

Size and shape analysis was performed to further characterize the difference between virgin powder and spatter particles. Analyses were performed via dynamic image analysis on a CamsizerX2 (Microtrac Retsch GmbH, Haan, Germany) and via static image analysis in a JEOL IT-500 scanning electron microscope (SEM) (JEOL Ltd., Tokyo, Japan). For SEM analysis, powders were dispersed onto 9mm adhesive carbon pads and a 12mm^2 region was imaged with the secondary electron detector.

4.2.3.3 QTA Property Analysis

After heat treatment, the QTA tensile bars were removed by hand and the remaining bodies (UTEP18/ramp and UTEP19/no ramp) were analyzed for surface integrity prior to sectioning. Surface roughness of the QTA's were characterized with a Keyence VR5000 (Keyence Corporation, Osaka, Japan) wide-area 3D measurement system utilizing the software provided by the manufacturer. Tensile testing was performed on an MTS Bionix (MTS, Minnesota, USA) and strain was monitored with a Zwick-Roell laserXtens 2-120 HP non-contact extensometer

(ZwickRoell GmbH & Co. KG, August, Germany). A 25kN load cell was utilized for all testing with a strain rate of 0.05mm/sec the 4mm diameter cross section samples and 0.03mm/s for 2.5mm diameter samples. Fracture surfaces of select bars were analyzed in a JEOL IT-500 scanning electron microscope (SEM) (JEOL Ltd., Tokyo, Japan) and the images were analyzed in FIJI [110] by manually outlining the defect area over the entire fracture area to determine the defect percent of the fracture surface.

Porosity analysis of metallographic cross sections were done with images acquired on a Keyence VHX 7000 (Keyence Corporation, Osaka, Japan) capable of full 3D stitching at 100x magnification. The Microscope was calibrated with the OEM's calibration procedure and reported 1.034 µm/pixel. MIPAR image analysis software (MIPAR, Worthington, OH, USA) was then used to segment the image and perform porosity analysis. Pores below $177\mu m^2$ were not counted and every pore identified was manually confirmed to reduce likelihood of mis-classification of imaging artifacts or other non-pore component features.

4.3 RESULTS AND DISCUSSION

This work has identified three possible results when a high energy laser beam first interacts with a metal surface. These include (1) a partial ejection of material from the interaction zone that solidifies before detaching from the plate (defined as a tail); (2) a full ejection of material from the laser/material interaction zone, or (3) a clean melt pool formation (no ejecta or tail identified). It is important to note that real-time imaging is required to discern ejection of spatter due to the similar appearance of a clean laser weld and a spatter inducing laser weld (to be described below with text associated with Figure 8). Alternatively, tails can be observed on the plates with an optical microscope after experimentation. Each of the 460 melt pools created on plates in this

117

work were observed live and imaged post experiment to determine which of the three results occurred. Table A and B in the Appendix contain the results for all melt conditions evaluated.

4.3.1.1 Experiment 1: Plate Scanning Ramp Rate Results

Plate melts observed by high-speed video on the AconityMIDI+ revealed that particles were ejected from the meltpool in the first several hundred microseconds of exposure. Prior work by Khairallah et al. and Zhao et al. identified this phenomenon as "back spatter" and occurs in less than 100µs of the laser interaction [2,111]. Khairallah et al. was able to simulate this and subsequently eliminate its occurrence experimentally by ramping the laser power during the first 100µs of the melt.

In this work, laser ramp rates from 5µs to 400µs were conducted and back spatter observed at 5µs, 50µs, and 100µs in every vector melted for IN718. At 200µs, back spatter was still observed in several vectors but not every vector. At a ramp of 300µs and 400µs, no back spatter was observed. Figure 50 highlights the development of back spatter with a 50µs ramp time in IN718 plate and the elimination of back spatter with a 300µs ramp time (video in supplemental data).
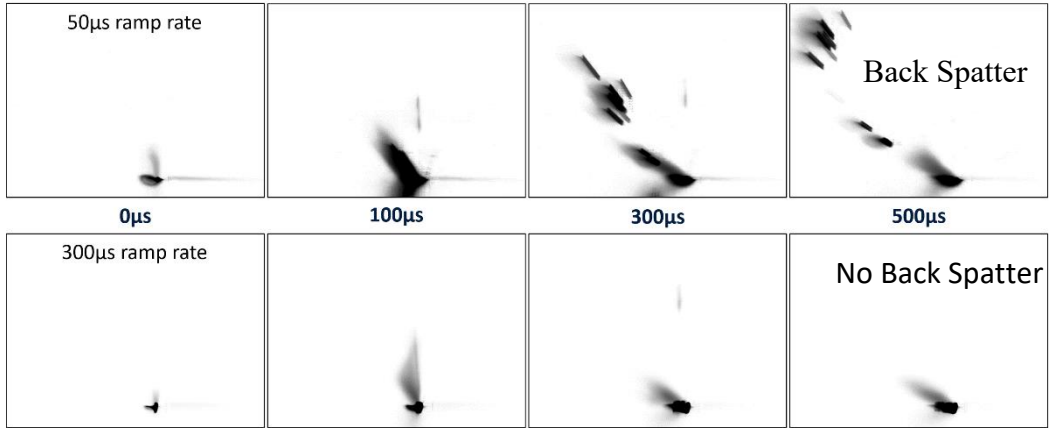
Figure 50 Top laser ramp to 280W at 50µs, bottom laser ramp to 280W over 300µs. Spatter is clearly evident in the 50 µs laser ramp rate sequence, while noticeably absent in the 300 µs sequence.

Post melt investigation of the plates indicated a distinct transition from back spatter>tail>clean melt. In IN718, a transition zone was identified at 200µs as seen in Figure 51 where a tail forms and freezes in place at the start of a vector.
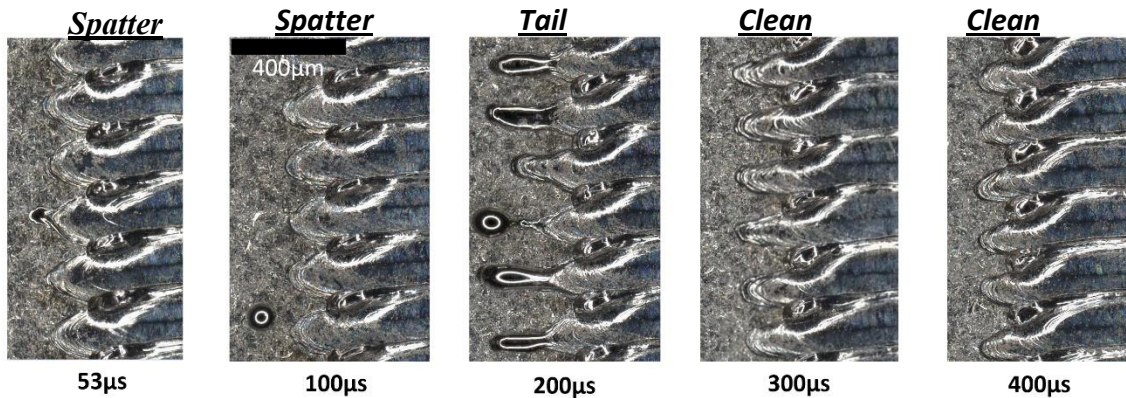
Figure 51 Resulting melt pool tails from laser ramp tests, spatter confirmed by high speed video

4.3.1.2 Experiment 2: Plate Scanning Ramp Rate, Scan Speed, Angle, Direction Results

As a follow-on to the experiment described above, a second set of experiments were conducted to expand the investigation to include scan speed, laser incident angle, vector direction, and ramp rate. The factors studied and described below are contained in Table 2. To investigate

the effect of scan speed, melts were performed at 75% and 50% nominal velocity (1000mm/s for IN718) while maintaining an equivalent power:velocity ratio (0.280 for IN718). The results of all melts performed on IN718 at 0° incident angle are shown in Figure 52. No back spatter or tails were observed at 50% velocity, 50% power conditions, indicating that lower processing speeds may have benefits with regard to spatter creation although lower processing speeds will negatively impact productivity.

IN718 Spatter/Tail Creation

- ■ Spatter + Tail
- ◆ Tails
- ● Clean

(y-axis: Power [w] @ Const. P/V = 0.28, range 0 to 300; x-axis: Ramp Time (µs), range 0 to 450)
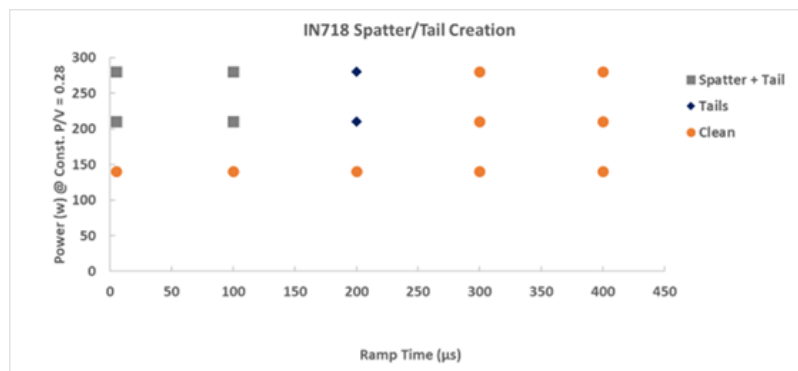
Figure 52 Scatter plot of constant P/V on IN718 versus Ramp Rate

To inspect the effect of incident angle, plate melts were performed at different distances from the scanner center. Figure 53 shows melts on IN718 without ramp at ≈15° incident angle, and spatter and tails were only observed when the laser travels away from the scanner while no tail or spatter is observed when the laser travels back towards the scanner. This observation challenges the use of recoil pressure induced by thermal gradients as a basis for ejection as described in [112,113] and indicates that the direction of recoil pressure relative to travel direction affects the melt pool shape. This experiment found that incident angle creates a complicated melt pool/spatter interaction, and, perhaps most importantly, that the direction of the scanning vector impacts this interaction.
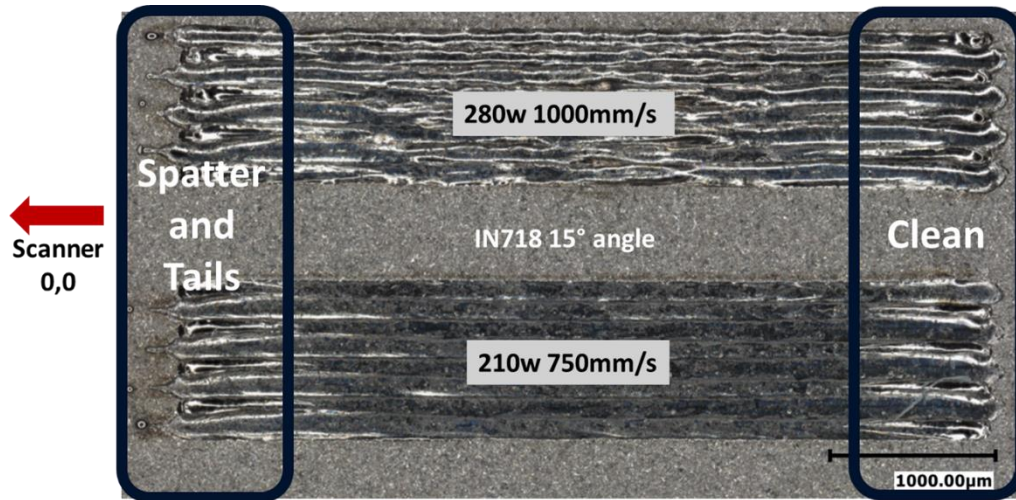
Figure 53 Optical microscope image of plate melt at high incident angle showing that a tail only forms when the laser scans away from the laser center point

Several prior works relate the ejection velocity to the recoil pressure to quantify a threshold value for laser processing parameters that prevent spatter[2,111,112]. Khairallah et al. defined a critical melt flow velocity for which a spatter particle equal in diameter to the laser beam would exceed the materials surface tension and generate a back spatter. This velocity was used to define the power ramp rate by ensuring the melt depth rate of change was less than V_{crit}, a value determined based on the materials surface tension, liquid density, and the beam radius [2]. Based on these works, a simplified figure (Figure 54) was created to describe the potential effect of scan speed, incident angle, scan direction, and ramp rate on direction of the induced recoil pressure and melt size. Lower scan velocities (500mm/s versus 1500mm/s) were shown to produce more vertical recoil pressure jets by Li et al. [113] and oblique incident angles relative to scan direction were shown to affect recoil pressure jets by Tsubouchi et al. [68], similar to the depiction in Figure 10.
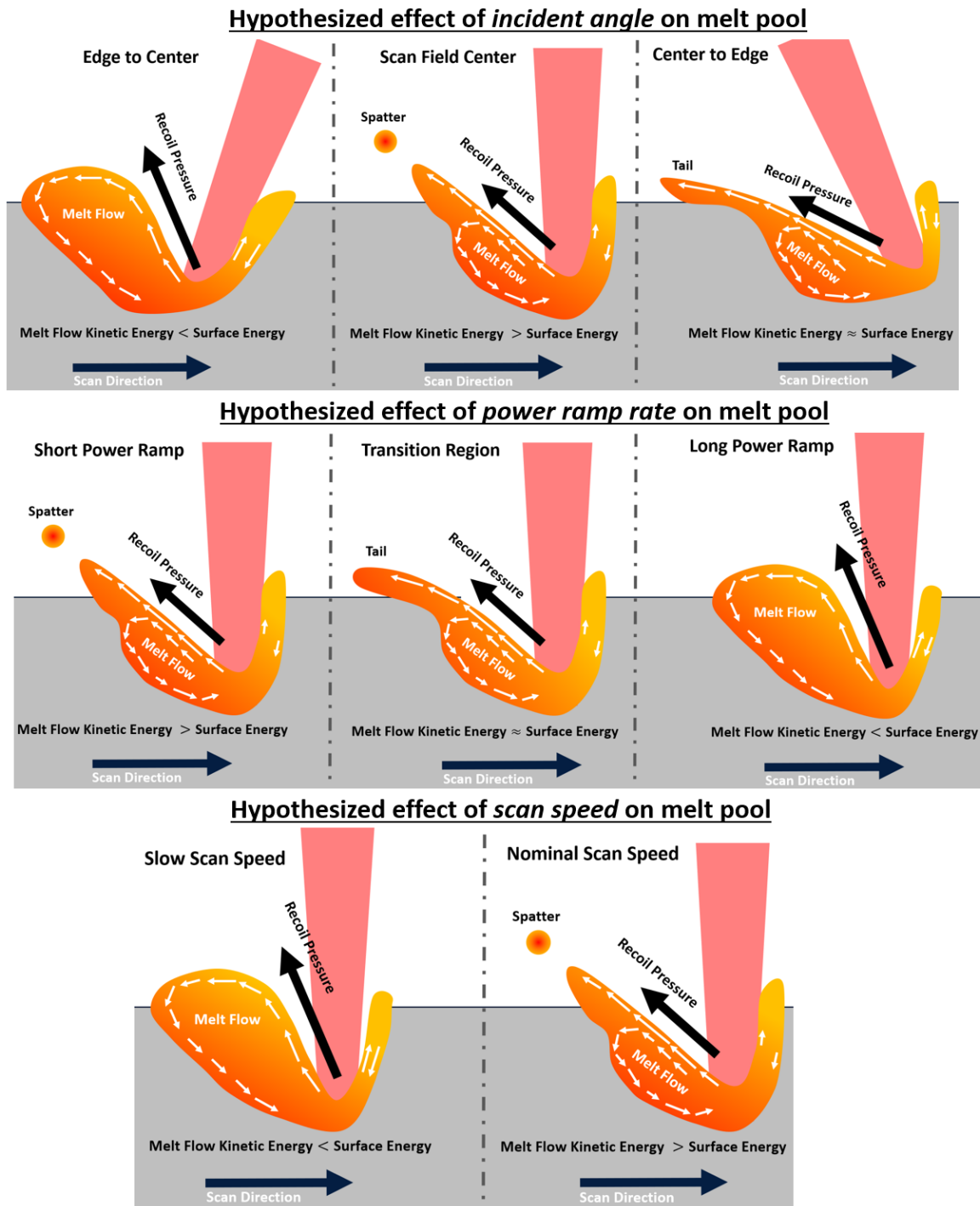
Figure 54 Hypothesized melt pool dynamics effecting spatter and tail formation based on experimental observations

As mentioned above, real-time monitoring was performed to visualize spatter using a high-speed camera (Photron SA-Z). However, as can be appreciated, using high-speed imaging is quite

costly in setup time, data acquisition and management, and actual financial investment. As a result, during this investigation, the authors identified a modern smartphone (Galaxy S21) was capable of capturing evidence of back spatter ejected during plate scans (full video in supplemental data). Figure 55 highlights the back spatter ejected from the melt pool without power ramp and the lack of back spatter when power ramp was 300µs. This approach is capable of classifying parameters with a Boolean indication of back spatter generation. In practice, after the melts are completed, they can be imaged with any optical microscope capable of 20x magnification to determine the presence of tails as defined in Figure 55. This method allows for users to obtain immediate feedback and potentially continuous health monitoring of their system over time.
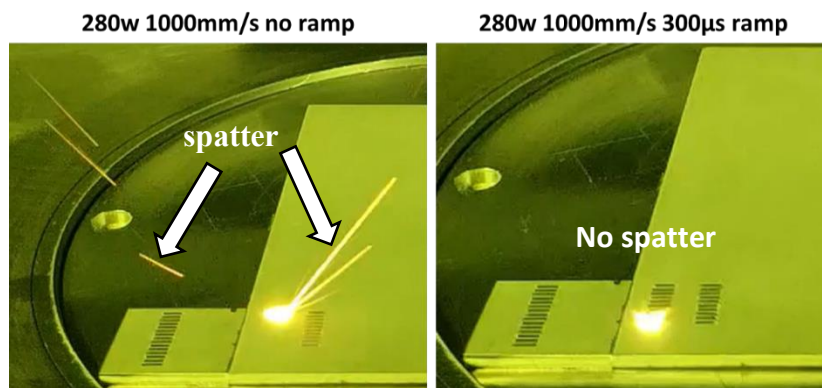
Figure 55 Low-cost melt pool analysis via Samsung Galaxy S21 full video in supplement (left) 280w 1000mm/s without ramp (right) 280w 1000mm/s 300µs

4.3.2 Spatter Analysis from Artifact Production

To understand the effect of laser ramping on spatter generation, the total number of vectors and number of laser "on" events was required. Table 12 details the results of a build file analysis that summarizes every vector from the slice file showing the artifact contains over 5.4km of weld. The average hatch vector length can be roughly estimated by dividing the total hatch weld distance by the number of vectors resulting in an average length of 3.47mm. At a scan speed of 1000mm/s the average vector takes 3470µs to complete. Based on the high-speed video, spatter is produced

continuously while the laser is at full power and the total reduction of spatter can be estimated as the percent of the total laser on scan time that the laser is ramping, which is roughly 7.2% of the overall build when accounting for both hatching and contour vectors. The actual reduction determined by the mass of collected spatter for UTEP18 w/ramp was 4.5%. Table 12 right summarizes estimation of spatter development assuming every time the laser turns on, it ejects material, and indicates why just eliminating a few spatter particles for every vector likely only reduces total spatter by a few grams. For example, if the 1,309,338 laser on events result in six spatter particles with $\sim 50\mu m$ diameter, the build would only generate 4.1g of spatter particles due solely to the laser on event.

Table 12 Summary of vector data to produce QTA for UTEP18/ramp and UTEP19/no ramp and summary of potential mass of spatter from vector start with range of assumption

Total Hatch Vectors	1,258,518	#
Total Hatch Distance	4,366,786	mm
Total Contour Starts	50,820	#
Total Contour Distance	1,123,794	mm
Total Hatch + Contour Starts	1,309,338	#
Total Hatch + Contour Distance	5,490,582	mm
Laser Ramp Distance	392,801	mm
% Build Laser Ramp	7.2%	
% Spatter Reduction	4.5%	

# of laser on events	Back Spatter Particles/Event	Equivalent Dia. (μm)	Total Mass of Back Spatter (g)
		10	0.03
		20	0.26
	6	30	0.89
		50	4.1
1309338		100	32.9
	1	97	5.0
	3	67	5.0
	6	53	5.0
	9	47	5.0

Surprisingly, the authors were unable to find significant research efforts quantifying total powder waste due to spatter for an LPBF build. The NextManufacturing website reports 10% waste of total part mass[114]. The QTA has a total solid volume of 25.8cm^3, so using IN718's theoretical density of 8.17 g/cm^3, the mass of a fully dense IN718 QTA is 210.8g. QTA UTEP18/ramp weighed 210g and produced 113.7g of spatter as shown in Table 13. The spatter is

greater than 50% of the part mass and significantly higher than the reported recyclable amounts of powder for a build [115,116].

Table 13 Spatter summary for UTEP 18 and UTEP 19

	Sieve Size	Spatter Behind Platform	Spatter in Powder Bed	Total Spatter	
UTEP18 Ramp	-230	**68g**	n/a	68g	113.7g
	+230	17.7g	28g	45.3g	
UTEP19 No Ramp	-230	**73g**	n/a	73g	119g
	+230	22.7g	23.3g	46g	

From the total spatter collected, ≈60% passed through the 230 mesh sieve and therefore would likely be reused in a production environment. Figure 56 highlights that this reusable powder's size distribution (from Camsizer X2 analysis) of the -230 mesh spatter particles for both UTEP 18 and UTEP 19 shift to a larger size than the virgin powder and this spatter induced change in particle size distribution may be a potential source of build-to-build variability. Further, qualitative SEM analysis of the Virgin IN718 vs the -230 mesh spatter behind platform reveals more fused spatter particles (Figure 56).
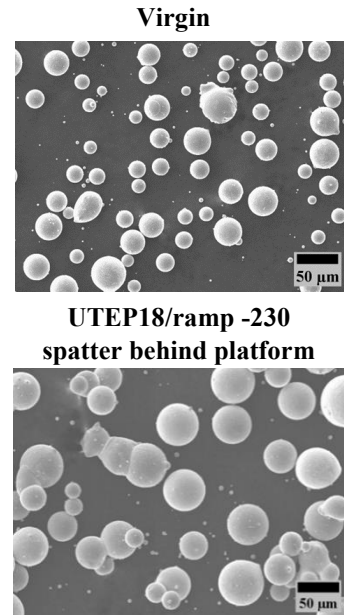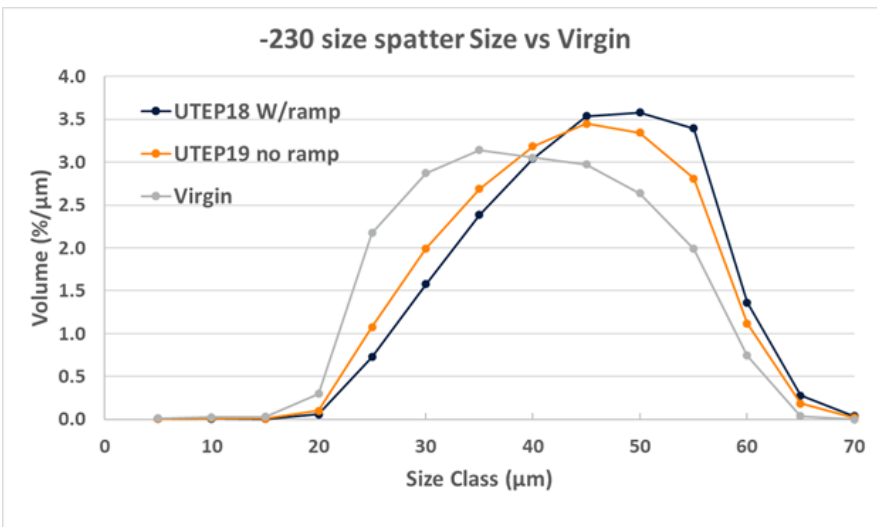
Figure 56 Powder size distribution of spatter vs virgin powder after sieving through 230mesh, representative SEM of (top right) Virgin IN718, (bottom right) UTEP18/ramp -230 spatter behind platform

4.3.3. QTA Analysis

4.3.3.1 QTA Surface Analysis

As described in the introduction, the motivation for this work was identified when high surface roughness in Ti64 was attributed to start of vector tails sticking through contours, and it was hypothesized that UTEP19/no ramp would have higher roughness than UTEP18/ramp. Both UTEP18/ramp and UTEP19/no ramp had vertical wall $S_a=8\pm1\mu m$ and $S_{pk}=14\pm1\mu m$. The similarity between UTEP18/ramp and UTEP19/no ramp indicates that tails are not protruding through the contour in IN718 builds. This result is not surprising as there were no observable tails with no laser ramping (UTEP19/no ramp) during the plate melt experiments.

4.3.3.2 QTA Metallography

The metallographic analysis of the QTA included ≈10.5 cm^2 for each specimen with a summary of the data shown in Table 14. The following describes analyses using the QTA, a holistic method the authors believe provides a significant advance over the use of cubes and tensile bars commonly used in LPBF research and part qualification [23]. It is the intent of the following to emphasize the ability of this approach to identify specific microsecond control issues associated with the LPBF processing route of real parts. A total of 2,109 pores were identified, and no pore with equivalent diameter greater than 50µm was identified more than 500µm away from the part edge. For both UTEP18/ramp and UTEP19/no ramp, defects were concentrated where part thickness was less than 1mm, highlighting the utility of the QTA to evaluate the LPBF process holistically as shown in Figure 57. UTEP18/ramp had more pores concentrated in thin regions, which is attributed to laser ramping for 300µs (300µm at 1000mm/s scan speed) creating shallow

126

melt pools at the start of the vector, and in some thin regions, this encompasses the full vector length (walls <0.5mm). In order to prevent this occurrence, the scan velocity must be controlled in a similar manner to the laser ramp to allow for full melt of the vector start[2].

Table 14 Porosity analysis summary of UTEP18/ramp and UTEP19/no ramp

	Pore Count	Total Area Measured (cm³)	% porosity	Max Equivalent Diameter (μm)	Average Equivalent Diameter (μm)	Max Caliper Diameter (μm)
UTEP 18 (Ramp)	1187	10.5	0.12	194	32.5	388
UTEP 19 (No Ramp)	922	11.1	0.08	184	28.1	350
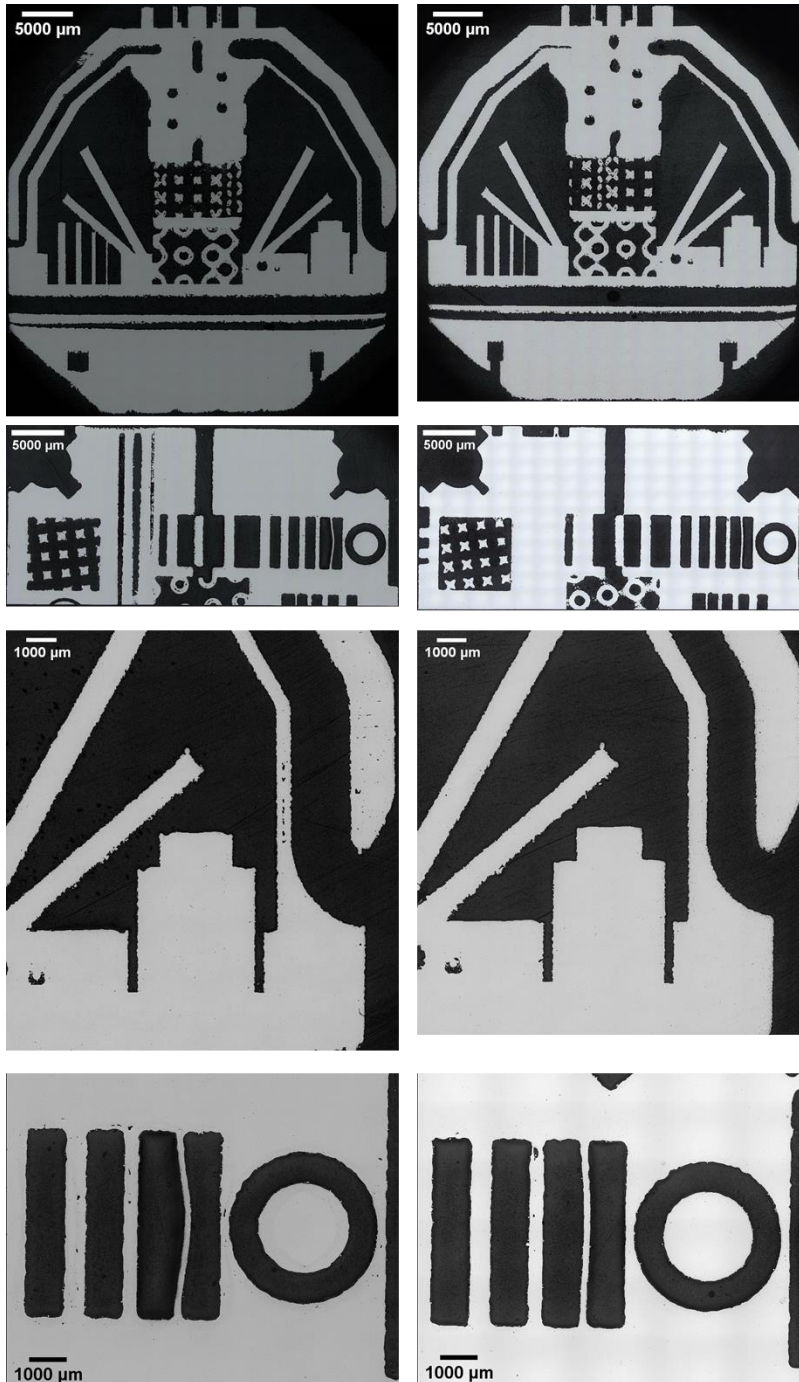
Figure 57 Porosity analysis of UTEP18/ramp and UTEP19/no ramp

4.3.3.3 QTA Mechanical Properties

Tensile testing is ubiquitous in LPBF research, and the results below question the utility of tensile testing to determine process sensitivity. As shown in Table 15, the net shape sub-size

ASTM E8 bars with as-built surface condition were able to exceed the ASTM 3055 standard for yield and ultimate strength. Further, a two-tail t-test showed no significant variation in UTEP18/ramp and UTEP19/no ramp yield strength or ultimate strength, despite the increased lack of fusion defects detected in UTEP18/ramp. However, a statistically significant difference in elongation to failure was identified between UTEP18/ramp and UTEP19/no ramp as seen in Table 15. It has been reported that tensile strength is not sensitive to defect populations below 1% but elongation to failure has been shown to be sensitive [32,99].

Table 15 Summary of tensile data

	0.2% Yield Strength (MPa)	Ultimate Strength (MPa)	Elongation at Failure (%)
UTEP 18 (Ramp)	1136 ± 12	1267 ± 21	12.8 ± 1.8
UTEP 19 (No Ramp)	1134 ± 24	1281 ± 17	17.8 ± 1.4
p value two-tail	0.83	0.19	0.00007

The fracture surface of bar 1 from each build was analyzed to compare porosity. The fracture analysis is presented in Figure 58, and both samples showed lack of fusion type defects near the sample edge indicated by unmelted or partially melted powder. The number of pores and area of pores in UTEP18/ramp was more than double UTEP19/no ramp with an area greater than 1% of the fracture surface. This level of porosity is in line with the defect volume required to affect tensile results [99,117]. UTEP19/no ramp fracture analysis revealed a defect area 5x higher than the metallographic porosity analysis and the tensile results showed no indication of poor performance. It is well known that a material's tensile properties are sensitive to microstructure and insensitive to defect populations below 1% if defects are considered uniformly distributed, yet the metal AM industry still utilizes tensile performance as a machine quality control method. This work further highlights that defects in LPBF AM are not uniformly distributed and therefore the

bulk porosity metric will not capture geometric specific properties. Based on this preliminary work, it would appear that machine quality control should be separated from materials performance characterization, and the authors plan on developing a more detailed approach for machine quality control and materials performance characterization for metal AM (LPBF, in particular) to be described in a future publication.

UTEP18/ramp Bar 1 Top
Defect Count = 10
Relative Defect Area = 1.13%
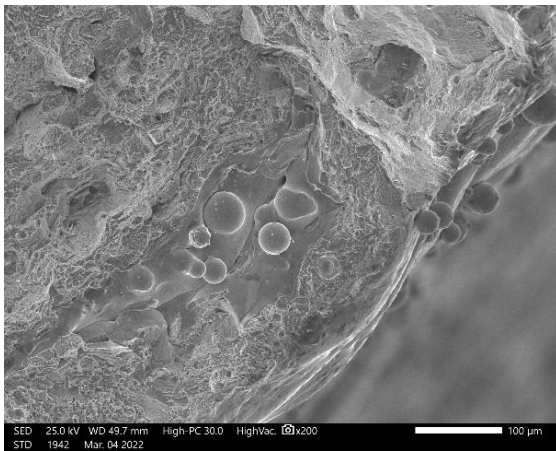
UTEP19/no ramp Bar 1 Top
Defect Count = 4
Relative Defect Area = 0.42%
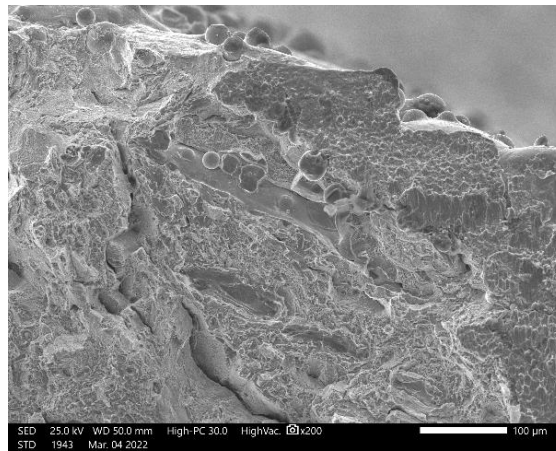
Figure 58 left) Lack of fusion defect near contour of UTEP18/ramp; Right) smaller lack of fusion defect in UTEP19/no ramp near contour

4.4 CONCLUSIONS

Laser powder bed fusion is a complex manufacturing process where every microsecond influences the component's integrity. This work demonstrates the importance of evaluating the impacts of microsecond control in LPBF, particularly laser power ramping, that could positively impact part quality but have not been investigated previously on complex geometries representative of real parts. Although this work was performed with a constant laser beam diameter on a single alloy (IN718), the methods described allow for rapid evaluation of any alloy

on any LPBF machine. The following bullets highlight conclusions that can be determined from this research.

4.4.1 Microseconds impact on back spatter and tails formation

- It is possible to eliminate spatter and the formation of frozen tails at the start of vectors in IN718 by ramping the laser power linearly from 0W to 280W over the first 300μs of the melt.

- Eliminating back spatter during LPBF fabrication can reduce total waste by ~4.5% in a single build to build comparison for a complex part (40mmx40mmx40mm, total volume of 25.8cm^3; QTA as described in [109]) built with 1,309,338 "laser ON" events and totaling 5.4 km of melt.

- The total amount of spatter collected was more than 50% of the total mass of the fabricated geometry (115g spatter for 210g part), significantly higher than previously reported.

- Laser incident angle relative to the vector travel direction can dictate whether a spatter, tail or clean melt occurs, indicating laser power, scan speed, spot size, and material properties are not sufficient to identify if a spatter/tail will occur.

4.4.2 Microsecond impact on part quality

- Controlled laser ramping without modification of the scanning speed results in lack of fusion defects at the start of vectors increasing porosity from 0.08% to 0.12% in a build-to-build comparison. The effect is magnified in the 2.5mm diameter sub-size tensile bar with porosity found to exceed 1% in the fracture surface analysis.

- The yield and ultimate strength were not statistically different between the two builds despite the difference in porosity, although the elongation to failure was statistically

different between the two builds. The lack of sensitivity to defects in tensile strength is well documented, and therefore, the authors recommend tensile testing should not be used to characterize machine performance.

- Most commercial LPBF systems limit what users can adjust, including laser power ramping, and a possible solution is scan strategy modification without elimination of spatter and tails by increasing hatch offset and modifying contours. This solution was shown in the introduction as a method for reducing surface roughness in the example by 50%.

4.4.3 Microsecond impact on investigation

- A method to determine appropriate ramp rate (and other parameters) without the need for high-speed monitoring is proposed requiring only a modern smartphone and an optical microscope.

- LPBF processing settings not frequently known to the user (scanner delays, skywriting times, etc.) and the high cost associated with investigating microsecond events slows advancements and often limits knowledge to the specific make and model of the machine being used.

There are 1,309,338 laser "on" events in the small 25cm^3 (0.21kg) part described in this work, and the user of a commercial LPBF machine cannot adjust or monitor any parameter related to these events. Due to the significant impacts that events taking microseconds have on surface roughness, defect populations, and spatter, it is clear that the removal of these settings from the "black box" is necessary before any effort related to standardizing materials properties across machines will be successful. The authors believe "intelligent" control of these events along with other advancements in removing variation from builds due to chamber gas flow, scanning

strategies, and other variables, will ultimately lead to repeatable and reproducible fabrication of components not only within single machines, but across machines as well.

Future work will include investigation into the total recyclable powder and spatter across common LPBF alloys and platforms as well as advancing the laser power ramp control to include galvanometer speed control. It is anticipated that a holistic approach and the removal of the black box will enable industry to move beyond cubes and tensile bars as the quality control metric.

necessarily representing the official policies or endorsements, either expressed or implied, of

AFRL, NASA, NIST or the U.S. Government.

Chapter 5: Path from Metal Art to Metal Manufacturing

At the onset of this work, the end game was a sensitivity analysis of structure and properties for constant input parameters like laser power, scan speed, and hatch space on at least three different LPBF machine makes/models. This required the development of a test artifact that enabled evaluation of structures and properties as a function of part complexity and the ability to control the build parameters. The QTA was developed along with evaluation procedures for this purpose. The scan strategy dictates the thermal history of the part at a micron scale and must be fully defined to perform any analysis of sensitivity to machine make/model. Unfortunately, it is not possible to fully define the scan strategy on any commercial LPBF machine today. This inconvenient truth has led to a proposed solution and potential significant impact on LPBF manufacturing of metal.

5.1 WHAT IS PREVENTING LPBF FROM REACHING ITS POTENTIAL?

There are over twenty metal LPBF machine manufacturers today and many have proven capable of producing high quality metal parts certifiable for use in space, aerospace, oil and gas, and medical industries. The report from the FAA – EASA joint workshop on qualification and certification in additive manufacturing in 2018 highlighted several success stories in the aerospace industry such as the GE part family of qualified CoCr parts used in the GE9X engine[118]. However, this workshop and other similar events site common issues with materials, design, machines, and controls that limit broader adoption due to reliability and repeatability concerns.

A primary motivator for adopting AM in the Air Force today is reduced lead time, lower cost, and increased performance. An extreme example of this is seen in the need for a latrine cover

quoted at $8,500 that was produced via material extrusion at a cost of less than $500 (not accounting development time)[119].   Another example includes a non-critical seal retention handle[120]. When attempting to procure via traditional methods, no bids from the industrial base were received at a fixed price >$2,000. The Air Force Rapid Sustainment Office (AFRSO) was able to print the part for <$200.   The cost of development, and likely other factors, were not included in the report [120].

Based on the last four years of work in the field of LPBF AM, I will include my opinions, thoughts, and recommendations throughout Chapter 5. Additive manufacturing is an amazing tool. But like all tools, it must be used in scenarios where cost savings, lead time reductions, or performance increases are achievable for AM to be effective. In many cases, the options appear to be the traditional way (the way it was made originally) or additive manufacturing. I was unable to find a decision tree that allowed for the selection of the best manufacturing method that may be neither the traditional way nor additive way. Significant cost and time savings could be achieved by streamlining the selection approach to enable all manufacturing to compete for part creation.

Most recently, an article published in September 2022 entitled "The Strategy for American Leadership in High-Consequence Additive Manufacturing", a result of the National Science and Technology Council and Materials Genome Initiative, listed 6 key areas to enable critical part production with AM[121]:

1. Well-defined requirements
2. Validated performance modeling and analysis capabilities
3. Well-characterized materials and materials designed for AM
4. In-situ process monitoring and control with known measurement uncertainties
5. Tailored post-processing and non-destructive evaluation (NDE)
6. Secure, registered, interoperable data

The six pains highlighted in this report are undoubtedly important, yet none focus on ensuring the process itself is capable of producing reliable and reproducible components. The article references the need for advanced process control to enable feedforward or AI/ML informed scanning strategy and simply states that today's software tools limit toolpath options. The entire LPBF community is providing endless investment in attempting to make a repeatable and reproducible process through "band-aids" without addressing the core problems of the process itself.

The missing link is the AM toolpath control and, more importantly, **toolpath transparency**. The industry accepts that the process control happens at the microsecond level but is content to represent the process parameters with a simple excel sheet. In a recent article focused on the melt pool level simulation, the authors identify the melt pool depth will increase after the hatch turnaround and near overhanging regions due to heat accumulation or lack of time for heat dissipation[40]. The authors qualitatively confirm the prediction by experimental analysis of the melt pool structure which is shown in Figure 59.**Error! Reference source not found.** through a notional rendering. Unfortunately, this leaves the author, reader, and industry with no ability to apply this knowledge due to a simple statement made in the text, "Although skywriting was enabled, the ramp-up and ramp-down time is not known, and hence a constant power is assumed throughout the simulation."[40].
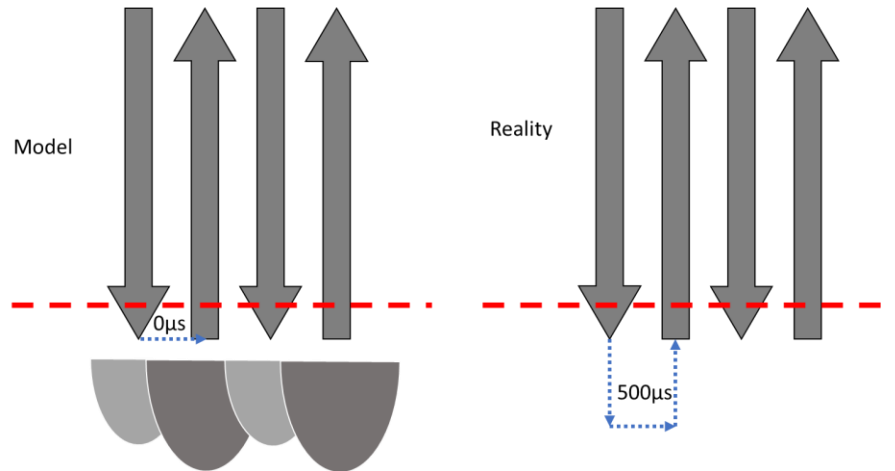
Figure 59 diagram of vector turnaround melt pools and the reality of skywriting time

The lack of machine "state" documentation (gas flow, spotsize, oxygen content) and toolpath transparency render the vast majority of information in the public domain useless. Without transparency in the actual processing conditions (providing spatially and temporally resolved laser beam power and on/off condition for each layer, along with environment chamber conditions such as O_2 concentration, humidity, actual build plate position, and laser optic cleanliness), it is my argument that additional investment in attempting to scale LPBF into a real manufacturing process is futile. Demonstrations of certified components will continue, but the qualification process will remain too costly for the promised impact of AM to be realized.

5.2 How Do Other Metal Manufacturing Methods Certify Parts

Production of critical parts is achievable with casting, forging, and wrought alloys. But how does the process work? There are hundreds of aerospace material specifications, MIL-standards, guidelines, and handbooks for design, material selections, process selection, control,

testing, and life cycle management. In traditional manufacturing of aircraft structures, the Air Force points to the Aircraft Structural Integrity Program (ASIP) which details the five tasks and sub tasks presented in Table 16. Lack of knowledge and standards in the blue boxes are currently preventing further adoption of metal AM for aerospace structure. The table also serves as a reminder that printing metal does not wholly solve problems and that it is only a piece of the larger system around aircraft structures.

Table 16 annotated table form MIL-STD-1530D[1]

TABLE I. USAF Aircraft Structural Integrity Program Tasks.

TASK I	TASK II	TASK III	TASK IV	TASK V
DESIGN INFORMATION	DESIGN ANALYSES & DEVELOPMENT TESTING	FULL-SCALE TESTING	CERTIFICATION & FORCE MANAGEMENT DEVELOPMENT	FORCE MANAGEMENT EXECUTION
5.1.1 ASIP Master Plan	5.2.1 Material and Structural Allowables	5.3.1 Static Tests	5.4.1 Structural Certification	5.5.1 L/ESS Execution
5.1.2 Design Service Life & Design Usage	5.2.2 Loads Analysis	5.3.2 First Flight Verification Ground Tests	5.4.2 Strength Summary & Operating Restrictions (SSOR)	5.5.2 IAT Execution
5.1.3 Structural Design Criteria	5.2.3 Design Loads/Environment Spectra	5.3.3 Flight Tests	5.4.3 Force Structural Maintenance Plan (FSMP)	5.5.3 DADTA Updates
5.2.1 Durability and Damage Tolerance Control	5.2.4 Stress and Strength Analysis	5.3.4 Durability Tests	5.4.4 Loads/Environment Spectra Survey (L/ESS) System Development	5.5.4 L/ESS and IAT System Updates
5.1.5 Corrosion Prevention & Control (CPC)	5.2.5 Durability Analysis	5.3.5 Damage Tolerance Tests	5.4.5 Individual Aircraft Tracking (IAT) System Development	5.5.5 NDI Updates
5.1.5.3 Nondestructive Inspection (NDI)	5.2.5 Damage Tolerance Analysis	5.3.6 Climatic Tests	5.4.6 Force Management Database Development	5.5.6 Structural Risk Analysis Updates
5.1.6 Selection of Materials, Processes, Joining Methods, & Structural Concepts	5.2.7 Corrosion Assessment	5.3.7 Interpretation and Evaluation of Test Findings	5.4.7 Technical Orders	5.5.7 CPC Plan and Corrosion Assessment Updates
	5.2.8 Sonic Fatigue Analysis	5.3.8 Resolution of Test Findings		5.5.8 Analytical Condition Inspection
	5.2.9 Vibration Analysis			5.5.9 FSMP Updates
	5.2.10 Aeroelastic and Aeroservoelastic Analysis			5.5.10 Technical Order Updates
	5.2.11 Mass Properties Analysis			5.5.11 Repairs
	5.2.12 Survivability Analysis			5.5.12 Force Management Database Execution
	5.2.13 Design Development Tests			5.5.13 Structural Certification Updates
	5.2.14 Structural Risk Analysis			5.5.14 Economic Service Life Analysis Updates
	5.2.15 Economic Service Life Analysis			5.5.15 Others as Required

Note: Numbers refer to and are hyperlinked to sections of this document.

Materials and structural allowables described in ASIP require established data for a material, the type of data that is found in Metallic Materials Properties Development Standardization Handbook (MMPDS). Materials Allowables are defined by MMPDS as *"A bulk material property derived from the statistical reduction of data from a stable process. The amount of data required to derive these values is governed by the statistical significance (or basis) and methods defined in Chapter 9. Application of material allowables may require additional considerations for use in design."*[122] MMPDS represents the alloy produced under a relevant standard, but each chemistry can have multiple standards and therefore datasets. IN718 has data for nine different AMS specifications that represent different production methods, forms, and applications. Furthermore, each can have multiple datasets based on thickness and loading direction relative to forming direction. AMS 5662N for precipitation hardened IN718 bars contains A basis data for eight thickness ranges each with data for longitudinal and transverse loading (i.e. 16 total ultimate strength allowables). Despite the range of design allowables for a single specification, it does not list a manufacturer, machine, make, model, serial number or software version and the AMS spec does not either. The material properties are therefore a function of the chemistry, thermal/mechanical history, the shape/size/surface of the part, and the loading conditions. The specification will often define bounds for max/min component size, the technical requirements (chemistry, tensile properties, microstructure, defect limits), and the quality assurance provisions to include acceptance criteria. The determination of whether a material requires different design allowable data for thickness or anisotropy is done based on statistical analysis of data defined in MMPDS chapter 9[123]. Many fear geometry specific based properties for AM but traditional manufacturing has already overcome this concern.

The acceptance criteria for a part manufactured according to AMS 5662N are listed in Table 17. The terms "melt" or "heat" and "lot" or "batch" are utilized in casting and forging to define intervals for testing. Composition analysis must be performed on each melt/heat defined as the charge used to create the cast or wrought stock after the final chemistry addition to the melt. A melt can be used for many lots or batches which are defined as going through heat treatment together in a single furnace. At a minimum one or two tensile samples are required per batch/lot. The combination of chemistry and tensile performance informs the quality of the materials microstructure. Tensile properties are sensitive to microstructure changes that thermal and mechanical history introduce. However tensile properties are not sensitive to defects and in general defect population in a tensile specimen vs the actual part may, and often do, vary [99].

Table 17 List acceptance criteria

Melt/Heat	Chemistry				
Lot/Batch	Tensile	Hardness	Microstructure	Grain Size	Stress rupture
Part/Piece	Tolerance				

The process described above does not result in part certification but creates confidence in material properties and serves as a basis for design allowable data. When this material is to be used as a part either cast, forged, machine or a combination thereof it must be certified. Typically, casting and forgings from a well-established firm will destructively test a first article to include cut ups and potentially instrumented load bearing tests. During this process, the part level inspection procedures are developed and documented. Nondestructive inspection methods are established and utilized in the serial production of subsequent parts. Beyond the first article, the inspection frequency is set based on criticality and supplier/buyer criteria. **In many regards the supplier/buyer agreement is the most important criteria for a given standard making new entrants into the manufacturing industry for critical components challenging.**

5.3 HOW HAS LASER POWDER BED FUSION MANAGED QUALIFICATION THUS FAR?

There is a path to certification today for flight critical components; however, the path is not scalable in time or cost. Dr. Mark Benedict of AFRL stated that it currently takes roughly 18 months and \$1,500,000 to develop materials data for a new LPBF machine within the Rapid Sustainment Office (RSO) directorate at an America Makes event. This development process may or may not enable trust and final component inspection is potentially cost prohibitive for commercial opportunities especially by small and mid-sized business. As part of my work related to GTADExP and DRIVE AM, I was able to travel to the Advanced Technology and Training Center (ATTC) Dayton and Middle Georgia (part of the AF RSO) to build QTA's. They had 15 EOS M 290's between the two facilities and had performed an internal development study to optimize build parameters. Most materials, including the ones utilized to build artifacts, had s-basis data available for the "optimized" parameters. Despite the significant effort to develop these parameters and subsequent data, no artifacts were built successfully at either facility (4 build attempts with 3 artifacts in each attempt). Example of RSO qualification build and the result of using the exact same parameters on a qualification test artifact is shown in Figure 60. This means the materials allowables data does not directly translate to parts built with those parameters.
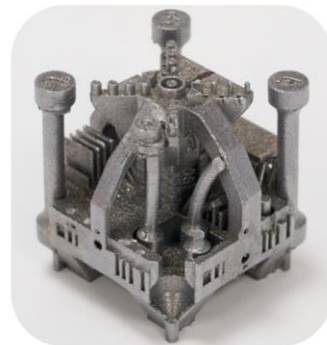
Figure 60 Example of RSO qualification build and the result of using the exact same parameters on a qualification test artifact

The current approach to LPBF qualification can be generalized and simplified as follows:

1. Identify potential component
2. Source powder/choose machine make/model/SN
3. Perform Design of Experiments to identify "optimal" parameters (based on historic knowledge and not standards)
4. Produce samples (fatigue, tensile, density, metallography) to develop material properties for that machine/make/model/serial number/software/firmware/scan parameters
5. Measure machine state
6. Lock down all settings
7. Repeat all the above for new machine/software/scan settings and more

The standards development community for AM has been very active over the past 5 years with SAE, ASTM, and NASA leading the way. Table 18 describes the relevant ASTM, NASA, and AMS specs/standards related to LPBF; only one alloy is included for alloy specific standards, but standards for several other alloys exist and follow a similar structure.

Table 18 Standards and Specs related to LPBF

	Org.	STD #	Title
Feedstock	AMS	7001	Nickel Alloy, Corrosion and Heat-Resistant, Powder for Additive Manufacturing, IN625
	ISO/ASTM	52907	Additive manufacturing — Feedstock materials — Methods to characterize metal powders
Material Properties	AMS	7000A	Laser-Powder Bed Fusion (L-PBF) Produced Parts, Nickel Alloy, Corrosion- and Heat-Resistant, IN625 Stress Relieved, Hot Isostatic Pressed and Solution Annealed
	ASTM	F3056	Additive Manufacturing Nickel Alloy (UNS N06625) with Powder Bed Fusion
Machine Parameters & IQ/OQ/PQ	AMS	7032	Machine Qualification for Fusion-Based Metal Additive Manufacturing
	AMS	7003A	Laser Powder Bed Fusion Process
	ISO/ASTM	52941	Additive manufacturing — System performance and reliability — Acceptance tests for laser metal powder-bed fusion machines for metallic materials for aerospace application
	ISO/ASTM	59204	Additive Manufacturing – Process Characteristics and Performance: Practice for Metal Powder Bed Fusion Process to Meet Critical Applications

	ISOASTM	52930	Additive manufacturing — Qualification principles — installation, operation, and performance (IQ/OQ/PQ) of PBF LB equipment
	NASA	6030	ADDITIVE MANUFACTURING REQUIREMENTS FOR SPACEFLIGHT SYSTEMS
	NASA	6033	ADDITIVE MANUFACTURING REQUIREMENTS FOR EQUIPMENT AND FACILITY CONTROL
Design	ISO/ASTM	52911	Additive manufacturing — Design — Part 1: Laser based powder bed fusion of metals
Personnel	ISO/ASTM	52941	Additive manufacturing — Qualification principles — Qualifying machine operators of laser metal powder bed fusion machines and equipment used in aerospace applications
	NASA	6033	ADDITIVE MANUFACTURING REQUIREMENTS FOR EQUIPMENT AND FACILITY CONTROL
In situ monitoring	ASTM	E3353	In-Process Monitoring Using Optical and Thermal Methods for Laser Powder Bed Fusion
Post processing	ASTM	F3530	Standard Guide for Additive Manufacturing — Design — Post Processing for Metal PBF LB
	ASTM	F3301	Standard for Additive Manufacturing – Post Processing Methods – Standard Specification for Thermal Post Processing Metal Parts Made Via Powder Bed Fusion
Facility	NASA	6033	ADDITIVE MANUFACTURING REQUIREMENTS FOR EQUIPMENT AND FACILITY CONTROL

The current standards cover most of the workflow related to LPBF part production. **However, it is important to note that specific standards for scan strategy and build file generation are not included, and in my opinion, this is the greatest need for the industry.**

5.3.1 Feedstock:

All standards acknowledge the "garbage in – garbage out" sentiment as it relates to feedstock and require the part produced to be validated with data tracked for feedstock usage, recycling, and storage. AMS specs go a step further to classify maximum oxygen levels based on powder size distribution as shown in Table 19 from AMS 7001. AMS 7001 also defines a minimum acceptable apparent density of $3g/cm^3$, or roughly 35% theoretical mean density (TMD); however, the minimum acceptable apparent density utilized for material acceptance in the W.M.

Keck Center for 3D innovation is 50% TMD. It is very important for standards to place limits and tolerances on acceptability; however, values that are not data backed will likely cause more harm than good. There is no reference to where this number came from, and no literature was identified to corroborate this value. The industry has not defined a spreadability metric in a standard but powder quality plus spreading method impact spreadability [76].

The major differentiator between NASA and the other specs is NASA requires a machine to never change alloy family, meaning if it is installed with Ti64, it can never be used to produce IN718 parts[27]. This is likely the correct approach for critical parts; however, no spec takes the next step to define if a facility can have two machines of different alloy families. **In my opinion isolating machines of different feedstocks to separate positive pressure rooms is necessary for flight critical parts.**

Table 19 AMS 7001 powder oxygen limits based on Particle size range[124]

	O Limit Wt.% Max	General Size Range	Fines Tolerance (Max)		Coarse Tolerance (Max)	
Class A	0.015 (150 ppm	>45 µm, <125 µm	10 wt%	<45 µm	>125 µm	10 wt%
Class B	0.030 (300 ppm)	>10 µm, <53 µm	5 wt%	<10 µm	>53 µm	10 wt%
Class C	0.040 (400 ppm	>5 µm, <30 µm	5 wt%	<5 µm	>30 µm	5 wt%

5.3.2 Finished part properties:

ASTM and AMS both have material property specifications for various alloys but currently only overlap with an IN625 spec. The specifications both report the same chemistry requirements apart from oxygen which is not mentioned in the ASTM F3065 but is limited to 0.03wt% in AMS 7000A[125]. Table 20 lists the tensile property minimums for equivalent thermal processing (HIP and solution annealed) with respect to AMS and ASTM as well as AMS 5666 bar S-basis data.

The ASTM minimum strength is considerably lower than the AMS minimum raising concerns as to how material produced via the same manufacturing process can have such variation in minimum part properties. ASTM F3056 references MIL-C-24615A Grade B as source for the material properties, which covers castings of IN625 last updated in 1988. AMS does not directly discuss the source for its material property minimums, although the UTS matches the S-basis properties found in MMPDS for IN625 bar (not casting). A value from literature of IN625 in the solution annealed state is also shown in Table 20, which complies well with AMS 7000A minimums with comfortable margins. Further analysis of literature creates a complicated process-structure-property story for LPBF IN625, and in the as-built state, the alloy maintains properties that can exceed the AMS 7000A minimum and can be further improved with aging with and without solution anneal[126,127]. Although the tensile properties can exceed minimums in a variety of conditions, the micro and nano structure contributions to strength vary greatly, which will significantly affect the other properties of the material such as high temperature properties and chemical/oxidation resistance[126]. Similar to the apparent density specification, the tensile property minimums are not tied to LPBF and are adapted from casting or wrought specifications that were developed before metal 3D printing was invented. **Standards are the source of confidence, and their ambiguity exacerbates the lack of trust in LPBF AM.**

Table 20 IN625 minimum tensile properties for traditional made bar, AMS LPBF and ASTM LPBF, AMS 5666 bar, and literature values for LPBF IN625[125]

IN625 in solution annealed condition	UTS (MPa)	YTS (MPa)	Elongation (%)
AMS 7000A	827	345	30
ASTM F3056	485	275	30
MMPDS-16 AMS 5666 S-basis 0.5-1" bar	827	414	30
Marchese et al. [126]	883±15	396±9	55±1

5.3.3 Process and Machine IQ/OQ/PQ

ASTM, AMS, and NASA standards and specifications cover many aspects related to establishing confidence in the repeatable production of parts with a LPBF machine. Figure 61 schematically represents the various domains of LPBF part production that must be controlled and documented. AMS and ASTM frequently refer to the Installation Qualification (IQ), Operational Qualification (OQ), Performance Qualification (PQ), and Material Qualification (MQ) to define distinct aspects of a qualified part production. NASA utilizes different verbiage but serves the same purpose, including creating and documenting a process that leads to repeatable performance. Figure 62 was taken from NASA-STD-6030 and clearly defined the various aspects of establishing trust in LPBF part quality, while much simpler Figure 63 was taken from AMS 7003A and has a strong correlation with NASA-STD-6030 in that the process qualification and control is established independent of part qualification/certification[26,128].
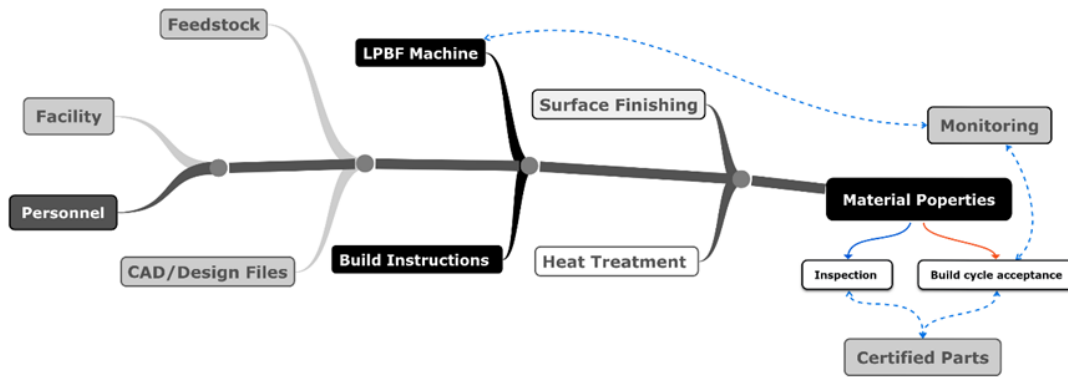
Figure 61 inputs that require control and documentation for LPBF production quality
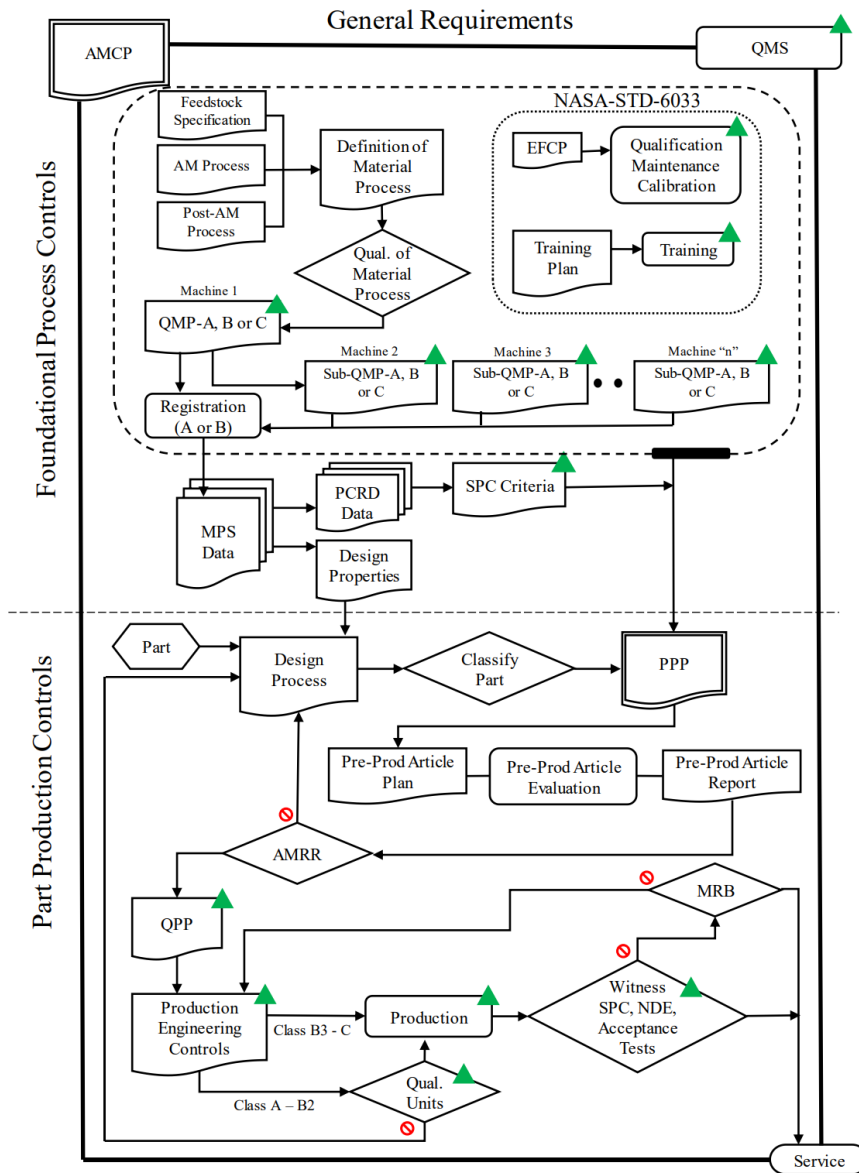
Figure 2—Key Products and Processes for NASA-STD-6030

Figure 62 Well defined workflow for the qualification and certification of materials, process, and parts made via additive manufacturing described in NASA-STD-6030[26]
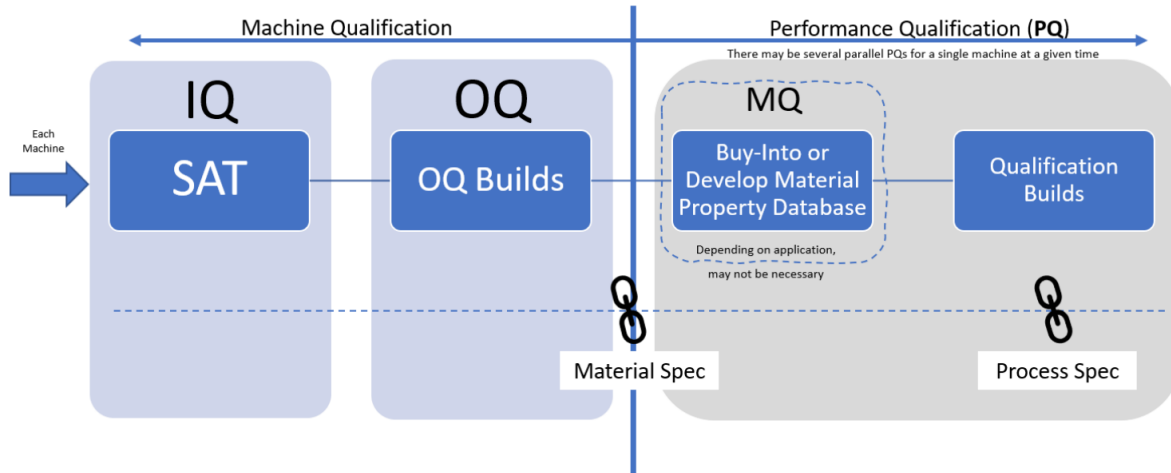
Figure 3 - Qualification flowchart

Figure 63 IQ, OQ, MQ, PQ workflow described in AMS 7003A[129]

Machine specific qualification standards are a focal point for NASA, AMS, and ASTM. Table 21 highlights the major similarities and differnecs in required documentation for the 6 LPBF machines subsystems to be qualified. 35 KPV's (key performance variables) are identified in AMS 7003A, while tolerances are excluded and left to the producer substantiating the tolerance with data[128]. In addition to the KPV's, another 25 variables are listed in the qualification and verification of AMS 7003A that must be documented periodically, potentially by the OEM during scheduled PM's. NASA and ASTM take slightly different approaches, but the result is the same; the part builder must somehow prove that, for example, the laser beam travel speed is reported accurately. Without industry accepted tolerances, the producer must establish the tolerance and prove that deviation within the tolerance limit does not detrimentally affect the outcome.

To further complicate matters, the machine user does not have access to all variables in order to validate or even document them. For example, the chamber oxygen is a key process variable. A variation of 100ppm vs 1000 ppm O2 can increase oxygen pick up by 200ppm in a

Ti64 parts[84]. The EOS M290 sensor Figaro KE-25 has a reported measurement uncertainty of 1% full-scale, which is roughly 230,000ppm when calibrated in atmosphere (air is 23wt% oxygen). Therefore, at the controlled level of 1000ppm, the actual oxygen level is 1000ppm ± 2300ppm. No standard specifically calls out a tolerance for oxygen sensor, but producers can show repeatability by producing the number and type of samples required in the standards. The standards define many more aspects of the process to measure to include spot size, scan speed, delays, gas flow and more.

Table 21 Comparison of LPBF machine qualification criteria listed in the relevant standards

Gas flow/filtration	ASTM	NASA	AMS		Computer control system	ASTM	NASA	AMS
Recirculation filter flow rate	✓	✓	✓		Software/firmware lock	✓	✓	✓
Velocity profile	✓				Time		✓	
					Scan strategy	✓		
Chamber Conditions	ASTM	NASA	AMS		**Laser**	ASTM	NASA	AMS
Shielding gas composition	✓	✓	✓		Power	✓±5%	✓	✓
Gas flow rates for supplement (purge)			✓		Waist location	✓	✓	✓
Moisture/humidity/dew point	✓	✓	✓		Astigmatism			✓
Chamber pressure (decay)	✓		✓		Beam quality factor	✓		✓
Oxygen sensor	✓	✓	✓		Thermal stability	✓		✓
Impurity concentration	✓				Power across build plate	✓	✓	✓
Chamber temperature	✓	✓			Spot size/shape across plate	✓	✓	✓
					Beam profile for each laser	✓	✓	✓
					Pulse characteristic	✓		✓
					On/off delays		✓	
Powder spreading/management	ASTM	NASA	AMS		**Beam Steering**	ASTM	NASA	AMS
Build Platform Positional Accuracy	✓	✓	✓		Travel speed	✓±5%	✓	✓
Re-coater speed	✓	✓	✓		Positional accuracy	✓0.06 mm	✓	✓
Build platform preheat	✓		✓		Scan field scaling	✓	✓	✓
Layer thickness and uniformity	✓							
Recoater blade material wear	✓							

ISO/ASTM 52930 does include a tolerance for select KPV's (ex. ±5% of true scan speed) and suggests measuring the true scan speed with an external timer [130]. ASTM 52941 also recommends a method to measure true scan speed by performing a star shaped plate melt and recording the time with a stopwatch[131]. There is no acceptable method or test or dataset for any

KPV, and almost all qualification requires one organization proving acceptable quality to another, regardless of the standards deployed. The primary method for developing that proof is through lots and lots of testing.

A major cost to qualification (time and monetary) is the number of test specimens per machine. Table 22 pulls the minimum number of builds/specimens for operational type qualification from AMS, 7032, ISO/ASTM 52930, and NASA-STD-6030 [26,130,132]. The exact language and intent of these samples does not translate across the different specifications but can be viewed as a bare minimum to be done on a new LPBF make/model machine. NASA-STD-6030 defines a material property suite (MPS) in addition to their qualified metallurgical process (QMP) which defines a "lot" mature property suite that requires a minimum of five feedstock lots and ten unique LPBF builds following the same build process (but not necessary on the same machine). The QMP is then mapped to an MPS which is why the number of specimens for NASA is lower to qualify a single machine vs ASTM and AMS. **According to NASA 6030 the cost of metal AM is reduced (slightly) as one scales to multimachine production, debunking another fallacy that LPBF has a flat cost vs quantity curve.**

Table 22 Number of samples required to qualify an LPBF machine to meet NASA, ASTM, and AMS recommendations.

Property	Quantity		
	NASA QMP-A	ASTM	AMS
Number of Builds	1	5	3
Feedstock lots	-	1	1
Tensile	15	50*	30
Tensile, in non-Z direction	-	-	2
High Cycle Fatigue (HCF)	10	-	12*
Low Cycle Fatigue (LCF)	5	-	-
Fracture Toughness	3	-	-
Tensile (at temperature)	6	-	-
Customized QMP	2	-	-
Chemistry	-	50*	3
Microstructure	>6cm^2	50*	3
Dimensional	-	50*	*
Roughness	-	50*	*

*recommended

The effort required to develop such data fosters an environment to hide the parameters as part of a company's proprietary information. While slow and expensive, the approach does enable PBF parts to attain air worthiness certification. After the completion of design allowables for a machine and process parameter set, the manufacturers can produce a first article for inspection, establish a continuous inspection plan and batch acceptance control plan. In forging or cast part production, every batch or lot must have a chemical composition check, at least one and often two tensile bars tested, and a metallography cut up. However, the lot size for cast or forging parts is typically defined by the heat treatment batch which can be significantly larger than the AMS 7000A definition of a batch for IN 625 produced in LPBF, which is build cycle based[125]. This tensile and chemical analysis per build is more burdensome on LPBF production cost due to the overall manufacturing cost. Unfortunately, for LPBF the data from a chemical or tensile bar built

alongside a part has little predictive power for the build quality. Casting and forging rely on historical data, a considerable array of standards for production, testing, inspection and design guides, and the ability to prove conformance to a materials design allowables database. A new casting house or forging press will have to prove itself capable of achieving a number of quality standards and even produce a number of test specimens, but in most cases, the alloy has historical data that reduces the need to develop an entire design allowables dataset. In essence, an LPBF machine is a casting or forging house in a box. **To provide certified material, each machine must be qualified with similar granularity as an entire casting/forging facility which can produce 10's of tons of metal vs a few hundred kilos of metal annually.**

All aspects of the process from design to deployment are interconnected forcing collaboration in an industry and time when being first to file is encouraged. A common philosophy of a rising tide lifts all boats has not been the mentality for AM, despite the number of steering committees, working groups, and non-profit knowledge sharing consortia. **A recent paper on structural integrity of various aluminum alloys in LPBF exemplifies this sentiment as follows "It must be noted that the detailed default EOS process parameters for other alloys are not provided for the sake of confidentiality."** [133] **Furthermore the chemistry of one of the alloys, "AD1", was deemed proprietary and not included. This statement violates the scientific method by preventing result reproduction. Unfortunately, this is not an isolated occurrence, and even if the parameters were included, the process would still not be repeatable due to the software and hardware black boxes that control the scanning strategy beyond the standard hatch space, laser power, and scan speed.** The reason the authors are forced to make this statement is the same reason the industry has been creating roadmaps for AM

154

to qualify and certify parts since pre-2010 - documenting what software version and parameter set used to generate a build file does not enable property data generated to grow beyond the exact software/firmware/make/model/serial number. **If the industry does not recognize this, the story will be the same in 2030.**

For LPBF to reduce time and cost to deploy <u>critical</u> parts, we must acknowledge that all LPBF machines operate under the same fundamental physics, and all have subsystems in place to manage and control these subsystems. Figure 64 calls out the six subsystems common to all LPBF machines. LPBF OEM's and machine users define their value in how they configure each subsystem for speed, quality, cost, and performance.

1) Laser source
2) Beam steering system
3) Powder and platform management system
4) Gas flow and filtering system
5) Environmental control chamber
6) Computer control system
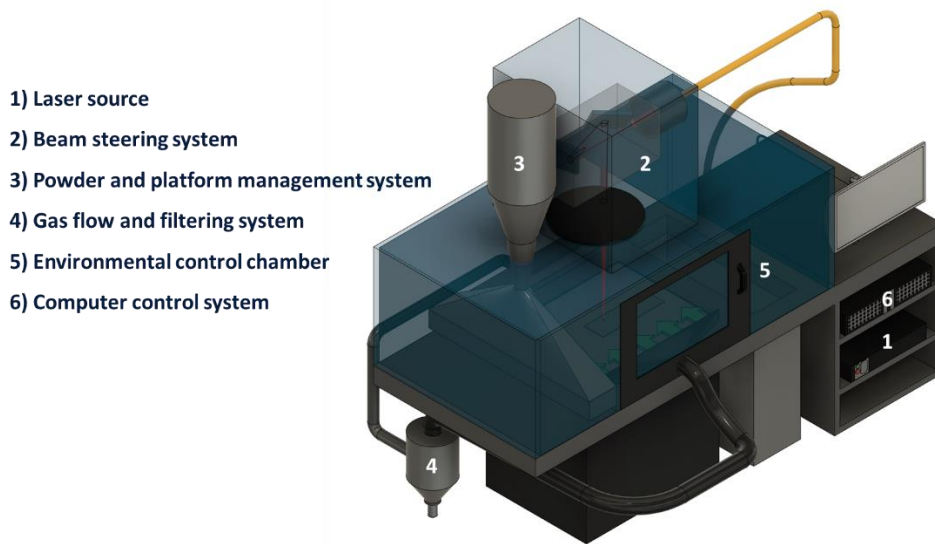
Figure 64 Notional Laser Powder Bed Fusion Machine and its subsystems

5.4 APPROACH GOING FORWARD

Before a metal part created by laser powder bed fusion can be deployed in a critical structure, it must be selected as a potential manufacturing process. The material, process, and

joining methods must meet five criteria defined in MIL-STD-1530D Aircraft Structural Integrity

Program[1].

1. Stability
2. Producibility
3. Characterization of mechanical and physical properties
4. Predictability of structural performance
5. Supportability

This approach requires new materials and processes creating parts entering the aircraft

structures to be substantiated by analysis across each of those five criteria, along with risk

mitigation strategies validated by test data. As an underlying assumption, this process relies on

material and structural allowables such as data found in MMPDS [122]. The development of

material properties must be done only once a material standard exists and a stable manufacturing

process is available. Material properties for design allowables cannot be developed as part of

material and process development [122]. **LPBF AM has struggled to establish a stable**

manufacturing process because the parameters are optimized for each machine, material,

and even part geometry forcing allowables type data development to be specific to machine

make/model, alloy, and often each build layout [26,134]**.**

After evaluating the standards, specs, and handbooks listed in Table 23 no mention of

design allowables tied to a forging press or furnace was found. The need for material property

development per LPBF machine is the fundamental difference between LPBF and traditional

manufacturing. In my opinion, had machine to machine scatter for LPBF been like traditional

manufacturing we would not have deviated from casting and forging standards and been able to

comply to MMPDS type design allowables more quickly.

Table 23 list of standards, specifications, and handbooks reviewed for traditional manufacturing

AMS4471	Cast Aluminum Alloy Composite 4.6Cu - 3.4Ti - 1.4B - 0.75Ag - 0.27Mg (205.0/TiB2/3p-T7P) Investment Cast, Solution and Precipitation Heat Treated
AMS5383	Nickel Alloy, Corrosion and Heat-Resistant, Investment Castings 52.5Ni - 19Cr - 3.0Mo - 5.1Cb(Nb) - 0.90Ti - 0.60Al - 18Fe Vacuum Melted Homogenization and Solution Heat Treated
AMS5662	Nickel Alloy, Corrosion- and Heat-Resistant, Bars, Forgings, Rings, and Stock for Forgings and Rings 52.5Ni - 19Cr - 3.0Mo - 5.1Cb (Nb) - 0.90Ti - 0.50Al - 18Fe Consumable Electrode or Vacuum Induction Melted 1775 °F (968 °C) Solution Heat Treated, Precipitation-Hardenable
AMS4928	Titanium Alloy Bars, Wire, Forgings, Rings, and Drawn Shapes 6Al - 4V Annealed
AMS4992	Casting, Structural Investment, Titanium Alloy 6Al - 4V Hot Isostatically Pressed
AMS4289	Aluminum Alloy Castings 7.0Si - 0.55Mg - 0.12Ti (F357.0-T6) Solution and Precipitation Heat Treated
AMS5666K	Nickel Alloy, Corrosion- and Heat-Resistant, Bars, Forgings, Extrusions, Rings, and Stock for Forgings, Extrusions, and Rings 62Ni - 21.5Cr - 9.0Mo - 3.65Cb (Nb) Annealed
MIL-T-46035B	TITANIUM ALLOY: HIGH STRENGTH, WROUGHT (FOR CRITICAL COMPONENTS)
MIL-T-9047G	TITANIUM AND TITANIUM ALLOY BARS (ROLLED OR FORGED) AND REFORGING STOCK, AIRCRAFT QUALITY
MIL-F-83142A	FORGING, TITANIUM ALLOYS, PREMIUM QUALITY
MIL-F-7190B	FORGING, STEEL, FOR AIRCRAFT/AEROSPACE EQUIPMENT AND SPECIAL ORDNANCE APPLICATIONS
MIL-STD-2175	CASTINGS,CLASSIFICATION AND INSPECTION OF
MIL-STD-1869	TURBINE BLADES AND VANES , CAST; ACCEPTANCE CRITERIA FOR
MIL-STD-781D	RELIABILITY TESTING FOR ENGINEERING DEVELOPMENT, QUALIFICATION, AND PRODUCTION
MIL-STD-1530D	AIRCRAFT STRUCTURAL INTEGRITY PROGRAM (ASIP)
MIL-HDBK-1587	MATERIALS AND PROCESS REQUIREMENTS FOR AIR FORCE WEAPON SYSTEMS
MIL-STD-1916	DOD PREFERRED METHODS FOR ACCEPTANCE OF PRODUCT
MIL-HDBK-61B	CONFIGURATION MANAGEMENT GUIDANCE
JSSG-2006	DEPARTMENT OF DEFENSE JOINT SERVICE SPECIFICATION GUIDE AIRCRAFT STRUCTURES
MIL-HDBK-516C	AIRWORTHINESS CERTIFICATION CRITERIA
MIL-A-21180D	ALUMINUM-ALLOY CASTINGS, HIGH STRENGTH

AM is fundamentally different than other manufacturing methods due to voxel level control. To account for this, LPBF machine qualification backed by materials data has been adopted. However, two qualified machines with identical beam size, recoater, scanner calibration confirmation, feedstock, and gas flow but different make/model cannot utilize the same material qualification data and must develop their own. The reason for this is simple, equivalent hardware controlled differently results in different outcomes. **The keystone of the qualification arch will be transparency in the complete build file**. **The approach will require a fundamental shift in the value LPBF machine manufacturers and machine users add by taking the cover off the**

black box and the hidden aspects of processing parameters. The following sections include my recommendations for achieving relevant design allowables in LPBF AM from facility to build file.

5.4.1 Facility

A poorly controlled facility with an excellent LPBF operator and machine can result in flawed materials. A single foreign particle can result in catastrophic failure of metallic components, the challenge of preventing and inspecting for these types of defects is a major cause for concern in powder bed fusion. The UA flight 232 crash in 1989 was due to a hard alpha inclusion in a titanium turbine disk that caused catastrophic engine failure and complete loss of flight controls. The failure resulted in the loss of life for 112 of 296 passengers and served as a wakeup call to the manufacturing and maintenance industries. As a result, SWRI was awarded a contract in 1995 to develop a software for Design Assessment of Reliability with Inspection, a software that supports damage tolerant design and inspection of cyclically loaded metal parts [135–137]. **It is important that the AM industry does not wait for a hard Fe-Ti intermetallic inclusion to cause loss of life before action is taken.**

Recent and preliminary work for fatigue testing of Ti64 samples produced from AP&C feedstock known to contain trace amounts of tungsten inclusions revealed they were not the source of crack initiation with six sampled tests at 690MPa with R=0.1 (Figure 65). Figure 65 compares sample #49 (25,287 cycles) to #19 (512,986 cycles), a vastly different life despite the similar size and location of the defect within the specimen. While Sample #19 is clearly a gas pore, sample #49 indicated low z elements to include carbon and oxygen, potentially from the carbon fiber brush

recoater or another source yet to be determined. Although not statistically significant, this early

indication points to the need to remove all potential forms of contamination in the facility when

possible.
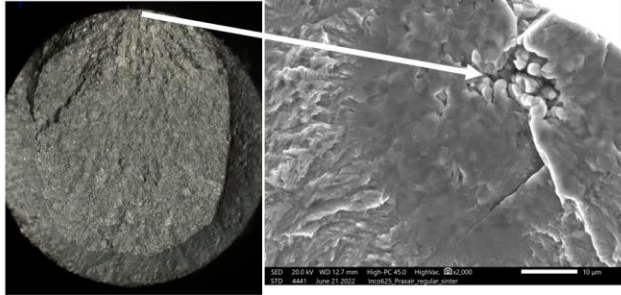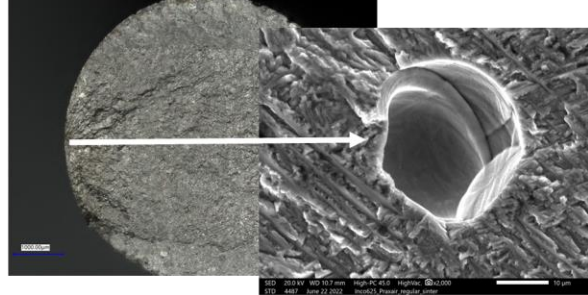
Bar ID	Cycles to failure	Failure location	Origin type	Defect from edge (μm)	Defect size (mm)	Crack growth area (mm²)
14	192,812	Gage	Contamination	Core (2414)	190	10.9
19	512,986	Gage	Gas Pore	Surface (81)	28	3.4
26	259,334	Gage	Gas Pore	Core (875)	41	3.2
11	309,768	Gage	Gas Pore	Core (359)	41	4.4
66	149,765	Gage	Gas Pore	Core (2209)	58	10.0
49	25,287	Gage	Contamination/ Lack of fusion	Surface (65)	49	3.1

Figure 65 preliminary results of uniaxial fatigue of Ti64 parts built in an EOS M290 with surface prepared in accordance with ASTM E466

I recommend that facilities confine machines of different chemistry families in separate

buildings or in separate positive pressure rooms. In addition, the clothing and tools used by

personnel working in those rooms should cover exposed skin and loose hair. The challenges in

statistically determining if a particular contaminant will or will not result in detrimental

performance is not bearable by a single entity. Therefore, the recommendation is to eliminate

sources of contamination until sufficient data exists to determine if a certain contaminant can cause

detrimental effects to performance.

5.4.2 Machine Qualification

In my opinion, the machine qualification must capture the quality, calibration, verification, and maintenance of the 6 subsystems called out in Figure 64. The effort is independent of material and is only to confirm the machine is operating as intended. The qualification of these subsystems must include an extended version performed during installation (IQ) and quality control testing that is less intensive that could be performed prior to a build or even during a build. Furthermore, the qualification of the hardware should not be confused with the digital system control. For example, skywriting and timing delays should be isolated from the qualification of the laser beam profile and power.

Machine qualification is a challenging topic due to the combinatorial effect of subsystems and the influence of the hidden/back box parameters. For this reason, I will define machine qualification for closed systems that do not give users access to raw sensor or control information and machines that do. For closed systems this means users can check that the machine is not changing over time and document how a machine interprets certain tasks but does not allow for calibration. For open systems the recommendation is more specific and enables calibration.
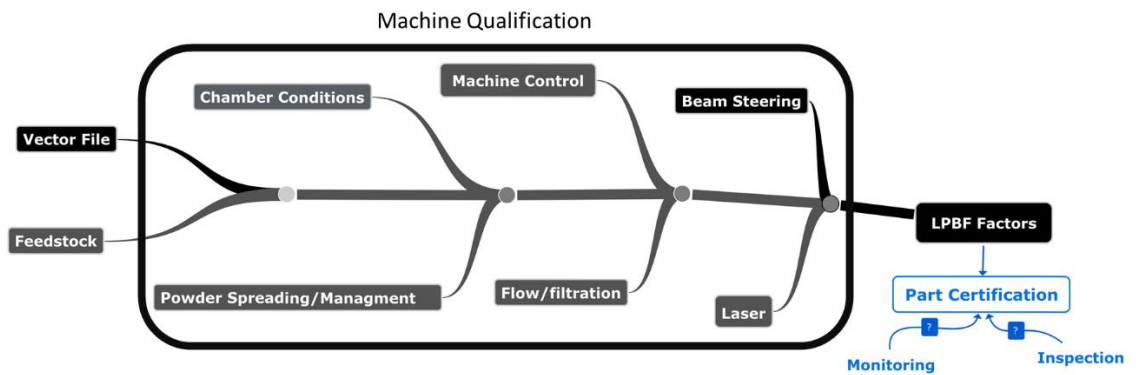
Figure 66 major consideration of LPBF qualification subsystems

5.4.2.1 Laser and Beam Steering

The laser source and beam steering system qualification are to be combined since many aspects of these subsystems are difficult to effectively isolate. Additionally, the following recommendation can likely be applied to closed architecture machines with creative manipulation of the machine controls (forcing single vector melts via wall thickness less than beam compensation, adding ghost parts to control intervector time). To fully leverage these recommendations complete control is required to implement adjustments based on findings.

Beam profile measurement devices typically start at $20,000 and require trained users which creates a roadblock to machine users in documenting their beam size. To monitor beam quality the industry has adopted methods to qualify general beam quality through plate melt testing. This approach has been addressed as an appropriate solution in AMS7003A with proper validation thorough quantitative means to be determined by the machine user[128]. During my time at the Keck Center, I have seen the installation of four LPBF machines and taken EOS self-care training to be certified to maintain the EOS M 290. Plate melt testing of some variety was

used by each as part of machine calibrations; however, there is no standard or NIST traceable plate material specifications for such a test. Although plate melting was done by each OEM in addition to the power and profile measurements there was no quantification of the melts on plate, only qualitative information was gathered. It is recommended that plate melting can be used to validate focal plane location, incident angle effect, laser power, scan speed and spot size concurrently. Table 24 lists the various quality control aspects related to laser and scanner functions described as key process variables in ASTM. AMS, and NASA standards along with potential methods to quantify or qualify them.

Table 24 Approaches to laser and scanner quality control/calibration

	Plate scan
Focal plane	Plate scan
Beam waist	Plate scan potential Measurement device
Waist/power/speed	Plate scan
Timing	Plates scan
Scanner black box	Plate scan or command vs true
Position accuracy	Plate scan
Scan field scaling	Plate scan
Beam travel speed	Plate scan + true position
Beam profile	Measurement device
Thermal lensing	Plate scan
Multi laser alignment	Plate scan

The challenge in performing accurate and repeatable plate melting tests is not trivial, which is why it should not be left to the OEM or end user to establish and should be supported by standards. The material, surface finish, scan setting, atmosphere, gas flow, scan direction relative to gas flow, and plate position all impact the results as found during work performed as part of this

dissertation. The following section highlights lessons learned to guide the development of a plate scan quality standard.

Based on availability, cost, and quality, it is recommended to use 304SS with brushed finish #3 as it comes with an adhesive film to protect the surface until use. These plates are available through McMaster-Carr for $1.50 per 1"x 1" x0.125" plate and are supplied with certificate of traceability. Bead blasted surfaces have been predominantly used in the research as part of this work, but that approach introduces user-based variability, and is therefore unacceptable as basis of a global standard. By standardizing the material type, size, and condition with a readily available material, the industry can create a quality check that is visual and a micrograph with annotations could be included as part of IQ/OQ/PQ and potentially build (lot) acceptance. It is recommended that an unbiased or not for profit create a database for this application.

An example to identify the focal plane relative to build plane on an AconityMINI is shown below in Figure 67. The left most melt is at the working plane of the LPBF machine, and the build platform was subsequently moved 0.5mm up for each melt. In this example, the build plane was positioned at the focal waist of the beam.
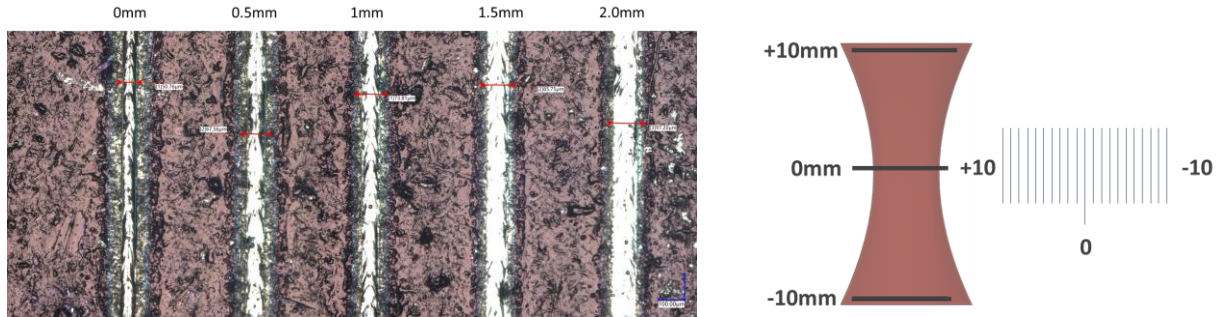
Figure 67 example of focal plane to beam waist test via melts on plate

To evaluate the scanner interpretation of a slice file and include aspects of the controls that are hidden to the user, a series of plate melts can be performed to shed light on potential quality concerns. The primary concerns highlighted in the NASA, AMS, and ASTM standards related to scanner controls are scan speed, positioning accuracy, and timing, all of which can be analyzed with plate melts. Scan speed can be evaluated by performing a series of pulses utilizing the pulse width modulation function (note: not all systems enable this function, but the lasers are typically capable). **To accomplish this, I recommend setting the pulse width to the system clock rate (typically 10µs), the modulation frequency to 10kHz, and the scan speed to 1,000mm/s at a laser power of 75w if spot size is roughly 80µm d4σ. These setting will result in center-to-center pulse distance of 100µm.** Performing a series of five 10mm long vectors in three locations of the print bed should be sufficient to determine the scan speed to less than 50mm/s. The plate can then be analyzed, and average pulse width distance measured. Figure 68 shows the results of pulsed conducted under the previously described setting highlighting the utility in identify galvo deceleration due to skywriting time that is too short. If there is no deceleration the distances between pulses should not change at the beginning or end of vectors.

164

V = 1000mm/s
Pulse width = 10µs
Frequency = 10kHz
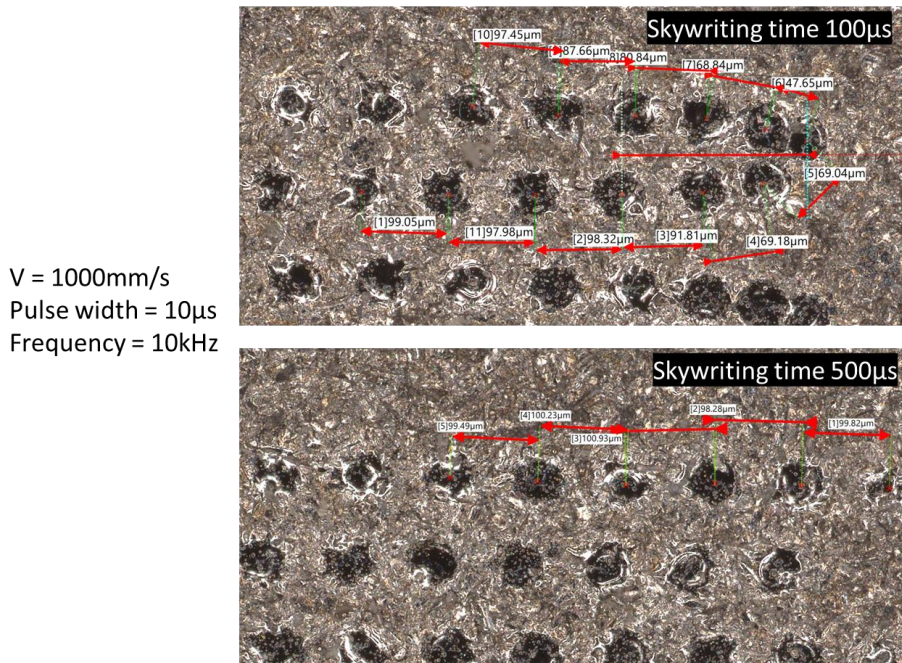
Figure 68 laser beam modulation method to determine scanner speed

In addition to scan speed and skywriting timing, it is important to evaluate when skywriting is applied, and the laser on/off timing is synchronized with the position. Figure 69 enables a direct comparison of an EOS LPBF machine (right) to and AconityMIDI+ (left) for Ti64 plates. A major difference between the two is the lack of skywriting implementation during sharp contours for EOS and the lightly reduced short vector heat buildup in the midi+, which limits the melt pool size increase as compared with the EOS. These differences are due to the skywritng time difference of 1ms for AconityMIDI+ and 0.5ms for EOS. This example, which contains less than 20 vectors for each sample combined with detailed analysis provides more insight into the LPBF machine/process quality than any build of a cube could. **With a goal of machine-to-machine repeatability this example raises the question; how can we attempt part equivalency if a simple test cannot produce identical results?**
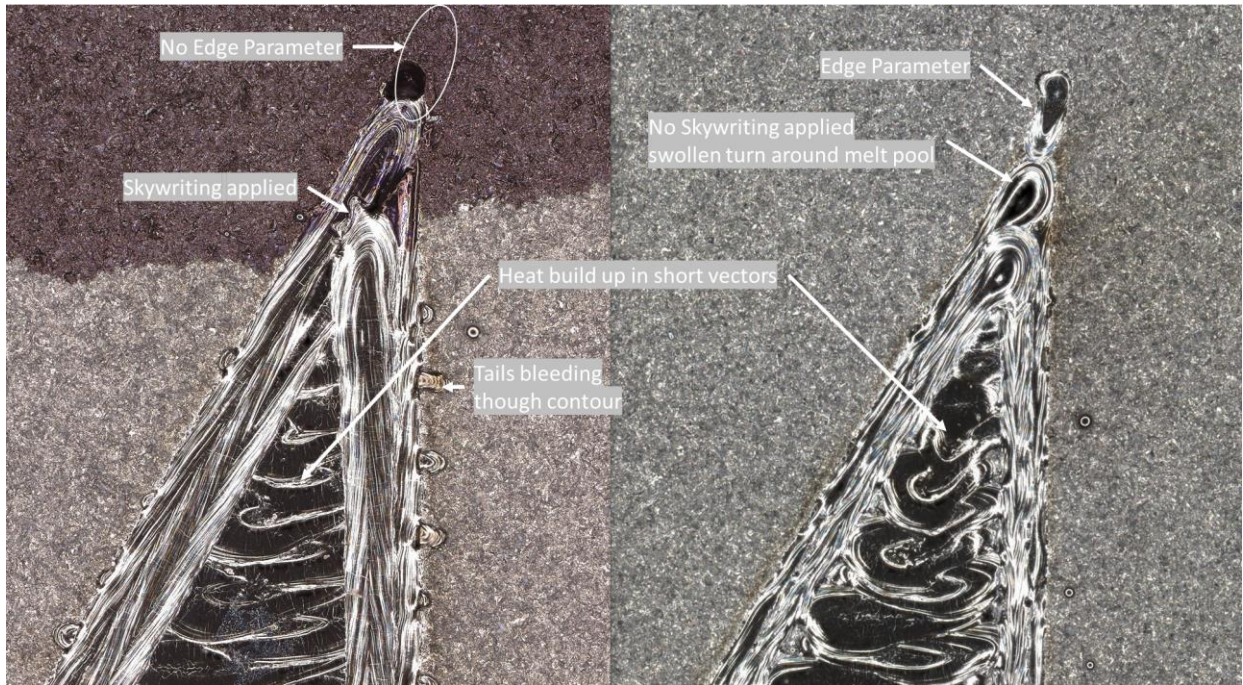
Figure 69 Aspect of ultimate layer scan highlight different scanner and digital file preparation defects

5.4.2.2 Chamber

The chamber as designed serves multiple functions, but the primary purpose is environmental control. Most metals used in LPBF are sensitive to oxidation at high temperatures and control of the residual oxygen in the chamber is required. The effect of chamber oxygen of 200ppm vs 1000 ppm was shown to result in a 150ppm oxygen pick up of Ti64 parts built in an EOS M290 with Linde ADDvance O_2 system to control the oxygen content level. The EOS M 290 utilizes a Figaro GS Oxygen sensor KE-25, which reports an error of ±1% full scale (approximately 230,000ppm since the sensor is calibrated with atmosphere) meaning the measurement error would be 2300ppm making control to 1000ppm impossible; however, there is no documentation available to my knowledge of EOS reporting accuracy of their oxygen sensor. SLM Solutions and Renishaw systems utilize the BOSCH LSH25 sensor, which can be sourced

from an auto parts store, and does not have a reported standard error for the application of controlling oxygen below 1000ppm in the public domain to my knowledge. **Sensors designed for full scale use (atmosphere to 1ppm) are unlikely to provide accuracy and repeatability at both extremes. Therefore, it is recommended the industry adopt a two-sensor approach that enables chamber control down to <10ppm±5ppm. Furthermore, NIST tracible calibration gas at approximately 100ppm oxygen should be utilized to certify sensors on during preventative maintenance.** By adopting this change, it is anticipated that powder degradation over time will decrease and the repeatability of all material properties collected will increase since oxygen leads changes in strength, hardness, ductility, facture toughness, and detrimental inclusions [84,85].

The chamber must also provide a stable thermal environment as temperature changes in the machine and optics can cause a variety of errors to include beam focal shift and loss of positional accuracy. Periodic layer lines shown in Figure 70 were due to the chiller for an LPBF machine maintaining a set point of $21 \pm 2.7°C$ and was remedied by refining the temperature limit to $\pm0.5°C$. **It is recommended that the temperature in the scanner and the collimator be monitored in addition to the chamber temperature near the optics and be maintained within ±1°C for the entirety of builds.** Future work should incorporate plate scans with precisely controlled cooling temperature to identify what thermal shift results in measurable differences in absolute positional accuracy of laser marking.
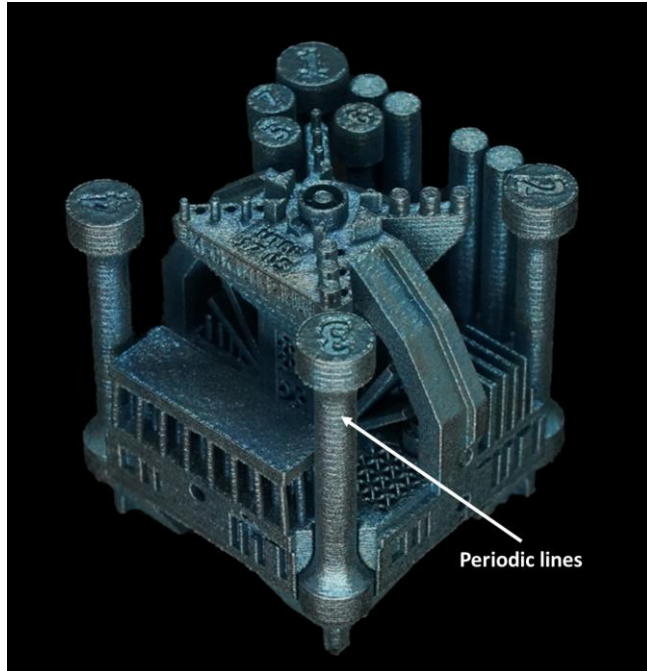
Figure 70 IN718 QTA built with chiller set to ± 2.7°C with visible periodic layer lines

5.4.2.3 Powder Spreading and Management System

There are now three major methods for spreading a thin layer of metal powder in LPBF. These include: gravity fed to a spreader (Renishaw 500Q, SLM 125, SLM 280, EOS M400, Additive Industries), volume displacement to a spreader (EOS M290, Aconity machines, DMG Mori machines, Trumph machines), and recently developed non-contact gravity deposited and vacuum removal (only VELO3D WO 2018/075741 A1). Except for the VELO 3D non-contact system, every LPBF machine has a blade, brush, or roller that pushes the powder mass across the print platform. The powder spreading system includes the material type, shape, travel speed, dosing factor, and layer thickness all impact the quality of the deposited layer even with identical feedstock [76,77,79]. The effect of these factors extends beyond establishing guidance on effective layer thickness as the recoating imparts a force on the parts and powder bed causing anisotropy in surface roughness, dimensional accuracy and even build failures. Unpublished work

to isolate the effect of incident angle, gas flow, and rake direction identified the face to the recoater vs away from the recoater had statistically different surface roughness. There is still a void in standards and literature related to the topic of powder spreading quality.

The objective of recoating is to simply apply a uniform layer of powder as quickly as possible without disturbing the parts being printed or contaminating the material. The constraints lead to a similar conclusion that VELO3D must have come to, the powder should be deposited gently, and excess removed to minimize contact and prevent contamination. The control of such a system appears daunting and is likely a core reason for the success. The industry, however, must still find a way to determine spreadability quality based on clear metrics. **The recommended metrics are as follows: effective layer thickness (min, max, variance across bed), free from potential foreign material contamination, and an imparted force metric and metric for qualifying a spreading method.** Effective layer thickness maximum should be feedstock and recoating method insensitive as they both play a role in the layer quality. Although there is not significant literature on this topic, Wischeropp et al. determined the effective layer thickness to be as much a 4-5x the nominal layer thickness [138] **To achieve all three metrics, a novel approach, or novel approaches to spreading and monitoring are required. Potential solutions include a brush style recoater made from metal brush fibers of the same alloy family being printed, fluidization or ultrasonic vibration to reduce particle friction, and monitors that can measure the effective layer thickness.**

5.4.2.4 Gas Flow and Filtration

Gas flow has received significant press in recent years with Renishaw, Velo3D, GE Additive, and Additive Industries highlighting improvements or optimizations of gas flow in their systems and the importance of gas flow in terms of quality[92–94]. Despite the OEM's claims to quality, there is no gas flow minimum or maximum requirement. It is still common practice to wipe the system's optical inlet glass prior to starting a build, and indication of poor gas flow. From personal experience, some machines have a visible amount of soot deposited on the lens after a single build, which is completely unacceptable. In addition, gas flow that does not effectively remove byproducts is known to reduce quality by attenuating the laser beam resulting in reduced melt pool depths [90]. At a minimum the gas flow should be uniform across the print area, unlike the region highlighted in Figure 71 where the powder is asymmetrically blown off the corner of the build area in an EOS M 290.

Gas flow may be acceptable against a defined minimum and maximum velocity and uniformity, but gas flow induced flaws can still occur if the scan strategy ignores the effect of gas flow relative to vector direction. **The bottom of Figure 71 the vectors traveling parallel with the gas flow have increased variability in melt pool penetration, which can be avoided by restricting the propagation direction of vectors.** Due to the challenges in measuring gas flow at low velocity it is recommended that OEM's prove gas flow quality for each machine make/model and customers only validate gas flow quality. Recommendations on methods for make/model flow qualification are outside of my domain of expertise and it is expected that experimental fluid mechanics will be required.
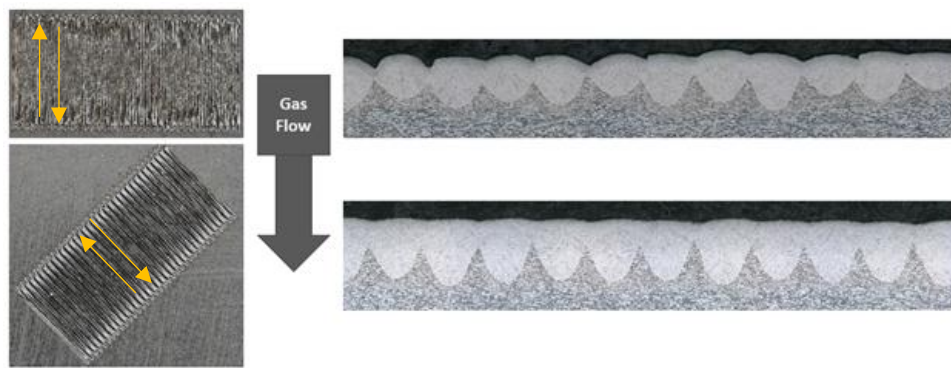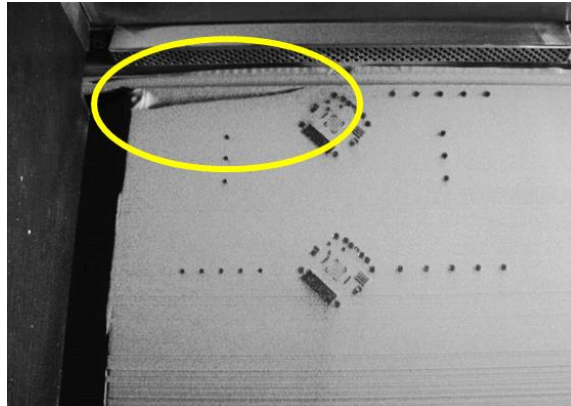
Figure 71 top) visual evidence of non-uniform gas flow in EOS M290 with blown powder in to left corner for duration of build, bottom) plate melt evaluation of melt pool depth variability based on strip propagation relative to gas flow

5.4.3 Process Parameter Development

Process parameter development shall be performed for laser powder bed fusion not for a machine make/model. Although some machines may utilize different laser spot size or laser powers the goal of parameter development is to optimize materials response to laser energy.

Performing bead on plate tests to establish process windows has been done by dozens of authors over the last decade; however, most bead on plate testing stops with simple hatching and

to the author's knowledge, no literature has developed a comprehensive understanding of the process parameter development that bead on plate enables [33,36,37,39,42,43,55,101,139–142]. Figure 72 defines the number of parameters that affect the LPBF process that can be interrogated with bead on plate testing and the type of analysis to be done to maximize the value of each melt pool.
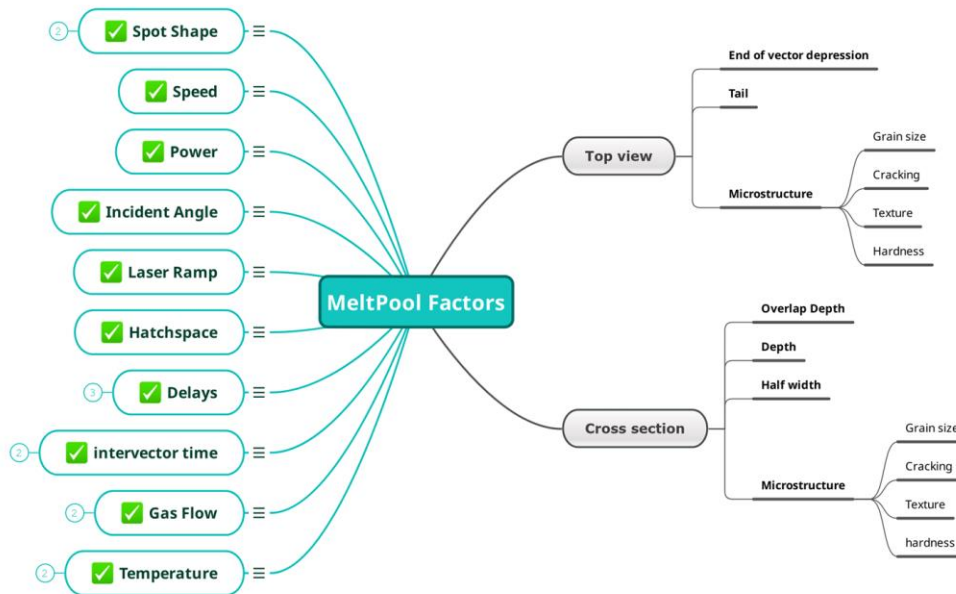
Figure 72 processing parameters that effect melt pool characteristics that inform the overall parameter development process before powder is ever purchased

I recommend the initial step of material qualification begin with power velocity mapping, an example of which is shown in Figure 73 as it will provide a general direction for all future testing. **A series of melts are to be performed at multiple powers and speeds to find the**

desired melt pool characteristics where the scan speed is near the balling limit and the melt pool depth to width ratio does not exceed 1.5 to stay below keyhole mode melting which is less stable[42,101]**.**
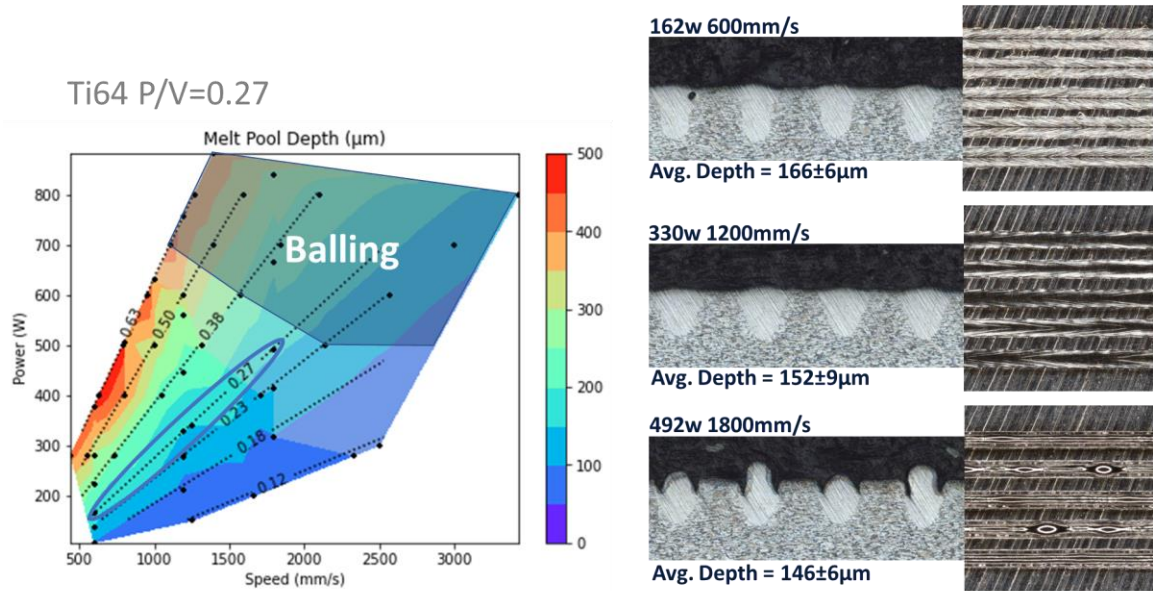
Figure 73 P/V map for Ti64 and representative melt pool images

The P/V map for common alloys in LPBF is presented in Figure 74 for a laser spot size of $d4\sigma = 75\mu m$. In general, near the transition melt mode, the P/V diagram is linear when beam size is held constant and has been shown to behave similarly for Cu, Mo, and Nb alloys in unpublished work by the author and by others [42,43].

6.5ms between melts 0.12mm hatch
P/V vs Melt Depth @ 1000mm/s d4σ=75μm
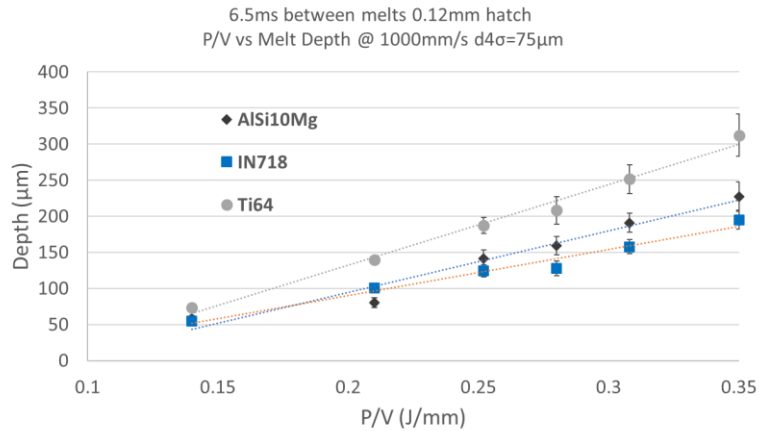
Figure 74 P/V map for Al10SiMg, IN718, and Ti64

Beyond P/V maps for a single spot size, the effect of spot size on microstructure must be evaluated. Spot sizes vary between systems and the laser beam diameter influences productivity, resolution, spatter, and microstructure. Through personal observation of VELO 3D Sapphire builds, and use of the AFX beam shaping laser, it is apparent that both research and production is being done with larger beam diameters (d4σ >150μm). The effect of spot size is known to affect microstructure and these microstructure variants can remain after heat treatment alloys like IN718 [46]. Each alloy has potentially different sensitivity to spot size, but this should be identified and used to establish machine classification. **For example, Alloy XYZ may need to generate material allowables data for a machine with beam size 70-140μm and data for a system with beam sizes 140-500μm. The initial screening can likely be achieved utilizing the plate melting.** The effect of laser spot size on melt pool formation at constant laser power and scan speed with various beam d4σ diameters on C103 plate is shown in Figure 75.

| Focal Plane: 0.0 mm | Focal Plane: 1.0 mm | Focal Plane: 2.2 mm |
| $d4\sigma \approx 50 \mu m$ | $d4\sigma \approx 70 \mu m$ | $d4\sigma \approx 120 \mu m$ |

$depth = 180 \mu m$ $depth = 140 \mu m$ $depth = 34 \mu m$
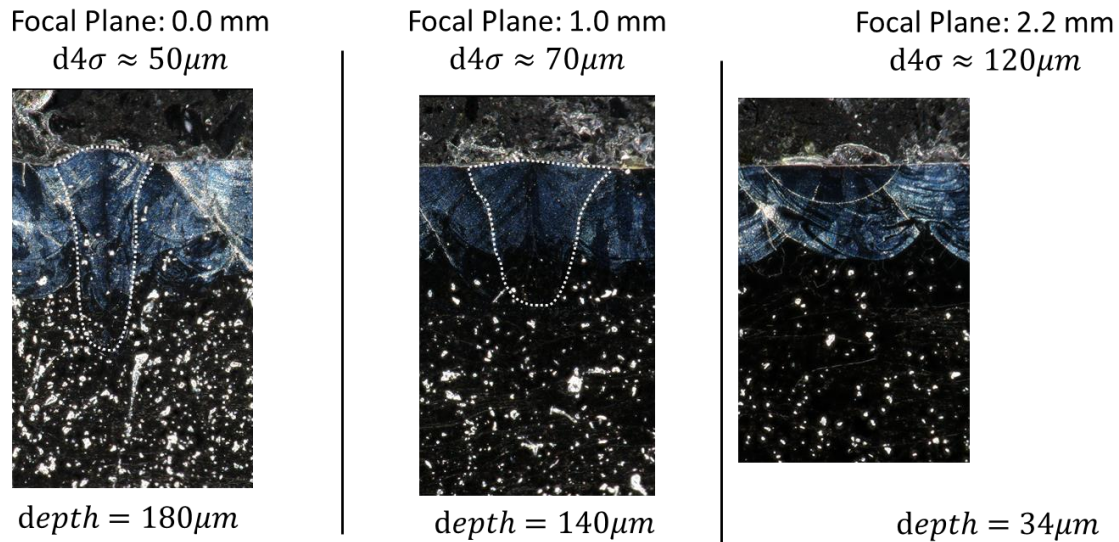
Figure 75 Effect of spot size on melt pool depth in C103

Once the knowledge of scan speed, spot size, and laser power sensitivity is established the effort can transition to hatching melts. During this step the material qualification should identify other practical bounds, such as minimum intervector time to maintain similar melt pool shape, effect of incident angle, effect of pre heat (heated build plate) and gas flow. The minimum intervector time can be determined by performing successively shorter vectors or by performing short vectors with successively long inter vector time. **An example of 1mm vector in IN718 with 1ms intervector time vs 3ms intervector time is shown in Figure 76. This example highlights the difference 2ms can have on melt pool shape.**
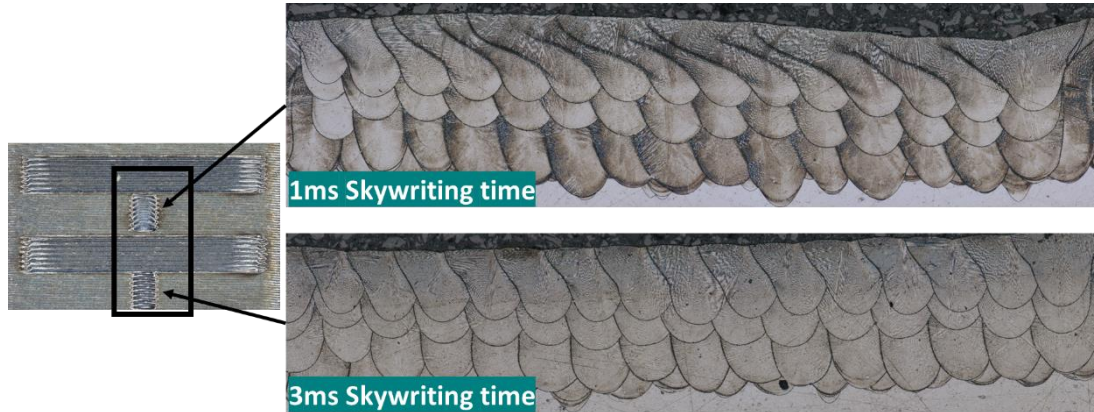
Figure 76 multi melt analysis to identify the minimum intervector time

Plate scans can also drive the industry toward standardizing uniformity across build platforms by quantifying the effect of incident angle and scanning direction on melt pool morphology. **The effect of gas flow (good or bad) can be defined by performing single vector melts with long (>1sec) delays between vectors.** Figure 77 below represents 135 single vector melts performed on Ti64 in an EOS M290 that were sectioned and measured for melt pool depth. This test was able to quantify up to a 30% reduction in penetration for the worst location as compared to the center of the platform. This effect could be removed by location specific laser power or speed to homogenize the melt pool across the platform. Evaluations based on incident angle enable lessons learned from single laser systems to be applicable to multi laser systems as well. Unfortunately, most literature in the public domain does not include incident angle or vector direction relative to gas flow.
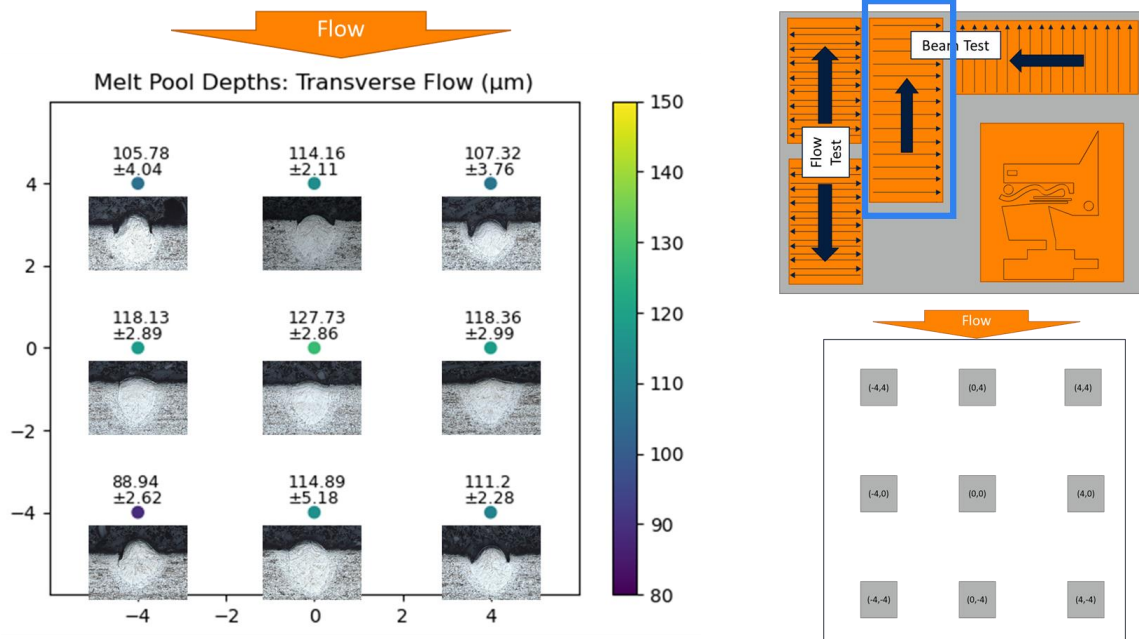
Figure 77 Effect of incident angle on melt pool depth

Upon the completion of the melt pool analysis for an alloy that fully defines the effects identified in Figure 72, the next step would be to define a set of rules in order to not violate known regions of the process space that result in melt pool shapes exceeding the target. With this knowledge, a scan strategy must be deployed that does not violate the rules. However, no such file preparation software based on rules exists today to my knowledge. **For the plate melt based material qualification to be successful, the industry needs to adopt an open, data driven build file generation and vector file format approach.**

5.5 CONCLUSION: BUILD FILE QUALIFICATION

Laser powder bed fusion of metals can produce parts for high performance applications. The critical hurdle to overcome for broad spread impact is reproducibility of material properties

globally. To my knowledge, there is no standard that mentions aspects of the build instructions other than the software/firmware and scan strategy must be locked once verified to produce acceptable quality. Current parameter development and optimization are done by the machine users and typically guided by OEM baseline parameters. As of today (December 2022), there is no unified build file format. The instructions defined in the build file utilize the same subsystems; however, the user cannot typically access how the selected parameters are executed. As described in the material development and machine qualification sections above, the impact of scan settings on melt pool formation is understood well enough to develop basic quality rules. The build files could then be analyzed and compared against a set of rules to verify that quality violations do not exist. Developing or utilizing such a tool today that is machine make/model agnostic is impossible, since the build files are typically proprietary, and the interpretation of the build file occurs on the machine, meaning there is no single source of truth prior to starting a build. Unfortunately, this means build file validation could only be enabled by the OEM's or through intercepting the build instructions controlling the machine during the build and reconstructing them. Most OEM's and early adopters protect their parameters, build file and control methodology, therefore it is unlikely that a solution to enable build file checking will be made available. One potential alternative would be a user adopted open vector format that contains all the information needed to build a part such as what was proposed by Dirks et al. [143]. **Ultimately, I believe any effort in material property development without transparency in build file information is futile.**

References

[1]   MIL-STD-1530D, DEPARTMENT OF DEFENSE STANDARD PRACTICE AIRCRAFT STRUCTURAL INTEGRITY PROGRAM (ASIP) NOT MEASUREMENT SENSITIVE, 2016. http://www.everyspec.com.

[2]   S.A. Khairallah, A.A. Martin, J.R.I. Lee, G. Guss, N.P. Calta, J.A. Hammons, M.H. Nielsen, K. Chaput, E. Schwalbach, M.N. Shah, M.G. Chapman, T.M. Willey, A.M. Rubenchik, A.T. Anderson, Y. Morris Wang, M.J. Matthews, W.E. King, Controlling interdependent meso-nanosecond dynamics and defect generation in metal 3D printing, Science (1979). 368 (2020) 660–665. https://doi.org/10.1126/science.aay7830.

[3]   T.T. Roehling, R. Shi, S.A. Khairallah, J.D. Roehling, G.M. Guss, J.T. McKeown, M.J. Matthews, Controlling grain nucleation and morphology by laser beam shaping in metal additive manufacturing, Mater Des. 195 (2020) 109071. https://doi.org/10.1016/j.matdes.2020.109071.

[4]   H. Yeung, J. Neira, B. Lane, J. Fox, F. Lopez, Laser path planning and power control strategies for powder bed fusion systems, in: Solid Freeform Fabrication 2016: Proceedings of the 27th Annual International Solid Freeform Fabrication Symposium - An Additive Manufacturing Conference, SFF 2016, 2016: pp. 113–127.

[5]   J.P. Oliveira, A.D. LaLonde, J. Ma, Processing parameters in laser powder bed fusion metal additive manufacturing, Mater Des. 193 (2020) 108762. https://doi.org/10.1016/J.MATDES.2020.108762.

[6]   J. Gockel, L. Sheridan, B. Koerper, B. Whip, The influence of additive manufacturing processing parameters on surface roughness and fatigue life, Int J Fatigue. 124 (2019) 380–388. https://doi.org/10.1016/j.ijfatigue.2019.03.025.

[7]   C. Kamath, Determination of Process Parameters for High-Density, Ti-6Al-4V Parts Using Additive Manufacturing, 2017.

[8]   H. Shen, P. Rometsch, X. Wu, A. Huang, Influence of Gas Flow Speed on Laser Plume Attenuation and Powder Bed Particle Pickup in Laser Powder Bed Fusion, JOM. 72 (2020) 1039–1051. https://doi.org/10.1007/s11837-020-04020-y.

[9]   H. Ali, H. Ghadbeigi, K. Mumtaz, Effect of scanning strategies on residual stress and mechanical properties of Selective Laser Melted Ti6Al4V, Materials Science and Engineering A. 712 (2018) 175–187. https://doi.org/10.1016/j.msea.2017.11.103.

[10] L.E.J. Thomas-Seale, J.C. Kirkman-Brown, M.M. Attallah, D.M. Espino, D.E.T. Shepherd, The barriers to the progression of additive manufacture: Perspectives from UK industry, Int J Prod Econ. 198 (2018) 104–118. https://doi.org/10.1016/j.ijpe.2018.02.003.

[11] M. Gorelik, Additive manufacturing in the context of structural integrity, Int J Fatigue. 94 (2017) 168–177. https://doi.org/10.1016/j.ijfatigue.2016.07.005.

[12] M. Seifi, M. Gorelik, J. Waller, N. Hrabe, N. Shamsaei, S. Daniewicz, J.J. Lewandowski, Progress Towards Metal Additive Manufacturing Standardization to Support Qualification and Certification, Jom. 69 (2017) 439–455. https://doi.org/10.1007/s11837-017-2265-2.

[13] R. Cunningham, S.P. Narra, C. Montgomery, J. Beuth, A.D. Rollett, Synchrotron-Based X-ray Microtomography Characterization of the Effect of Processing Variables on Porosity Formation in Laser Power-Bed Additive Manufacturing of Ti-6Al-4V, JOM. 69 (2017) 479–484. https://doi.org/10.1007/s11837-016-2234-1.

[14] H. Kyogoku, T.-T. Ikeshoji, A review of metal additive manufacturing technologies: Mechanism of defects formation and simulation of melting and solidification phenomena in

laser powder bed fusion process, Bulletin of the JSME Mechanical Engineering Reviews. 7 (2020). https://doi.org/10.1299/mer.19-00182.

[15]   A.A. Martin, N.P. Calta, S.A. Khairallah, J. Wang, P.J. Depond, A.Y. Fong, V. Thampy, G.M. Guss, A.M. Kiss, K.H. Stone, C.J. Tassone, J. Nelson Weker, M.F. Toney, T. van Buuren, M.J. Matthews, Dynamics of pore formation during laser powder bed fusion additive manufacturing, Nat Commun. 10 (2019) 1–10. https://doi.org/10.1038/s41467-019-10009-2.

[16]   R.C. Mcclung, M.P. Enright, Current Trends in Probabilistic Damage Tolerance with DARWIN Current Trends in Probabilistic Damage Tolerance, 2015.

[17]   L. Parry, I.A. Ashcroft, R.D. Wildman, Understanding the effect of laser scan strategy on residual stress in selective laser melting through thermo-mechanical simulation, Addit Manuf. 12 (2016) 1–15. https://doi.org/10.1016/j.addma.2016.05.014.

[18]   J. Robinson, I. Ashton, P. Fox, E. Jones, C. Sutcliffe, Determination of the effect of scan strategy on residual stress in laser powder bed fusion additive manufacturing, Addit Manuf. 23 (2018) 13–24. https://doi.org/10.1016/j.addma.2018.07.001.

[19]   Z. Chen, X. Wu, D. Tomus, C.H.J. Davies, Surface roughness of Selective Laser Melted Ti-6Al-4V alloy components, Addit Manuf. 21 (2018) 91–103. https://doi.org/10.1016/j.addma.2018.02.009.

[20]   P.J. DePond, G. Guss, S. Ly, N.P. Calta, D. Deane, S. Khairallah, M.J. Matthews, In situ measurements of layer roughness during laser powder bed fusion additive manufacturing using low coherence scanning interferometry, Mater Des. 154 (2018) 347–359. https://doi.org/10.1016/j.matdes.2018.05.050.

[21]   H. Yeung, B. Lane, J. Fox, Part geometry and conduction-based laser power control for powder bed fusion additive manufacturing, Addit Manuf. 30 (2019) 100844. https://doi.org/10.1016/j.addma.2019.100844.

[22]   A. Ladewig, G. Schlick, M. Fisser, V. Schulze, U. Glatzel, Influence of the shielding gas flow on the removal of process by-products in the selective laser melting process, Addit Manuf. 10 (2016) 1–9. https://doi.org/10.1016/j.addma.2016.01.004.

[23]   C.L. Druzgalski, A. Ashby, G. Guss, W.E. King, T.T. Roehling, M.J. Matthews, Process optimization of complex geometries using feed forward control for laser powder bed fusion additive manufacturing, Addit Manuf. (2020) 101169. https://doi.org/10.1016/j.addma.2020.101169.

[24]   T.G. Spears, S.A. Gold, In-process sensing in selective laser melting (SLM) additive manufacturing, (2011). https://doi.org/10.1186/s40192-016-0045-4.

[25]   ISO/ASTM 52942:2020(E), Additive manufacturing — Qualification principles — Qualifying machine operators of laser metal powder bed fusion machines and equipment used in aerospace applications, n.d.

[26]   NASA-STD-6030, ADDITIVE MANUFACTURING REQUIREMENTS FOR SPACEFLIGHT SYSTEMS, 2021. https://standards.nasa.gov.

[27]   NASA-STD-6033, ADDITIVE MANUFACTURING REQUIREMENTS FOR EQUIPMENT AND FACILITY CONTROL, 2021. https://standards.nasa.gov.

[28]   ISO/ASTM 52907:2019(E), Additive manufacturing-Feedstock materials-Methods to characterize metallic powders 1, n.d. http://www.iso.org.

[29]   K. Riener, N. Albrecht, S. Ziegelmeier, R. Ramakrishnan, L. Haferkamp, A.B. Spierings, G.J. Leichtfried, Influence of particle size distribution and morphology on the properties of

the powder feedstock as well as of AlSi10Mg parts produced by laser powder bed fusion (LPBF), Addit Manuf. 34 (2020) 101286. https://doi.org/10.1016/j.addma.2020.101286.

[30]   S. Vock, B. Klöden, A. Kirchner, T. Weißgärber, B. Kieback, Powders for powder bed fusion: a review, Progress in Additive Manufacturing. 4 (2019) 383–397. https://doi.org/10.1007/s40964-019-00078-6.

[31]   How do you densely pack a bunch of spheres? Ask an algorithm | Princeton University Department of Chemistry, (n.d.). https://chemistry.princeton.edu/news/how-do-you-densely-pack-bunch-spheres-ask-algorithm (accessed November 9, 2022).

[32]   J. v. Gordon, S.P. Narra, R.W. Cunningham, H. Liu, H. Chen, R.M. Suter, J.L. Beuth, A.D. Rollett, Defect structure process maps for laser powder bed fusion additive manufacturing, Addit Manuf. 36 (2020) 101552. https://doi.org/10.1016/J.ADDMA.2020.101552.

[33]   M. Khorasani, A. Ghasemi, M. Leary, L. Cordova, E. Sharabian, E. Farabi, I. Gibson, M. Brandt, · Bernard Rolfe, B. Rolfe, A comprehensive study on meltpool depth in laser-based powder bed fusion of Inconel 718, 120 (2022) 2345–2362. https://doi.org/10.1007/s00170-021-08618-7.

[34]   Q. Chen, Y. Zhao, S. Strayer, Y. Zhao, K. Aoyagi, Y. Koizumi, A. Chiba, W. Xiong, A.C. To, Elucidating the effect of preheating temperature on melt pool morphology variation in Inconel 718 laser powder bed fusion via simulation and experiment, Addit Manuf. 37 (2021) 101642. https://doi.org/10.1016/J.ADDMA.2020.101642.

[35]   J.S. Weaver, J.C. Heigel, B.M. Lane, Laser spot size and scaling laws for laser beam additive manufacturing, J Manuf Process. 73 (2022) 26–39. https://doi.org/10.1016/J.JMAPRO.2021.10.053.

[36] B. Zhang, R. Seede, L. Xue, K.C. Atli, C. Zhang, A. Whitt, I. Karaman, R. Arroyave, A. Elwany, An efficient framework for printability assessment in Laser Powder Bed Fusion metal additive manufacturing, Addit Manuf. 46 (2021). https://doi.org/10.1016/J.ADDMA.2021.102018.

[37] A.K. Agrawal, B. Rankouhi, D.J. Thoma, Predictive process mapping for laser powder bed fusion: A review of existing analytical solutions, Curr Opin Solid State Mater Sci. 26 (2022) 101024. https://doi.org/10.1016/J.COSSMS.2022.101024.

[38] A. Großmann, J. Mölleney, T. Frölich, H. Merschroth, J. Felger, M. Weigold, A. Sielaff, C. Mittelstedt, Dimensionless process development for lattice structure design in laser powder bed fusion, Mater Des. 194 (2020) 108952. https://doi.org/10.1016/J.MATDES.2020.108952.

[39] D.B. Hann, J. Iammi, J. Folkes, A simple methodology for predicting laser-weld properties from material and laser parameters, J Phys D Appl Phys. 44 (2011). https://doi.org/10.1088/0022-3727/44/44/445401.

[40] A. Olleak, F. Dugast, P. Bharadwaj, S. Strayer, S. Hinnebusch, S. Narra, A.C. To, Enabling Part-Scale Scanwise process simulation for predicting melt pool variation in LPBF by combining GPU-based Matrix-free FEM and adaptive Remeshing, Additive Manufacturing Letters. 3 (2022) 100051. https://doi.org/10.1016/J.ADDLET.2022.100051.

[41] Y. Yang, A. Großmann, P. Kühn, J. Mölleney, L. Kropholler, C. Mittelstedt, B.X. Xu, Validated dimensionless scaling law for melt pool width in laser powder bed fusion, J Mater Process Technol. 299 (2022). https://doi.org/10.1016/J.JMATPROTEC.2021.117316.

[42] W.E. King, H.D. Barth, V.M. Castillo, G.F. Gallegos, J.W. Gibbs, D.E. Hahn, C. Kamath, A.M. Rubenchik, Observation of keyhole-mode laser melting in laser powder-bed fusion

additive manufacturing, J Mater Process Technol. 214 (2014) 2915–2925. https://doi.org/10.1016/j.jmatprotec.2014.06.005.

[43] Y. He, M. Zhong, J. Beuth, B. Webler, A study of microstructure and cracking behavior of H13 tool steel produced by laser powder bed fusion using single-tracks, multi-track pads, and 3D cubes, J Mater Process Technol. 286 (2020) 116802. https://doi.org/10.1016/j.jmatprotec.2020.116802.

[44] G. Kasperovich, J. Haubrich, J. Gussone, G. Requena, Correlation between porosity and processing parameters in TiAl6V4 produced by selective laser melting, Mater Des. 105 (2016) 160–170. https://doi.org/10.1016/j.matdes.2016.05.070.

[45] Y. Mahmoodkhani, U. Ali, F. Liravi, R. Esmaeilizadeh, E. Marzbanrad, Determination of the Most Contributing Laser Powder Bed Fusion Process Parameters on the Surface Roughness Quality of Hastelloy X Components, Global Power Propulsion Society. (2018) 1–8.

[46] T.D. McLouth, G.E. Bean, D.B. Witkin, S.D. Sitzman, P.M. Adams, D.N. Patel, W. Park, J.M. Yang, R.J. Zaldivar, The effect of laser focus shift on microstructural variation of Inconel 718 produced by selective laser melting, Mater Des. (2018). https://doi.org/10.1016/j.matdes.2018.04.019.

[47] A.M. Mancisidor, F. Garciandia, M.S. Sebastian, P. Álvarez, J. Díaz, I. Unanue, Reduction of the residual porosity in parts manufactured by selective laser melting using skywriting and high focus offset strategies, in: Phys Procedia, 2016: pp. 864–873. https://doi.org/10.1016/j.phpro.2016.08.090.

[48] G.E. Bean, D.B. Witkin, T.D. McLouth, D.N. Patel, R.J. Zaldivar, Effect of laser focus shift on surface quality and density of Inconel 718 parts produced via selective laser melting, Addit Manuf. 22 (2018) 207–215. https://doi.org/10.1016/j.addma.2018.04.024.

[49] Y. Ekubaru, O. Gokcekaya, T. Ishimoto, K. Sato, K. Manabe, P. Wang, T. Nakano, Excellent strength–ductility balance of Sc-Zr-modified Al–Mg alloy by tuning bimodal microstructure via hatch spacing in laser powder bed fusion, Mater Des. 221 (2022) 110976. https://doi.org/10.1016/J.MATDES.2022.110976.

[50] P. Promoppatum, S.-C. Yao, Influence of scanning length and energy input on residual stress reduction in metal additive manufacturing: Numerical and experimental studies, J Manuf Process. 49 (2020) 247–259. https://doi.org/10.1016/j.jmapro.2019.11.020.

[51] Q. Chen, H. Taylor, A. Takezawa, X. Liang, X. Jimenez, R. Wicker, A.C. To, Island scanning pattern optimization for residual deformation mitigation in laser powder bed fusion via sequential inherent strain method and sensitivity analysis, Addit Manuf. 46 (2021) 102116. https://doi.org/10.1016/J.ADDMA.2021.102116.

[52] H. Ali, L. Ma, H. Ghadbeigi, K. Mumtaz, In-situ residual stress reduction, martensitic decomposition and mechanical properties enhancement through high temperature powder bed pre-heating of Selective Laser Melted Ti6Al4V, Materials Science and Engineering A. 695 (2017) 211–220. https://doi.org/10.1016/j.msea.2017.04.033.

[53] S.Z. Uddin, L.E. Murr, C.A. Terrazas, P. Morton, D.A. Roberson, R.B. Wicker, Processing and characterization of crack-free aluminum 6061 using high-temperature heating in laser powder bed fusion additive manufacturing, Addit Manuf. 22 (2018) 405–415. https://doi.org/10.1016/j.addma.2018.05.047.

[54] M. Malỳ, C. Höller, M. Skalon, B. Meier, D. Koutnỳ, R. Pichler, C. Sommitsch, D. Paloušek, Effect of process parameters and high-temperature preheating on residual stress and relative density of Ti6Al4V processed by selective laser melting, Materials. 16 (2019). https://doi.org/10.3390/ma12060930.

[55] K. Kempen, B. Vrancken, S. Buls, L. Thijs, J. van Humbeeck, J.-P. Kruth, Selective Laser Melting of Crack-Free High Density M2 High Speed Steel Parts by Baseplate Preheating, (2014). https://doi.org/10.1115/1.4028513.

[56] B. Diehl, A. Nassar, Reducing near-surface voids in metal (Ti-6Al-4V) powder bed fusion additive manufacturing: the effect of inter-hatch travel time, Addit Manuf. 36 (2020) 101592. https://doi.org/10.1016/j.addma.2020.101592.

[57] G. Strano, L. Hao, R.M. Everson, K.E. Evans, Surface roughness analysis, modelling and prediction in selective laser melting, J Mater Process Technol. 213 (2013) 589–597. https://doi.org/10.1016/j.jmatprotec.2012.11.011.

[58] S. Kleszczynski, A. Ladewig, K. Friedberger, J. zur Jacobsmühlen, D. Merhof, G. Witt, POSITION DEPENDENCY OF SURFACE ROUGHNESS IN PARTS FROM LASER BEAM MELTING SYSTEMS, (n.d.).

[59] S. Rott, A. Ladewig, K. Friedberger, J. Casper, M. Full, J.H. Schleifenbaum, Surface roughness in laser powder bed fusion – Interdependency of surface orientation and laser incidence, Addit Manuf. 36 (2020) 101437. https://doi.org/10.1016/j.addma.2020.101437.

[60] D. Pradhan, G.S. Mahobia, K. Chattopadhyay, V. Singh, Effect of surface roughness on corrosion behavior of the superalloy IN718 in simulated marine environment, J Alloys Compd. 740 (2018) 250–263. https://doi.org/10.1016/j.jallcom.2018.01.042.

[61] Y. Tian, D. Tomus, P. Rometsch, X. Wu, Influences of processing parameters on surface roughness of Hastelloy X produced by selective laser melting, Addit Manuf. 13 (2017) 103–112. https://doi.org/10.1016/j.addma.2016.10.010.

[62] B.R. Whip, Effect of Process Parameters on the Surface Roughness and Mechanical Performance of Additively Manufactured Alloy 718, (2018). http://rave.ohiolink.edu/etdc/view?acc_num=wright1526993831680976.

[63] ISO/ASTM 52902, Additive manufacturing - test artifact - geometric capability assessment of additive manufacturing systems, (2019). https://doi.org/10.1520/52902-19.

[64] C.L. Druzgalski, A. Ashby, G. Guss, W.E. King, T.T. Roehling, M.J. Matthews, Process optimization of complex geometries using feed forward control for laser powder bed fusion additive manufacturing, Addit Manuf. 34 (2020). https://doi.org/10.1016/J.ADDMA.2020.101169.

[65] J. Pedro Fernandes dos Santos, R. Manuel dos Santos Oliveira Baptista Supervisor, M. Luisa Coutinho Gomes de Almeida, M. Luisa Coutinho Gomes de Almeida Carlos Manuel Alves da Silva, GEOMETRY SPECIFIC SCAN STRATEGY FOR SELECTIVE LASER MELTING (SLM) Mechanical Engineering Examination Committee, 2017.

[66] Y. Zhou, F. Ning, Build Orientation Effect on Geometric Performance of Curved-Surface 316L Stainless Steel Parts Fabricated by Selective Laser Melting, J Manuf Sci Eng. 142 (2020). https://doi.org/10.1115/1.4047624.

[67] S. Sendino, M. Gardon, F. Lartategui, S. Martinez, A. Lamikiz, The effect of the laser incidence angle in the surface of l-pbf processed parts, Coatings. 10 (2020) 1–12. https://doi.org/10.3390/COATINGS10111024.

[68]   K. Tsubouchi, T. Furumoto, M. Yamaguchi, A. Ezura, S. Yamada, M. Osaki, K. Sugiyama, Evaluation of spatter particles, metal vapour jets, and depressions considering influence of laser incident angle on melt pool behaviour, International Journal of Advanced Manufacturing Technology. 120 (2022) 1821–1830. https://doi.org/10.1007/S00170-022-08887-W/FIGURES/12.

[69]   A. Charles, A. Elkaseer, L. Thijs, V. Hagenmeyer, S. Scholz, Effect of process parameters on the generated surface roughness of down-facing surfaces in selective laser melting, Applied Sciences (Switzerland). 9 (2019) 1–13. https://doi.org/10.3390/app9061256.

[70]   D. Wang, S. Mai, D. Xiao, Y. Yang, Surface quality of the curved overhanging structure manufactured from 316-L stainless steel by SLM, International Journal of Advanced Manufacturing Technology. 86 (2016) 781–792. https://doi.org/10.1007/s00170-015-8216-6.

[71]   H. Lee, C.H.J. Lim, M.J. Low, N. Tham, V.M. Murukeshan, Y.J. Kim, Lasers in additive manufacturing: A review, International Journal of Precision Engineering and Manufacturing - Green Technology. 4 (2017) 307–322. https://doi.org/10.1007/s40684-017-0037-7.

[72]   XM200C | Xact Metal | Affordable Metal Powder-Bed Fusion 3D Printing, (n.d.). https://xactmetal.com/affordable-metal-3d-printing-xm200c/ (accessed November 9, 2022).

[73]   L.R. Goossens, Y. Kinds, J.-P. Kruth, B. van Hooreweder, on the Influence of Thermal Lensing During Selective Laser, Solid Freeform Fabrication Symposium – An Additive Manufacturing Conference. (2018) 2267–2274. https://www.researchgate.net/publication/329814587.

[74]   Scanlabs, Installation and Operation The RTC ® 5 PC Interface Board and RTC ® 5 PC / 104- Plus Board, (2010) 1–467.

[75]   J. Romano, T. Brezoczky, D. Christansen, B. Buller, A. Vitanov, A. Brudny, OPERATION OF THREE-DIMENSIONAL PRINTER COMPONENTS, 2018.

[76]   L.C. Capozzi, A. Sivo, E. Bassini, Powder spreading and spreadability in the additive manufacturing of metallic materials: A critical review, J Mater Process Technol. 308 (2022) 117706. https://doi.org/10.1016/J.JMATPROTEC.2022.117706.

[77]   G. Miao, W. Du, Z. Pei, C. Ma, A literature review on powder spreading in additive manufacturing, Addit Manuf. 58 (2022) 103029. https://doi.org/10.1016/J.ADDMA.2022.103029.

[78]   Z. Snow, R. Martukanitz, S. Joshi, On the development of powder spreadability metrics and feedstock requirements for powder bed fusion additive manufacturing, Addit Manuf. 28 (2019) 78–86. https://doi.org/10.1016/j.addma.2019.04.017.

[79]   L.I. Escano, N.D. Parab, L. Xiong, Q. Guo, C. Zhao, K. Fezzaa, W. Everhart, T. Sun, L. Chen, Revealing particle-scale powder spreading dynamics in powder-bed-based additive manufacturing process by high-speed x-ray imaging, Scientific Reports 2018 8:1. 8 (2018) 1–11. https://doi.org/10.1038/s41598-018-33376-0.

[80]   H. Fox, A.B. Kamaraj, D. Drake, Investigating the effect of powder recoater blade material on the mechanical properties of parts manufactured using a powder-bed fusion process, Manuf Lett. 33 (2022) 561–568. https://doi.org/10.1016/J.MFGLET.2022.07.071.

[81]   T.P. Le, X. Wang, K.P. Davidson, J.E. Fronda, M. Seita, Experimental analysis of powder layer quality as a function of feedstock and recoating strategies, Addit Manuf. 39 (2021) 101890. https://doi.org/10.1016/J.ADDMA.2021.101890.

[82]   P. Bidare, I. Bitharas, R.M. Ward, M.M. Attallah, A.J. Moore, Laser powder bed fusion at sub-atmospheric pressures, Int J Mach Tools Manuf. 130–131 (2018) 65–72. https://doi.org/10.1016/j.ijmachtools.2018.03.007.

[83]   P. Bidare, I. Bitharas, R.M. Ward, M.M. Attallah, A.J. Moore, Laser powder bed fusion in high-pressure atmospheres, International Journal of Advanced Manufacturing Technology. 99 (2018) 543–555. https://doi.org/10.1007/s00170-018-2495-7.

[84]   K. Dietrich, J. Diller, S. Dubiez-Le Goff, D. Bauer, P. Forêt, G. Witt, The influence of oxygen on the chemical composition and mechanical properties of Ti-6Al-4V during laser powder bed fusion (L-PBF), Addit Manuf. 32 (2020). https://doi.org/10.1016/j.addma.2019.100980.

[85]   C. Pauzon, A. Raza, E. Hryha, P. Forêt, Oxygen balance during laser powder bed fusion of Alloy 718, Mater Des. 201 (2021) 109511. https://doi.org/10.1016/J.MATDES.2021.109511.

[86]   (74) Gone with the wind - how gas flow governs LPBF performance | LinkedIn, (n.d.). https://www.linkedin.com/pulse/gone-wind-how-gas-flow-governs-lpbf-performance-marc-saunders/ (accessed October 27, 2022).

[87]   3Din30: We're Not Just Blowing Smoke - YouTube, (n.d.). https://www.youtube.com/watch?v=8FIEzKbXHoY (accessed October 27, 2022).

[88]   Introduction "IN THIS WHITE PAPER WE WILL EXPLORE THE ADDITIVE INDUSTRIES DESIGN APPROACH OF THE SHIELDING GAS CONFIGURATION OF THE METALFAB1 WITH THE AID OF COMPUTATIONAL FLUID DYNAMICS," (n.d.).

[89] R. Ding, J. Yao, B. Du, K. Li, T. Li, L. Zhao, Y. Guo, Effect of shielding gas volume flow on the consistency of microstructure and tensile properties of 316l manufactured by selective laser melting, Metals (Basel). 11 (2021) 1–14. https://doi.org/10.3390/met11020205.

[90] H. Shen, P. Rometsch, X. Wu, A. Huang, Influence of Gas Flow Speed on Laser Plume Attenuation and Powder Bed Particle Pickup in Laser Powder Bed Fusion, JOM. 72 (2020) 1039–1051. https://doi.org/10.1007/s11837-020-04020-y.

[91] J. Reijonen, A. Revuelta, T. Riipinen, K. Ruusuvuori, P. Puukko, On the effect of shielding gas flow on porosity and melt pool geometry in laser powder bed fusion additive manufacturing, Addit Manuf. 32 (2020) 101030. https://doi.org/10.1016/j.addma.2019.101030.

[92] (74) Gone with the wind - how gas flow governs LPBF performance | LinkedIn, (n.d.). https://www.linkedin.com/pulse/gone-wind-how-gas-flow-governs-lpbf-performance-marc-saunders/ (accessed October 27, 2022).

[93] Introduction "IN THIS WHITE PAPER WE WILL EXPLORE THE ADDITIVE INDUSTRIES DESIGN APPROACH OF THE SHIELDING GAS CONFIGURATION OF THE METALFAB1 WITH THE AID OF COMPUTATIONAL FLUID DYNAMICS," (n.d.).

[94] 3Din30: We're Not Just Blowing Smoke - YouTube, (n.d.). https://www.youtube.com/watch?v=8FIEzKbXHoY (accessed October 27, 2022).

[95] TRUMPF: Ask the Expert – TruPrint 5000 gas flow design - YouTube, (n.d.). https://www.youtube.com/watch?v=g1cQAbAiZI4 (accessed November 9, 2022).

[96]   B. Roidl, T. Fauner, G.E. Additive, Gas Flow White Paper Continuous Improvement in Gas Flow Design, (n.d.).

[97]   T.G. Gallmeyer, S. Moorthy, B.B. Kappes, M.J. Mills, B. Amin-Ahmadi, A.P. Stebner, Knowledge of process-structure-property relationships to engineer better heat treatments for laser powder bed fusion additive manufactured Inconel 718, Addit Manuf. 31 (2020). https://doi.org/10.1016/j.addma.2019.100977.

[98]   M. Leary, M. Khorasani, A. Sarker, J. Tran, K. Fox, D. Downing, A. du Plessis, Surface roughness, Fundamentals of Laser Powder Bed Fusion of Metals. (2021) 179–213. https://doi.org/10.1016/B978-0-12-824090-8.00023-8.

[99]   T. Voisin, N.P. Calta, S.A. Khairallah, J.B. Forien, L. Balogh, R.W. Cunningham, A.D. Rollett, Y.M. Wang, Defects-dictated tensile properties of selective laser melted Ti-6Al-4V, Mater Des. 158 (2018) 113–126. https://doi.org/10.1016/j.matdes.2018.08.004.

[100]   Z. Snow, A.R. Nassar, E.W. Reutzel, Invited Review Article: Review of the formation and impact of flaws in powder bed fusion additive manufacturing, Addit Manuf. 36 (2020) 101457. https://doi.org/10.1016/j.addma.2020.101457.

[101]   C. Zhao, N.D. Parab, X. Li, K. Fezzaa, W. Tan, A.D. Rollett, T. Sun, Critical instability at moving keyhole tip generates porosity in laser melting, Science (1979). 370 (2020) 1080–1086. https://doi.org/10.1126/SCIENCE.ABD1587/SUPPL_FILE/ABD1587_S9.MP4.

[102]   S. Tammas-Williams, P.J. Withers, I. Todd, P.B. Prangnell, The Influence of Porosity on Fatigue Crack Initiation in Additively Manufactured Titanium Components, Sci Rep. 7 (2017) 1–13. https://doi.org/10.1038/s41598-017-06504-5.

[103] M. Komarasamy, S. Shukla, S. Williams, K. Kandasamy, S. Kelly, R.S. Mishra, Microstructure, fatigue, and impact toughness properties of additively manufactured nickel alloy 718, Addit Manuf. 28 (2019) 661–675. https://doi.org/10.1016/j.addma.2019.06.009.

[104] D.B. Witkin, D. Patel, T. v. Albright, G.E. Bean, T. McLouth, Influence of surface conditions and specimen orientation on high cycle fatigue properties of Inconel 718 prepared by laser powder bed fusion, Int J Fatigue. 132 (2020) 105392. https://doi.org/10.1016/j.ijfatigue.2019.105392.

[105] D.B. Witkin, D.N. Patel, H. Helvajian, L. Steffeney, A. Diaz, Surface Treatment of Powder-Bed Fusion Additive Manufactured Metals for Improved Fatigue Life, J Mater Eng Perform. 28 (2019) 681–692. https://doi.org/10.1007/s11665-018-3732-9.

[106] A.R. Balachandramurthi, J. Moverare, N. Dixit, R. Pederson, Influence of defects and as-built surface roughness on fatigue properties of additively manufactured Alloy 718, Materials Science and Engineering A. 735 (2018) 463–474. https://doi.org/10.1016/j.msea.2018.08.072.

[107] Y. GUO, L. JIA, B. KONG, N. WANG, H. ZHANG, Single track and single layer formation in selective laser melting of niobium solid solution alloy, Chinese Journal of Aeronautics. 31 (2018) 860–866. https://doi.org/10.1016/J.CJA.2017.08.019.

[108] J.R. Zhuang, Y.T. Lee, W.H. Hsieh, A.S. Yang, Determination of melt pool dimensions using DOE-FEM and RSM with process window during SLM of Ti6Al4V powder, Opt Laser Technol. 103 (2018) 59–76. https://doi.org/10.1016/J.OPTLASTEC.2018.01.013.

[109] H.C. Taylor, E.A. Garibay, R.B. Wicker, Toward a common laser powder bed fusion qualification test artifact, Addit Manuf. 39 (2021) 101803. https://doi.org/10.1016/J.ADDMA.2020.101803.

[110] J. Schindelin, I. Arganda-Carreras, E. Frise, V. Kaynig, M. Longair, T. Pietzsch, S. Preibisch, C. Rueden, S. Saalfeld, B. Schmid, J.Y. Tinevez, D.J. White, V. Hartenstein, K. Eliceiri, P. Tomancak, A. Cardona, Fiji: an open-source platform for biological-image analysis, Nature Methods 2012 9:7. 9 (2012) 676–682. https://doi.org/10.1038/nmeth.2019.

[111] C. Zhao, Q. Guo, X. Li, N. Parab, K. Fezzaa, W. Tan, L. Chen, T. Sun, Bulk-Explosion-Induced Metal Spattering During Laser Processing, (2019). https://doi.org/10.1103/PhysRevX.9.021052.

[112] J. Yin, D. Wang, L. Yang, H. Wei, P. Dong, L. Ke, G. Wang, H. Zhu, X. Zeng, Correlation between forming quality and spatter dynamics in laser powder bed fusion, Addit Manuf. 31 (2020) 100958. https://doi.org/10.1016/J.ADDMA.2019.100958.

[113] S. Ly, A.M. Rubenchik, S.A. Khairallah, G. Guss, M.J. Matthews, Metal vapor micro-jet controls material redistribution in laser powder bed fusion additive manufacturing, Scientific Reports 2017 7:1. 7 (2017) 1–12. https://doi.org/10.1038/s41598-017-04237-z.

[114] Details and cost, (n.d.). https://engineering.cmu.edu/next/facilities/details-cost.html (accessed May 4, 2022).

[115] K. Gruber, I. Smolina, M. Kasprowicz, T. Kurzynowski, Evaluation of Inconel 718 Metallic Powder to Optimize the Reuse of Powder and to Improve the Performance and Sustainability of the Laser Powder Bed Fusion (LPBF) Process, Materials. 14 (2021). https://doi.org/10.3390/MA14061538.

[116] N.E. Gorji, P. Saxena, M. Corfield, A. Clare, J.P. Rueff, J. Bogan, P.G.M. González, M. Snelgrove, G. Hughes, R. O'Connor, R. Raghavendra, D. Brabazon, A new method for assessing the recyclability of powders within Powder Bed Fusion process, Mater Charact. 161 (2020) 110167. https://doi.org/10.1016/j.matchar.2020.110167.

[117] W. Everhart, E. Sawyer, T. Neidt, J. Dinardo, B. Brown, The effect of surface finish on tensile behavior of additively manufactured tensile bars, J Mater Sci. 51 (2016) 3836–3845. https://doi.org/10.1007/s10853-015-9702-9.

[118] FAA-EASA Q&C workshop2018, n.d. http://www.tc.faa.gov/its/worldpac/techrpt/tc20-16.pdf (accessed January 14, 2022).

[119] $10,000 Toilet Seats and Data Rights: The Air Force's New Dilemma | Military.com, (n.d.). https://www.military.com/dodbuzz/2018/06/20/10000-toilet-seats-and-data-rights-air-forces-new-dilemma.html (accessed December 3, 2022).

[120] T. Grohoske, USAF Rapid Sustain Office (RSO) Advance Manufacturing Program Office (AMPO), 2021.

[121] M. Benedict, S. Moylan, S. Al-Abed, C. Ashforth, K. Chou, M. di Prima, A. Elwany, M. Gorelik, A. Lewis, T. Luxton, B. Marshall, W. Mullins, L. Sapochak, R. Russell, J. Warren, D. Wells, The Strategy for American Leadership in High-Consequence Additive Manufacturing, (n.d.). https://doi.org/10.6028/NIST.AMS.600-10.

[122] MMPDS_CHAPTER_1, (n.d.).

[123] MMPDS_CHAPTER_9, (n.d.).

[124] AMS7001_Nickel Alloy, Corrosion and Heat-Resistant Powder for AM, (n.d.).

[125] AMS7000A, (n.d.).

[126] G. Marchese, M. Lorusso, S. Parizia, E. Bassini, J.W. Lee, F. Calignano, D. Manfredi, M. Terner, H.U. Hong, D. Ugues, M. Lombardi, S. Biamino, Influence of heat treatments on microstructure evolution and mechanical properties of Inconel 625 processed by laser powder bed fusion, Materials Science and Engineering: A. 729 (2018) 64–75. https://doi.org/10.1016/J.MSEA.2018.05.044.

[127] C.U. Brown, G. Jacob, M. Stoudt, S. Moylan, J. Slotwinski, A. Donmez, Interlaboratory Study for Nickel Alloy 625 Made by Laser Powder Bed Fusion to Quantify Mechanical Property Variability, J Mater Eng Perform. 25 (n.d.). https://doi.org/10.1007/s11665-016-2169-2.

[128] AMS7003A, Laser Powder Bed Fusion Process, (n.d.).

[129] AMS7003_Laser Powder Bed Fusion Process, (n.d.).

[130] ISO/ASTM 52930:2021, Additive manufacturing-Qualification principles-Installation, operation and performance (IQ/OQ/PQ) of PBF-LB equipment, n.d. https://www.iso.org/obp.

[131] ISO/ASTM 52941:2020, Additive manufacturing-System performance and reliability-Acceptance tests for laser metal powder-bed fusion machines for metallic materials for aerospace application, 2020. www.iso.org/obp.

[132] AMS 7032, Machine Qualification for Fusion-Based Metal Additive Manufacturing, n.d. www.osha.gov/pls/publications/pubindex.list.

[133] P.D. Nezhadfar, S. Thompson, A. Saharan, N. Phan, N. Shamsaei, Structural integrity of additively manufactured aluminum alloys: Effects of build orientation on microstructure, porosity, and fatigue behavior, Addit Manuf. 47 (2021) 102292. https://doi.org/10.1016/J.ADDMA.2021.102292.

[134] AIA Additive Manufacturing Working Group, Report: Recommended Guidance for Certification of AM Components AIA Additive Manufacturing Working Group, 2020.

[135] National Transportation Safety Board, (2016). http://www.ntsb.gov/investigations/dms.html (accessed November 11, 2022).

[136] DARWIN Background | Southwest Research Institute, (n.d.). https://www.swri.org/darwin-background (accessed November 11, 2022).

[137] SwRI receives FAA grant to assess fracture risk in aircraft engines | Southwest Research Institute, (n.d.). https://www.swri.org/press-release/swri-receives-faa-grant-assess-fracture-risk-aircraft-engines (accessed November 11, 2022).

[138] T.M. Wischeropp, C. Emmelmann, M. Brandt, A. Pateras, Measurement of actual powder layer height and packing density in a single layer in selective laser melting, Addit Manuf. 28 (2019) 176–183. https://doi.org/10.1016/j.addma.2019.04.019.

[139] C. Tenbrock, F.G. Fischer, K. Wissenbach, J.H. Schleifenbaum, P. Wagenblast, W. Meiners, J. Wagner, Influence of keyhole and conduction mode melting for top-hat shaped beam profiles in laser powder bed fusion, J Mater Process Technol. 278 (2020) 116514. https://doi.org/10.1016/J.JMATPROTEC.2019.116514.

[140] L. Schmidt, K. Schricker, J.P. Bergmann, C. Junger, Effect of Local Gas Flow in Full Penetration Laser Beam Welding with High Welding Speeds, Applied Sciences 2020, Vol. 10, Page 1867. 10 (2020) 1867. https://doi.org/10.3390/APP10051867.

[141] C. Brock, R. Hohenstein, M. Schmidt, Mechanisms of vapour plume formation in laser deep penetration welding, Opt Lasers Eng. 58 (2014) 93–101. https://doi.org/10.1016/J.OPTLASENG.2014.02.001.

[142] J.P. Oliveira, T.G. Santos, R.M. Miranda, Revisiting fundamental welding concepts to improve additive manufacturing: From theory to practice, Prog Mater Sci. 107 (2020) 100590. https://doi.org/10.1016/J.PMATSCI.2019.100590.

[143] S. Dirks, A. Collet, J.H. Schleifenbaum, Open Vector Format for Laser-Based Computer-Aided Manufacturing, in: Progress in Additive Manufacturing 2020, ASTM International, 2022: pp. 117–130. https://doi.org/10.1520/stp163720210013.

Vita

Hunter Cole Taylor was not accepted into the Governor's Academy for Engineering Studies at L.C. Bird high school in Chesterfield, VA. He went on to graduate from Virginia Tech with a B.S. in Materials Science and Engineering in 2015. That summer he represented the USA as 1 of 25 members of the national ultimate frisbee team at the world championships in London Unfortunately, this meant nothing to his future job prospects. After 6 months of post-graduation delivering Chinese food he realized a degree without hard work has no value. Eventually, he began work as a materials engineer at MATSYS Inc. where he learned about small business, powder metallurgy, and research. In 2018, his future wife was restationed to Ft. Bliss in El Paso TX and a new job hunt began. After a meeting and tour with Dr. Wicker he enrolled in a PhD program and started as a research assistant in the W. M. Keck Center for 3D Innovation.

During his time as a Research Assistant, he participated in a number of proposals and publications. He also led the proposal for the Global Test Artifact Data Exchange Program that was awarded $1,000,000 by NIST and was the first author on two journal publications related to laser powder bed fusion. Hunter also led the development and delivery of training courses related to laser powder bed fusion as part of DRIVE AM.

In addition to his research activities, Hunter founded Tailored Alloys with Laszlo Kecskes based on two novel ideas for alloy development and wedding bands in 2019. The company was awarded an NSF STTR in 2020 entitled "Additive Manufacturing of High Conductivity- High Strength Copper-Based Alloys" based on the novel alloy development approach. Hunter has been on four patent applications to date with many more in progress. Today, he leads Tailored Alloys, which has grown to three full-time employees.

Contact Information: htaylor@tailoredalloys.com